Additional Sex Combs-Like Family Genes Regulate Embryonic Development

BY

Andrea McGinley
B.S. Marietta College, 2007

THESIS

Submitted in partial fulfillment of the
Requirements for the degree of
Doctor of Philosophy in Biological Sciences
in the Graduate College of the
University of Illinois at Chicago, 2014
Chicago, Illinois

Defense committee:
Jennifer Schmidt, Chair
Qun-Tian Wang, Advisor
Peter Okkema
Teresa Orenic
Hans-Georg Simon, Northwestern University

ACKNOWLEDGEMENT

I would like to thank my thesis adviser, Tian Wang, for her continued support since joining her lab. This work would not be possible without her energy, intellect, and insatiable hunger for science to guide me. I also thank my committee members Jennifer Schmidt, Teresa Orenic, and Pete Okkema for introducing me to developmental biology and encouraging me throughout my training. I thank my committee member Hans-Georg Simon for generously sharing his time and the expertise of his lab during the formative stages of my manuscript. I thank Eric Svensson for his service on my committee and critical insights in heart morphogenesis. I thank Robert Dettman for sharing his knowledge of and enthusiasm for epicardial biology. I am indebted to the rest of the Wang lab for their encouragement and friendship over the years, and especially to Hsiao Lei Lai for many thoughtful discussions.

Lastly, I would like to thank my family, especially my parents, Clint and Mary, for raising me; Bill and Dale, for supporting me; and my dearest husband Mc, for everything.

TABLE OF CONTENTS

TABLE OF CONTENTS (continued)

TABLE OF CONTENTS (continued)

LIST OF TABLES

LIST OF FIGURES

LIST OF FIGURES (continued)

LIST OF ABBREVIATIONS

A/P	anterior/posterior
AV	atrioventricular
B6	C57BL/6
BOS	Bohring Opitz Syndrome
BrdU	bromodeoxyuridine
CHD	congenital heart disease
CMFDA	5-chloromethylfluorescein diacetate
CNC	cardiac neural crest
DA	ductus arteriosus
DAB	3,3'-diaminobenzidine
DAPI	4',6-diamidino-2-phenylindole
DMEM	Dulbecco's Minimal Essential Media
E	embryonic day
EdU	5-ethynyl-2′-deoxyuridine
EMT	epithelial-to-mesenchymal transition
FBS	fetal bovine serum
FHF	first heart field
H&E	hematoxylin and eosin staining
HBSS	Hank's balanced salt solution
Hox	homeotic gene
IVS	interventricular septum
LV	left ventricle
MeOH	methanol
ml	milliliter

LIST OF ABBREVIATIONS (continued)

mm	millimeter
OCT	optimal cutting temperature medium
P	postnatal day
PBS	phosphate-buffered saline
PcG	Polycomb Group
PDA	patent ductus arteriosus
PFA	paraformaldehyde
PhoRC	Pho-Repressive Complex
PRC1	Polycomb Repressive Complex 1
PRC2	Polycomb Repressive Complex 2
PR-DUB	Polycomb Repressive Deubiquitinase complex
qRT-PCR	quantitative real-time polymerase chain reaction
RT-PCR	reverse transcription polymerase chain reaction
RV	right ventricle
SHF	second heart field
TF	transcription factor
TrxG	trithorax Group
TUNEL	terminal deoxynucleotidyl transferase dUTP nick end labeling
ug	microgram
um	micrometer
UV	ultraviolet
VSD	ventricular septum defect
WGA	wheat germ agglutinin

SUMMARY

The Polycomb Group (PcG) and trithorax Group (TrxG) proteins regulate gene expression during development (Chen and Dent, 2013). PcG and TrxG are repressors and activators of gene transcription, respectively, that function at the level of chromatin in large multiprotein complexes (Schwartz and Pirrotta, 2008). Chromatin consists of DNA wrapped around histone proteins to facilitate its compaction and storage in the nucleus. PcG and TrxG proteins use posttranslational modifications of histone proteins and the local movement of nucleosomes to alter the chromatin landscape and effect gene transcription (Sparmann and van Lohuizen, 2006). PcG proteins establish and regulate the repressive histone marks H3K27 trimethylation and H2AK119 ubiquitination (Cao *et al*., 2002; de Napoles *et al*., 2004). TrxG proteins generate the histone mark H3K4 trimethylation and use chromatin remodeling of nucleosomes to activate gene expression (Byrd and Shearn, 2003).

The activities of PcG and TrxG proteins are antagonistic and integrated. They frequently regulate the same target genes, but at different stages of development or in different tissues (Chen and Dent, 2013; Sparmann and van Lohuizen, 2006; Kennison and Tamkun, 1988). During differentiation PcG complexes repress unneeded lineage-specific genes while TrxG complexes activate lineage-specific genes needed by the cell (Boyer *et al*., 2006; Fisher and Fisher, 2011). PcG and TrxG are best known for their regulation of *Hox* genes, where they maintain the proper expression domains of *Hox* along the anteroposterior axis (Deschamps and van Nes, 2005; Beuchle *et al*., 2001). Loss of PcG proteins causes ectopic *Hox* expression outside the normal expression domain; loss of TrxG proteins causes reduced *Hox* expression within the normal expression domain (Kennison, 1995; Struhl and Akam, 1985; Ingham, 1985). PcG and TrxG are regulated by a third class of genes known as Enhancers of trithorax and

Polycomb (ETP). ETP members genetically interact with both *PcG* and *TrxG* and are important for maintaining the proper expression domains of PcG/TrxG targets (Coleno-Costes *et al*., 2012).

Additional sex combs (*Asx*) is an ETP gene identified in *Drosophila*. It is involved in the classic ETP functions of regulating *Hox* genes and patterning along the anteroposterior axis (Milne *et al*., 1999). *Asx* has three mammalian homologs: *Additional sex combs-like 1* (*Asxl1*), *Asxl2*, and *Asxl3*. ETP function is conserved for both *Asxl1* and *Asxl2* (Fisher *et al*., 2010a; Baskind *et al*., 2009). Mammalian ASXL proteins are activators and repressors of gene transcription, depending on their interacting partners and cellular context. Both ASXL1 and ASXL2 regulate the PcG complexes Polycomb repressive complex 2 (PRC2) and Polycomb repressive deubiquitnase (PR-DUB). ASXL1 and ASXL2 are required for localization of PRC2 to target genes and the repression of targets via H3K27me3 (Abdel-Wahab *et al*., 2012; Lai and Wang, 2013). Both partner with BAP1 in the PR-DUB complex and are required for BAP1's deubiquitination of H2K119ub1 and the repression of target genes (Scheuermann *et al*., 2010; Lai and Wang, 2013). ASXL1 and ASXL2 interact with diverse protein partners to direct these activities in a tissue- and loci-dependent manner (Lee *et al*., 2010; Park *et al*., 2011; Cho *et al*., 2006).

ASXL proteins have divergent functions in developing tissues. *Asxl1* is most highly expressed in the developing and adult hematopoietic system (Fisher *et al*., 2010b). Loss of *Asxl1* causes dysregulation of hematopoietic progenitor proliferation and differentiation (Fisher *et al*., 2010b; Abdel-Wahab *et al*., 2013; Wang *et al*., 2014). Further, *ASXL1* mutation is frequently found in individuals with myeloid cancers (Gelsi-Boyer *et al*., 2012). In contrast, *Asxl2* is most highly expressed in the developing and adult heart (Baskind *et al*., 2009; McGinley *et al*., 2014). Loss of *Asxl2* causes excessive postnatal growth of the heart and progressive contractility defects

(Lai *et al*., 2012; Lai and Wang, 2013). Failure to maintain PRC2-mediated repression of target genes in hematopoietic and cardiac tissues contributes to *Asxl1*$^{-/-}$ and *Asxl2*$^{-/-}$ phenotypes, respectively (Abdel-Wahab *et al*., 2012; Lai and Wang, 2013).

The high expression levels of *Asxl2* in the developing heart and its requirement in the adult heart led us to examine whether *Asxl2* also regulates cardiovascular development. We also investigated whether *Asxl1* exhibits functional redundancy with *Asxl2* in cardiovascular development. Here we report findings that ASXL2 and ASXL1 have divergent functions in the developing cardiovascular system. ASXL2 regulates cardiac morphogenesis: *Asxl2*$^{-/-}$ animals have overgrowth of the left ventricle and interventricular septum myocardium in late fetal development. ASXL2 is also required for the fetal-neonatal circulatory transition, as *Asxl2*$^{-/-}$ animals are unable to close the ductus arteriosus after birth, resulting in neonatal death. Minor defects in the epicardium were also observed that resolve during development. In contrast, ASXL1 regulates development of the endocardial cushions and has no apparent effect on the myocardium. *Asxl1*$^{-/-}$ animals have inlet-type ventricular septal defects and atrioventricular canal defects at high penetrance that are associated with early defects in formation of the endocardial cushions.

ASXL2 and ASXL1 have roles outside the cardiovascular system as well. I report here that ASXL2 is required for proper melanocyte distribution in the embryo and adult and that ASXL1 is required for lung maturation, early eye development, and craniofacial development. Taken together, these data demonstrate non-overlapping functions for ASXL2 and ASXL1 in the cardiovascular system and other developing tissues. These studies add ASXL2 and ASXL1 to the growing list of chromatin-associated epigenetic factors that regulate cardiovascular development.

I. GENERAL INTRODUCTION

1.1 Development of multicellular organisms requires heritable gene regulation

1.1.1 A need for cellular memory

The development of multicellular organisms involves the adoption, maintenance, and modification of cell identity. Although every cell in an organism contains the same genome, different cell types perform different functions. Cells adopt different identities by expressing different genetic programs. Development involves gradually establishing these identities and expression signatures for each cell type. Development begins with a totipotent one-cell zygote, able to become any cell of the body. These totipotent cells divide to create pluripotent progenitors. Pluripotent progenitor cells can become many, but not all cell types. As development proceeds, gradual lineage restriction towards multipotent progenitors occurs. Eventually progenitors are fated to generate only one cell type.

In the developing heart, cardiomyocytes are derived from BRY^+ multipotent mesoderm progenitors. Lineage restriction produces $MESP1^+$ mesoderm progenitors, which can become only a subset of mesoderm tissues, including cardiac muscle, skeletal muscle, blood cells, and vascular cells (Kitajima *et al*., 2000; Chan *et al*., 2013). These cells are exposed to multiple secreted signaling factors, including BMP, FGF, and antagonists of WNT (Schultheiss *et al*., 1997; Sirbu *et al*., 2008; Marvin *et al*., 2001). This signaling leads to lineage restrictions in which a subset of the $MESP1^+$ cells become cardiac cells. The cardiac cells begin expressing the master cardiac transcription factors (TF) NKX2.5 and GATA4 and a suite of downstream cardiac-specific genes (Lints *et al*., 1993; Oka *et al*., 2006). Whereas the signaling molecules inducing NKX2.5 and GATA4 are short-lived, both transcription factors continue to be expressed into adulthood (Oka *et al*., 2006; Lien *et al*., 1999).

The temporary nature of patterning information during development requires that some system of cellular memory exist for progenitor cells to pass information to their progeny in a lineage. Cells use annotations of the genome to instruct proper expressions at a given time. The annotations must be faithful, capable of maintaining the same information for multiple cell divisions, as progenitor cells divide many times to make copies of themselves and expand a pool of like progenitors. Yet the system must also be malleable, as developing cells alter their gene expressions during differentiation into mature cell types.

1.1.2 Epigenetics is a system of cellular memory

Epigenetics is a system of cellular memory used during development to record information and transmit it to future cell generations. Epigenetics is defined here as heritable changes in a cell that are not due to changes in the DNA sequence itself. The inherited information can be saved in several forms, including posttranslational modifications of histones, chromatin remodeling patterns, DNA methylation, and in non-coding RNAs (reviewed in Margueron and Reinberg, 2010). There is considerable cooperation and crosstalk between these mechanisms. For the purposes of understanding the ASXL proteins, I will describe two of these mechanisms further: histone modification and chromatin remodeling.

1.1.3 Chromatin based epigenetic regulation of gene expression

Histone modifications and chromatin remodeling act at the level of chromatin. In eukaryotic cells, DNA is wrapped around nucleosomes and assembled into chromatin. Stacking of nucleosomes allows for the compaction and efficient storage of DNA. Each nucleosome contains an octamer of histone proteins around which approximately 147 basepairs of DNA is wrapped. The histone proteins have N-terminal tails that emerge from the nucleosome. These histone tails can be post-translationally modified by phosphorylation, acetylation, methylation,

ubiquitination and sumoylation, to alter DNA-histone affinity and/or the affinity of specific chromatin regions for regulatory proteins. Histone modifications can also regulate gene expression by physically changing the chromatin's configuration to be more or less accessible to transcription. For example, acetylation of lysine residues causes a decrease in the positive charge of the nucleosome, reducing its affinity for DNA (Hizume *et al*., 2010). Nucleosome arrays with acetylated histones are less compact, and acetylation of histones directly enhances transcription by RNA Polymerase III (Tse *et al*., 1998).

Chromatin remodeling complexes utilize energy from ATP to move nucleosomes and facilitate access to DNA by transcriptional machinery and regulatory factors (reviewed in Clapier and Cairns, 2009). Nucleosomes can slide along the DNA, be removed, or have their histone composition changed by chromatin remodelers to either activate or repress gene transcription. Chromatin remodelers also utilize histone modifications. For example, the loosening of nucleosomal-DNA interaction by histone acetylation is used by SWI/SNF family complexes to facilitate nucleosome sliding (Chatterjee *et al*., 2011).

Covalent modifications of histones and nucleosome patterns are copied during the cell cycle, passing regulatory information onto daughter cells epigenetically (Clapier and Cairns, 2009). This allows cells with a common progenitor to maintain memories of relevant gene expression modules, stored within the structure of their chromatin.

1.2 PcG and TrxG complexes establish a system of cellular memory during development

PcG and TrxG proteins act in large multi-protein complexes to generate and maintain histone post-translational modifications. TrxG proteins also participate in chromatin remodeling. Chromatin modifications mediated by PcG and TrxG proteins are heritable across cell

generations (Dejardin and Cavalli, 2005). Thus, a cell and its descendents can be programmed to behave in the same way. After transient patterning signals are gone, PcG and TrxG proteins or their marks remain on the chromatin to propagate proper gene expression in descendent cells. Together the PcG and TrxG complexes form a system of cellular memory that is critical for proper development.

The activities of PcG and TrxG proteins are mutually antagonistic; whereas PcG proteins generate repressive, chromatin-condensing marks, TrxG proteins generate activating, open-chromatin associated marks. PcG and TrxG complexes are found enriched at developmental target genes (Voight *et al*., 2013). In early embryos most developmental target genes are marked by a flexible chromatin configuration. Both PcG and TrxG proteins are present at these genes, and are believed to keep them in a poised state whereby they can be repressed or activated upon receipt of the appropriate signal (Boyer *et al*., 2006). Upon cell differentiation, the appropriate lineage-specific genes are maintained in an active state by TrxG proteins, whereas genes for alternate lineages are permanently repressed by PcG proteins (Steffen and Ringrose, 2014).

1.2.1 Mechanisms of PcG function

PcG proteins assemble into at least four different complexes: PhoRC, PRC2, PRC1, and PR-DUB (Schwartz and Pirrotta, 2007). The current model of PcG regulation is that Polycomb Repressive Complex 2 (PRC2) binds to sites known as Polycomb Response Elements (PREs). These PREs may be in close proximity to the target gene, or lie very far away on the chromosome. PRC2 contains the histone methyltransferases EZH2/EZH1 which are responsible for creating the H3K27me3 mark, a hallmark of repressed loci and PcG activity. Finally, Polycomb Repressive Complex 1 (PRC1) is recruited to the loci by binding to H3K27me3 (Boyer *et al*., 2006). PRC1 is important for the long-term maintenance of repression (Schwartz

and Pirrotta, 2008). PRC1 also ubiquitinates histone H2AK119, a mark associated with gene repression (Endoh *et al*., 2012). H2A ubiquitination is required for the binding of poised RNA Polymerase II, preventing transcriptional elongation of the target gene (Stock *et al*., 2007). More recently, another PcG complex, PR-DUB was identified that antagonizes the H2AK119ub1 mark generated by PRC1. PR-DUB contains the deubiquitinase BAP1 and ASXL1/2. Interestingly, both the ubiquitinating activity of PRC1 and the deubiquitinating activity of PR-DUB are needed for repression, underscoring a need for balance in the distribution and cycling of H2AK119ub1.

1.2.2 Mechanisms of TrxG function

The mechanism of TrxG function is less well understood compared to that of PcG function. TrxG complexes function by enzymatically modifying histone tails, or by remodeling chromatin. Chromatin remodeling complexes can reposition, remove, and add alternate histone subunits to nucleosomes to change transcriptional access to target genes. In mammals, three TrxG complexes exist: BRM, SET1-like, and MLL (Schuettengruber *et al*., 2007). The BRM complex contains Brahma, an ATP-dependent chromatin remodeler. The SET1-like complex contains the histone methyltransferase responsible for creating the H3K4me3 mark, a hallmark of activated loci and TrxG activity. Finally, the MLL complex contains proteins that mediate both chromatin remodeling and histone methyltransferase activity. The activities of TrxG and PcG proteins are antagonistic. For example, the TrxG histone methyltransferases ASH1 and TRX block PcG silencing by establishing the activating modifications H3K4me3, H3K9me3, and H4K20me3 (Klymenko and Muller, 2004).

1.3 Asx and ASXL proteins interact with PcG and TrxG proteins

The *Asxl* gene family consists of three mammalian homologs of the Drosophila *Additional sex combs* (*Asx*) gene: *Asxl1*, *Asxl2*, and *Asxl3*. Asx and the ASXL family are

members of the Enhancer of Trithorax and Polycomb (ETP) Group proteins. ETP genes like *Asx* genetically interact with both *PcG* and *TrxG* genes (Milne *et al*., 1999). Mutations in *Asx* result in both posterior (PcG-type) and anterior (TrxG-type) homeotic transformations (Sinclair *et al*., 1992). Asx localizes to over 90 loci on polytene chromosomes, over 60 of which colocalize with binding sites of PcG complexes (Sinclair *et al*., 1998).

Asx/ASXL proteins regulate PcG protein activity using multiple mechanisms. Asx participates in the PR-DUB complex with the histone deubiquitinase Calypso. In PR-DUB, Asx is required for the deubiquitination of the PRC1-generated mark H2AK119ub1, and the continued repression of the Hox gene *Ubx* in Drosophila (Scheuermann *et al*., 2010). ASXL1 and ASXL2 also function in mammalian PR-DUB with BAP1, the mammalian homolog of Calypso (Lai and Wang, 2013; Scheuermann *et al*., 2010; Dey *et al*., 2012). *Asxl1* also genetically interacts with the PRC1 member *Cbx2* during anteroposterior patterning, consistent with ASXL's role in regulating H2AK119ub1 levels (Fisher *et al*., 2010; Baumann and De La Fuente, 2011). ASXL1 and ASXL2 both have functional interactions with the PRC2 complex as well. Both ASXLs interact with PRC2 components to direct PRC2 to target genes and are required for normal distribution of the PRC2-generated H3K27me3 mark (Abdel-Wahab *et al*., 2013; Baskind *et al*., 2009; Lai and Wang, 2013).

1.3.1 The developmental functions of Asx and ASXL

Mutant mouse models have been studied for two mammalian homologs of *Asx*: *Asxl1* and *Asxl2*. These studies have provided insight into the developmental and adult functions of these genes in anteroposterior patterning, hematopoiesis, cardiac development and function, and several other processes. Both *Asxl1* and *Asxl2* are required for anteroposterior patterning of the mesoderm and exhibit both PcG and TrxG-type homeotic transformation of the axial skeleton

(Fisher *et al*., 2010; Basking *et al*., 2009). In *Asxl1*$^{-/-}$ animals this is due to misexpression of *Hox* genes in ectopic domains, and loss of *Hox* expression in normal domains (Fisher *et al*., 2010). The same cause is suspected, but not confirmed, for *Asxl2*$^{-/-}$ animals (Baskind *et al*., 2009).

Asxl1 is a critical regulator of cell identity during hematopoietic development. Hematopoiesis involves maintenance of a hematopoietic stem cell (HSC) pool which gives rise to lineage-specific progenitors. Blood cells are formed by the stepwise differentiation of these progenitors. Loss of *Asxl1* causes defects in the proliferation and differentiation of hematopoietic progenitors, leading to myelodysplasia and leukemia like syndromes (Wang *et al*., 2014; Abdel-Wahab *et al*., 2013). *ASXL1* is found to be frequently mutated in these human syndromes as well (Gelsi-Boyer *et al*., 2009). *Asxl1* mutation also leads to a number of developmental defects in the heart, lungs, eyes, and brain (McGinley *et al*., 2014; Wang *et al*., 2013; Abdel-Wahab *et al*., 2013; Fisher *et al*., 2010).

1.3.2 Do ASXL proteins regulate cardiovascular development?

Several lines of evidence suggested to us that ASXL proteins may regulate cardiovascular development. First, ASXL2 binds at a number of cardiac target genes and is required for their PRC2-mediated repression via H3K27me3 in the adult heart (Lai and Wang, 2013; Lai *et al*., 2012). Specifically, ASXL2 is required for mediating the conversion of dimethylation to trimethylation on H3K27 (Lai and Wang, 2013). Loss of *Asxl2* causes derepression of fetal β-MHC and other cardiac target genes (Lai *et al*., 2012). Does ASXL2 regulate fetal heart development in addition to adult cardiac function? *Asxl2* is highly expressed in the heart from E9.5-birth, so this appears likely (Baskind *et al*., 2009). Finally, congenital cardiac defects are found in 50% of Bohring-Opitz Syndrome patients, a developmental disorder caused by ASXL1/ASXL3 mutation (Hastings *et al*., 2011).

1.4 Roles of PcG and TrxG in the regulation of heart development

Here we investigate the roles of ASXL2 and ASXL1 in heart development in order to understand their functions in chromatin-based regulation of heart development. Towards this end, I review here the development of the heart and the known roles of PcG/TrxG members therein.

1.4.1 Heart development

The mammalian heart is a 4-chambered muscular organ designed to pump oxygenated blood throughout the circulatory system. The heart is the first functioning organ to develop in the embryo and its processes are highly conserved between species. Heart development begins at E7 in the pre-gastrulation mouse embryo. At this stage BRY^+ precardiac mesoderm cells in the epiblast layer migrate through the primitive streak (Evans, 2010). The cardiac mesoderm forms a horseshoe-shaped field of cells at the anterior end of the lateral plate mesoderm. Upon division of the mesoderm plate into two layers, cardiac progenitors reside in the splanchnic mesoderm layer. The cardiac fields on either side will be pushed towards the midline of the embryo and fuse together to form the primitive heart tube.

Two cell types are present in the primitive heart tube: an outer muscular myocardial layer, and an inner endothelial endocardium layer. Both cell types derive from a common $FLK1^+$ progenitor, a marker of early vascular cells (Kattman *et al*., 2006; Milgrom-Hoffman *et al*., 2011). The endocardial cells assemble into tubes comparable to the self-assembly of blood vessels during vasculogenesis. As the heart fields fuse, the endocardial tubes on each side will fuse at the midline and generate a single endocardially-lined heart tube. Thus the primitive heart tube consists of a single layer of myocardial muscle cells enveloping a layer of endocardial cells.

1.4.1.1 First heart field progenitors

The primitive heart tube is derived from an early-differentiating pool of progenitors within the cardiac field termed the first heart field (FHF). These cells will eventually become the left ventricle and atria of the heart. The transcription factor MESP1 is the earliest marker of cardiac mesoderm (Kitajima *et al*., 2000). MESP1 acts upstream of multiple cardiac-specifying transcription factors including NKX2.5, GATA4, and ISL1 (Bondue *et al*., 2011). After FHF recruitment into the primary heart tube, NKX2.5, GATA4, and Myocardin direct a transcriptional cascade of downstream cardiac-specific genes (Bruneau, 2002; Kuo *et al*., 1997; Wang *et al*., 2001). TBX5 expression is restricted to the FHF and regulates left ventricle maturation (Takeuchi *et al*., 2003). The voltage-gated ion channel HCN4 is expressed early and delineates the boundaries of the FHF (Spater *et al*., 2013). Contractile proteins like myosin light chain MLC2A, MLC2V, and alpha-cardiac actin are expressed, allowing the heart tube to contract (Evans, 2010; Franco *et al*., 1999). ISL1 is downregulated in the FHF and retained in the late-differentiating cardiac precursors of the second heart field (SHF) (Brown *et al*., 2005; Evans *et al*., 2010).

1.4.1.2 Second heart field progenitors

After formation of the primitive heart tube, the heart continues to receive cells from the second heart field (SHF). The SHF is a migratory progenitor population originally found in a crescent anterior to the FHF, extending from the pharyngeal arches to the inflow tract of the heart. Cells from the SHF become the right ventricle, outflow tract, and also contribute to the atria. The SHF is marked by the transcription factor ISL1 and migrates to both ends of the heart tube to join the inflow and outflow tracts (Cai *et al*., 2003). The SHF was originally conceived as a separate progenitor population from the FHF, defined by ISL1 expression. However, both are

derived from a common progenitor, and ISL1 is expressed broadly in cardiac mesoderm before the FHF forms the heart tube (Xavier-Neto *et al*., 2012). ISL1 is required to maintain the progenitor status of cardiac cells in the SHF, and is downregulated during differentiation (Brade *et al*., 2013). Like the FHF, cells from the SHF are multipotent: they can give rise to endocardial, myocardial, and smooth muscle lineages (Kattman *et al*., 2006; Milgrom-Hoffman *et al*., 2011). Their differentiation is regulated by many of the same transcription factors as the FHF, including NKX2.5 and GATA4, in addition to SHF-specific factors such as TBX20 (Xavier-Neto *et al*., 2012).

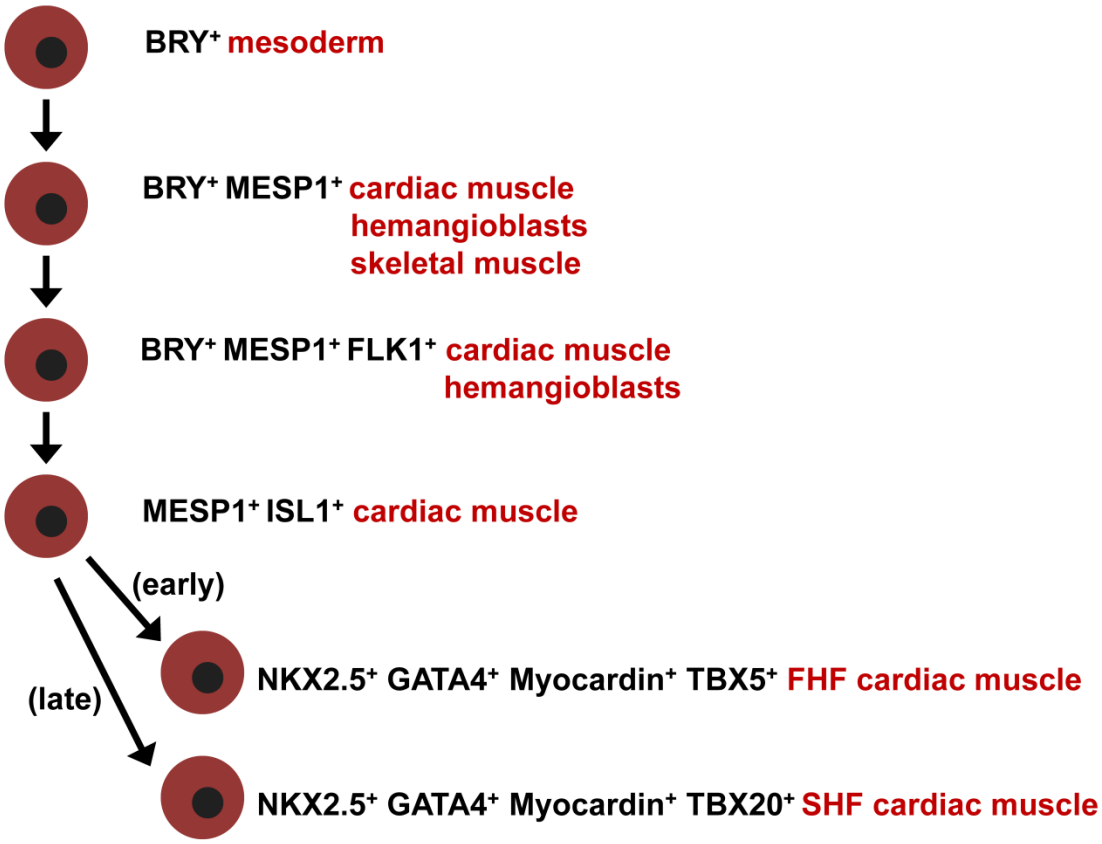

Figure 1: Lineage restrictions in cardiac progenitors of the first and second heart fields. Major transcription factors expressed during the differentiation of cardiomyocytes from the first and second heart fields (FHF, SHF) are depicted. The developmental potential of each progenitor is listed in red text. The FHF and SHF are both derived from $ISL1^+$ cells; FHF progenitors downregulate ISL1 and begin expressing transcription factors for muscle differentiation early, while SHF cells continue to express ISL1 and proliferate as progenitors before differentiating.

1.4.1.3 Cardiac neural crest

Migratory cardiac neural crest (CNC) cells join the heart from E9-12.5 and contribute to reshaping the aortic arches and outflow tract (Keyte and Hutson, 2012). CNC cells are essential for proper alignment of the outflow tract via two distinct mechanisms. First, the CNC gives rise to the aorticopulmonary septum that begins dividing the outflow tract at E9.5, and also makes contributions to the membranous ventricular septum (Kirby and Waldo, 1995). Proper rotation of the aorticopulmonary septum is required for the convergence of the aorta/pulmonary arteries with the ventricular septum. Second, the CNC controls extension of the outflow tract towards the septum by regulating FGF signaling in the pharyngeal arches as the CNC migrate through them on their way to the heart (Kirby and Waldo, 1995; Abu-Issa *et al*., 2002). CNC also form parasympathetic nerves in the heart, but not the cardiac conduction system, which is derived from myocardium (Keyte and Hudson, 2012; Christoffels and Moorman, 2009).

1.4.1.4 Epicardial cells

In addition to migratory SHF and CNC cells, a third population of cells migrates to the heart and shapes its development. The proepicardium is a transient organ located adjacent to the liver and inflow tract of the heart. Between E9-E11.5 cells from the proepicardium migrate over the surface of the heart and form the epicardium. Some cells of the epicardium undergo an epithelial-to-mesenchymal transition from E12.5-E14.5 and migrate into the subepicardial space between the epicardium and compact myocardium. Once in the subepicardium some of these cells will form surface-level coronary blood vessels. Other cells migrate into the myocardium to form coronary arteries and veins. The epicardium is multipotent: it gives rise to the smooth muscle cells and some endothelial cells of the coronary vasculature, as well as the cardiac fibroblast lineage and some scattered cardiomyocytes (Olivey and Svensson, 2010; Wilting *et*

al., 2007; Acharya *et al*., 2012; Cai *et al*., 2008; Zhou *et al*., 2008). The cardiac fibroblasts are an important group of cells present in greater numbers than cardiomyocytes themselves in the adult heart. They contribute to the growth of the myocardium by supplying pro-proliferative signals and synthesize extracellular matrix within the heart. Fibroblasts are first found in the heart at E12.5, and their population increases through the early postnatal period (Snider *et al*., 2009; Ieda *et al*., 2009).

1.4.2 Cardiac morphogenesis : partitioning and trabeculation

1.4.2.1 Partitioning

To form the adult atrial and ventricular chambers, the primitive heart undergoes a series of morphogenetic movements that partition the heart into 4 chambers. This process begins with cardiac looping, one of the earliest asymmetrical events in the developing embryo. At E8.5 the heart bulges outward towards the right side of the body, influenced by signals from the left/right asymmetrical patterning genes *nodal*, a member of the TGF-β family, and *Pitx2*, a homeobox transcription factor (Zhang *et al*., 2004). Looping shifts the inflow tract anteriorally, such that the future atrial chambers sit on top of the heart.

Endocardial cushions form valve tissue between the future chambers (reviewed in Combs and Yutzey, 2009). The endocardial cushions are mounds of loose mesenchymal cells in a rich extracellular matrix called cardiac jelly. The mesenchymal cells are formed by EMT of endocardial epithelial cells. Beginning at E9.5 cushions form within the outflow tract and atrioventricular canal. They will coalesce between the atrial and ventricular chambers of the heart when the heart completes looping, forming a ring of endocardial tissue that will become the atrioventricular valves and semilunar valves of the aorta/pulmonary artery.

Remodeling of the endocardial cushions occurs concurrently with ventricular and atrial septation. The septa divide the heart into left and right chambers and separate the flow of oxygenated and deoxygenated blood. Atrial septation is a multi-step process in which a septum grows from the anteromedial wall towards the endocardial cushions. A second septum grows from the endocardial cushions towards the upper wall, overlapping the first septum. Multiple cell populations contribute to atrial septation, including the atrioventricular canal cushions, mesenchymal cells of the dorsal mesocardium, FHF and SHF (Mommersteeg *et al*., 2006; Goddeeris *et al*., 2008; Hoffmann *et al*., 2009; Xie *et al*., 2012).

In comparison to atrial septation, ventricular septation is more straightforward. The interventricular septum (IVS) forms from ventricular myocardium that begins growing upwards from the apex of the heart towards the endocardial cushions at E10. The IVS lies between the SHF-derived right ventricle and the FHF-derived left ventricle. It appears the septum contains cells from both populations, although their relative contribution is disputed. Tracing using a mef2c-SHF-Cre line shows labeling in the entire IVS (Verzi *et al*., 2005). However, clonal analysis and tracing using *Mlc1v*, expressed in the right ventricle, and *Mlc3f*, expressed in the left ventricle, demonstrate that the septum has cells from both sides, with a majority from the left ventricle (Franco *et al*., 2006).

1.4.2.2 Trabeculation

Maturation of the ventricular chambers includes morphological remodeling by trabeculation. Trabeculation of the heart begins at E9.5 and is controlled by neuregulin and Notch signaling (Runge and Patterson, 2005; Grego-Bessa *et al*., 2007). The myocardial surface facing the endocardium develops ridges and a sponge-like arrangement. Trabeculation increases the surface area inside the heart and allows oxygenated blood to reach the compact layer.

Myocardial cells are arranged in a gradient of differentiation across the compact myocardium and trabeculae; cells in the trabeculae are most differentiated, while the compact layer is highly proliferative and less differentiated (Park *et al*., 2013; Pasumarthi and Field, 2002). Between E13-E14 the basal portions of the trabeculae undergo compaction and these trabecular myocytes rejoin the compact myocardial layer (Sedmera and McQuinn, 2008). Compaction of the trabeculae generates a dramatically thicker compact layer by E14.

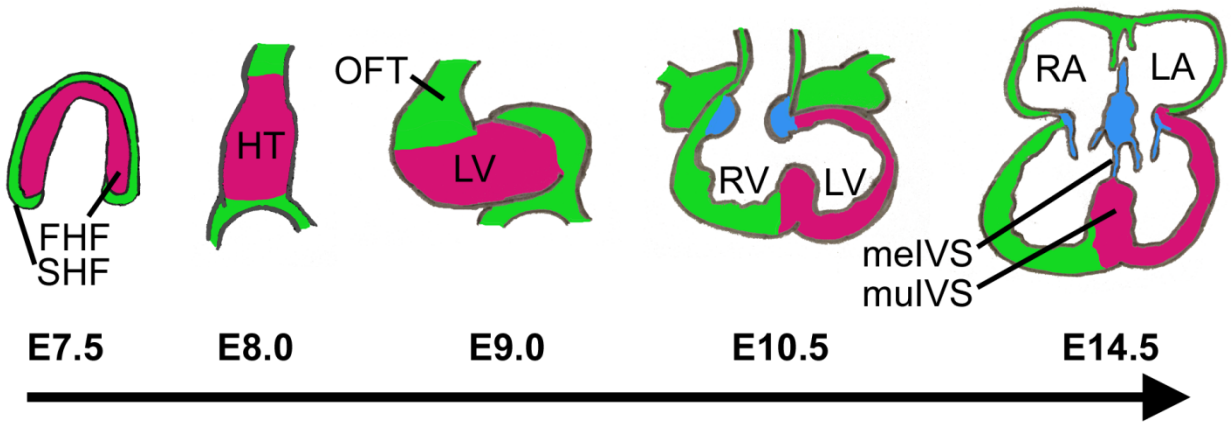

Figure 2: Derivatives of the first and second heart fields.

At E7.5 cardiac progenitors exist in two overlapping horseshoe-shaped domains known as the first heart field (FHF; pink) and second heart field (SHF; green). At E8.0 the FHF progenitors have formed the tubular heart, with inflow and outflow tracts derived from the SHF. During cardiac looping at E9.0, the tubular heart loops rightward and the inflow tract moves towards the outflow tract. Endocardial cushions (blue) form within the outflow tract and atria to separate the flow of oxygenated and deoxygenated blood. Endocardial cushions form the atrial septum, atrioventricular valves, and membranous septum (meIVS). MuIVS: Muscular IVS.

1.4.3 PcG and TrxG complexes in heart development

The role of epigenetic factors and chromatin dynamics during heart development has been gradually recognized (reviewed in Chang and Bruneau, 2012; Wang, 2012). The known functions of PcG and TrxG proteins in heart development are summarized below.

1.4.3.1 The PcG complex PRC2

The PcG complex PRC2 establishes H3K27me3-mediated repression of developmental genes. When EZH2, the H3K27 methyltransferase of PRC2, is inactivated in early cardiomyocytes, a thin myocardial wall with thickened trabeculae results, in addition to septal defects (Delgado-Olguin *et al*., 2012). If EZH2 is inactivated in the SHF, development of the heart is unperturbed until adult stages, when the hearts develop hypertrophy and fibrosis (Delgado-Olguin *et al*., 2012). This suggests that PRC2 has multiple functions in different tissues of the developing heart.

PRC2 often functions together with JARID2. JARID2 is one of a number of PcG proteins that are not 'core' required members of the major complexes, but rather interact with the PcG complexes in some contexts to facilitate recruitment or maintenance of binding. *Jarid2* is required for repressing cyclins and cell proliferation in cardiomyocytes (Toyoda *et al*., 2003). *Jarid2* is first expressed in the heart in the trabeculae at E10.5, which is consistent with a role in the repression of cardiomyocyte proliferation, as the trabeculae exhibit low proliferation (Toyoda *et al*., 2003). In *Jarid2*$^{-/-}$ mice double-outlet right ventricle and ventricular septal defects are present, indicating defects in looping (Lee *et al*., 2000). Differentiation of cardiomyocytes is also impaired and may be due to the ability of JARID2 to complex with NKX2.5 and GATA4 cardiac transcription factors and regulate their target gene expression (Kim *et al*., 2004).

1.4.3.2 The PcG complex PRC1

The PRC1 complex recognizes loci marked by H3K27me3 and maintains long-term gene repression (Boyer *et al*., 2006; Schwartz and Pirrotta, 2008). RAE28 is a core component of PRC1. In *Rae28*$^{-/-}$ mice outflow tract septation and valve development are impaired (Shirai *et al*., 2002). *Rae28* is required for maintaining cardiomyocyte expression of NKX2.5, suggesting that RAE28 may act on *Nkx2.5* indirectly, perhaps by repressing the expression of an *Nkx2.5* repressor (Koga *et al*., 2002; Shirai *et al*., 2002). The effect of RAE28 on cardiomyocytes is not the cause of the outflow tract defects. Given that *Rae28*$^{-/-}$ animals also exhibit defects in cranial neural crest derived tissues, the outflow septation defects are likely due to a requirement for PRC1 in the neural crest (Shirai *et al*., 2002; Takihara *et al*., 1997).

1.4.3.2 The TrxG protein BRG1

TrxG proteins have several known roles in heart development. The TrxG chromatin remodeling complex member BRG1 is essential for trabeculation. BRG1 is required in the endocardium to repress expression of the metalloproteinase ADAMTS1, which would otherwise cause premature cessation of trabeculation (Stankunas *et al*., 2007). In cardiomyocytes, BRG1 interacts with HDAC partners to repress adult α-myosin heavy chain (*α-MHC*) in fetal hearts and activates the fetal *β-MHC* during differentiation (Hang *et al*., 2010). During pathological hypertrophy, BRG1 mediates the switch back to the fetal *β-MHC* isoform (Hang *et al*., 2010).

1.5 Purpose of this study

PcG and TrxG proteins have multiple roles in embryonic development. A handful of studies have explored the function of proteins of these complexes in the heart, reviewed above. However, we lack an integrated vision of how the morphological changes during heart development are influenced by PcG and TrxG proteins. Further, how are the PcG/TrxG proteins

themselves regulated? ETP proteins are known to regulate the activities of PcG and TrxG members, but whether and how ETP proteins function in heart development was unknown prior to this study. ASXL2 and ASXL1 are ETP proteins that regulate the activity of two PcG complexes, PRC2 and PR-DUB. Here I investigate the role of ASXL2 and ASXL1 in cardiovascular development. We find that ASXL2 and ASXL1 have divergent roles in heart development. We also report roles for ASXL2 in the regulation of epicardial and melanocyte development, and for ASXL1 in the development of the lungs, eyes and palate.

II. MATERIALS AND METHODS

2.1 Animal breeding

All animal studies were performed in accordance with University of Illinois at Chicago ACC and IACUC policies. The *Asxl2*$^{-}$ allele has been backcrossed for more than 10 generations into the C57BL/6J genetic background and maintained as *Asxl2*$^{+/-}$ colonies. *Asxl1*^{tm1a} animals were generated by the European Conditional Mouse Mutagenesis Program and obtained from the European Mutant Mouse Archive (Strain EM:03996) and maintained in a C57BL/6NTac genetic background. For timed matings, noon on the date of vaginal plug was considered E0.5.

2.2 Quantitative real-time PCR

Total RNA was extracted from whole E18.5 or E17 hearts using TRIzol reagent (Invitrogen) and treated with DNase I (Fermentas) to ensure removal of genomic DNA. Quantitative real-time RT-PCR (qRT-PCR) was performed on an ABI Prism 7900HT sequence detection system (Applied Biosystems) using the *Power* SYBR Green RNA-to-C_T One-Step kit (Invitrogen). 100 ng total RNA was used as template in each reaction. Relative expression level of each gene was normalized against *β-actin* in the same sample and calculated using the ΔΔCt method.

2.3 Histology and immunostaining

Tissues for histology and immunostaining analysis of BrdU, EdU, and Nkx2.5 were fixed in 4% paraformaldehyde (PFA) overnight, dehydrated, and paraffin embedded using standard protocols. For EdU detection, a Click-iT EdU Alexa 488 kit (Invitrogen) was used prior to antibody staining. Tissues for immunostaining of cTnT and vimentin were fixed in 4% PFA overnight, cryoprotected in 30% sucrose and cryosectioned. Sections were air dried 10 min and permeabilized 5 min with 0.2% Triton X-100 before immunostaining. Tissues for analysis of

nuclear density were snap-frozen in OCT in a dry ice-hexane bath immediately after collection and sections were post-fixed for 10 minutes in 4% PFA before DAPI staining. All tissues for immunofluorescence were mounted using Vectashield mounting media with DAPI (Vector Labs, H-1200) and imaged on a Zeiss Axiovert 200 M microscope.

2.4 *In situ* hybridization

Whole-mount *in situ* hybridization was performed on E9.5 and E10.5 wildtype embryos as described previously (Piette *et al.,* 2008).

2.5 Morphometric analysis

Analysis of compact layer and trabeculated layer thickness was performed on H&E stained sections on E18.5 hearts. Individual hearts were isolated and embedded carefully to avoid differences in orientation within the trunk. Measurements were collected from 3 sections equidistant from the midpoint of the atrioventricular valves for each heart. The compact layer was defined as the region of the heart between the epicardium and the deepest invagination of the trabecular layer, marked by endothelial cell coverage of the trabeculae. The trabecular layer was measured from this point to the furthest extension of the trabeculae into the ventricular lumen. Width of the interventricular septum was measured across the thickest part of the muscular septum, excluding the papillary muscle. For each parameter, width was averaged from measurements at two randomly selected locations per section.

2.6 Proliferation analysis

For analysis of proliferation rate at E13.5, E15.5, and E17.5, timed pregnant females were administered a single dose of BrdU (100 µg/g body weight) by intraperitoneal injection. Females were sacrificed after two hours and samples were processed for paraffin embedding. Three to five matched sections through the midpoint of each heart were chosen for

immunostaining with anti-BrdU antibody and DAPI. Proliferation indices were calculated within the compact layer of the left and right ventricles or muscular interventricular septum by manually scoring the number of $BrdU^+$ and $BrdU^-$ nuclei. For tracing proliferation from E15.5 to E18.5, timed pregnant females were administered a single dose of EdU (50 μg/g body weight) intraperitoneally at E15.5. Females were sacrificed on E18.5 and samples were processed for paraffin embedding. For analysis of proliferation rate in the lung, anti-phosphorylated-serine 10-histone H3 (pH3) antibody was used to label mitotic nuclei. $pH3^+$ and $pH3^-$ nuclei from the distal portion of the lung lobes were manually scored for three sections per sample.

2.7 Measurement of cell density

DAPI staining was performed on 8 μm cryosections of fresh frozen E18.5 hearts. The number of nuclei within a 100 x 100 μm region of the LV compact layer or 200 x 200 μm region of the IVS was quantified. For the LV, 15-18 regions were analyzed per heart. For the IVS, 5-6 regions were analyzed per heart. Measurements were averaged from 5 samples per genotype.

2.8 Cesarean section recovery

Timed pregnant females were sacrificed by cervical dislocation on E19 under a warming lamp. The uterine wall was dissected open to expose each pup. Umbilical vessels were clamped and severed for each pup individually. Cotton swabs and warm saline were used to clean mucus from the mouth and nose, and pups were rubbed gently on the chest and back until regular breathing was established. Breathing activity and behavior were monitored for two hours, then pups were sacrificed by decapitation, fixed, and paraffin-embedded using standard protocols. Serial sections through the lung and heart regions were H&E stained and analyzed.

2.9 Vital dye-labeling of the epicardium *ex vivo*

Embryos were dissected from timed pregnant *Asxl2*$^{+/-}$ females on E12.5 into cold sterile Hank's Balanced Salt Solution (HBSS). Individual embryos were dissected to isolate the heart into clean HBSS. Hearts were transferred individually to the wells of a 48-well cell culture plate. Hearts were incubated in 1 ml of labeling solution (5 µg/ml CMFDA, Invitrogen C7025 in DMEM) 30 minutes at 37°C, rinsed in DMEM, and then cultured in DMEM with 10% FBS for 24 hours at 37°C to allow EMT to occur. After culturing, hearts were rinsed 3x in PBS, fixed 15 minutes in 4% PFA, rinsed in PBS and incubated in 30% sucrose 2 hours at 4°C. Hearts were then embedded in Neg-50 OCT, frozen, and stored at -20°C. Serial cryosections were prepared at 10 µm and collected on charged slides. Sections were post-fixed in 4% PFA 15 minutes and counterstained with DAPI before imaging.

2.11 Whole-mount PECAM-1 immunostaining of heart

Hearts were dissected from embryos, rinsed in PBS, and fixed in 4% PFA 4 hours at 4°C. Hearts were then rinsed 3x in PBS, and dehydrated in a series of MeOH washes: 15% for 24 hours; 30% for 24 hours; 50%, 70%, 95%, and 100% for 30 minutes each. Hearts were blocked in 5% H_2O_2 in MeOH 4 hours, rinsed in 100% MeOH, and rehydrated through a series of MeOH washes to PBS. Blocking in 5% normal goat serum and 0.1% Triton X-100 was performed, followed by incubation in primary antibody (1:200 rat-anti-PECAM-1) overnight. Hearts were washed in PBST 15 minutes 4x and incubated in secondary antibody (1:200 biotinylated goat-anti-rat) overnight, then washed in PBST 15 minutes 4x, and incubated in ABC reagent (Vector Labs) overnight. Hearts were washed as before and incubated in DAB reagent (Vector Labs) 6 minutes at room temperature until signal developed, then washed and stored in PBS for imaging.

III. ADDITIONAL SEX COMBS-LIKE 1 AND 2 REGULATE CARDIOVASCULAR DEVELOPMENT

3.1 Abstract

Congenital heart disease (CHD) is the most common birth defect. However, the majority of CHD cases have unknown etiology. Here we report the identification of ASXL2 and ASXL1, two homologous chromatin factors, as novel regulators of heart development. *Asxl2*$^{-/-}$ fetuses have reduced body weight and display congenital heart malformations including thickened compact myocardium in the left ventricle, membranous ventricular septal defect and atrioventricular valval stenosis. Although most *Asxl2*$^{-/-}$ animals survive to term, the neonates have patent ductus arteriosus and consequent lung hemorrhage and die soon after birth. *Asxl1*$^{-/-}$ fetuses have reduced body weight and display cleft palate, anophthalmia as well as ventricular septal defects and a failure in lung maturation. From these results, we conclude that normal heart development requires both ASXL proteins. In particular, ASXL2 plays an important role in heart morphogenesis and the transition from fetal to postnatal circulation.

3.2 Introduction

Congenital heart disease (CHD) is the leading cause of prenatal and birth defect-related death in the United States (Mitchell *et al.,* 2007; Baker *et al.,* 2012). The incidence of CHD is 1% of all live births, although this is likely an underestimate as many anomalies do not require clinical intervention and remain undiagnosed (Mitchell *et al.,* 2007; van der Bom *et al.,* 2012). In addition to the estimated 40,000 new cases of CHD diagnosed in U.S. infants each year, it is estimated that at least another 40,000 individuals are born with undiagnosed heart defects that

can contribute to disease later in their lives (Shieh and Srivastava, 2009; Lau *et al.,* 2011). For example, undiagnosed abnormalities of atrioventricular valve development often result in valve deterioration and replacement surgeries in young adults (Nemer *et al.,* 2008; Warnes *et al.,* 2008).

Only a fraction of CHD cases have been attributed to known genetic causes or *in utero* exposure to teratogens (Richards and Garg, 2010). Accordingly, in most cases a genetic cause of disease is not known and etiology is likely multifactorial in nature (Granados-Riveron *et al*, 2012; Gill *et al.,* 2003; Burn *et al.* 1998). A large inheritance study of CHD in Denmark over a 28-year period found strong familial clustering, even for sporadic cases of CHD with no known genetic cause (Oyen *et al.,* 2009). Similarly, an echocardiographic screen of immediate relatives of congenital bicuspid aortic valve (BAV) patients revealed a high rate of familial occurrence of undiagnosed BAV (Huntington *et al.*, 1997). These observations suggest that unidentified genetic components are at play among cases of CHD with unknown etiology.

A number of transcription factor pathways are known to play important roles in normal heart development, and not surprisingly, mutations in transcription factors have been implicated in multiple forms of CHD (Hatcher *et al.*, 2003; McCulley and Black, 2012). The action of transcription factors is often regulated by epigenetic factors, yet the epigenetic mechanisms governing cardiac development and disease are not well understood. Epigenetics describes the inheritance of gene expression pattern independently of DNA sequence (van Speybroeck *et al.,* 2002). The key mechanisms of epigenetic inheritance are histone modification, chromatin remodeling, DNA methylation and microRNA (Goldberg *et al.,* 2007). The precise and coordinated control of gene expression by epigenetic factors is critical for the regulation of many developing organs, including the heart (reviewed in van Weerd *et al.,* 2011; Zhou *et al.,* 2011;

Chang and Bruneau, 2012; Vallaster *et al.,* 2012; Wang, 2012). Epigenetic causes of CHD are promising candidates for intervention due to their ability to direct and maintain long-term changes to transcription (Matarazzo *et al.,* 2007; Ordovas and Smith, 2010; Kelly *et al.,* 2010; Nebbioso *et al.,* 2012). Therefore, identifying novel epigenetic causes of congenital heart disease will improve our ability to predict and manage CHD.

Here we report two novel causes of CHD in mice: mutation to the chromatin factors ASXL1 and ASXL2. The Additional Sex Combs-Like (ASXL) protein family is comprised of three homologs in mammals: ASXL1, 2 and 3 (Fisher *et al.,* 2003; Katoh and Katoh, 2003; Katoh and Katoh, 2004). The ASXL family proteins have been implicated in a variety of diseases. Germline and hematopoietic-specific deletions of *Asxl1* cause myelodysplastic syndrome-like disease in mice (Abdel-Wahab *et al.,* 2013; Wang *et al.,* 2013). Similarly, somatic mutation or deletions of human *ASXL1* are frequently found in patients with cancers of the myeloid lineage (Gelsi-Boyer *et al.,* 2009; Bejar *et al.,* 2011; Jankowska *et al.,* 2011). In addition, mutations in all three *ASXL* genes have been implicated in solid tumors, such as breast cancer and melanoma (reviewed in Katoh 2013). Finally, germline mutations of *Asxl1*, and more recently *Asxl3*, cause Bohring-Opitz syndrome, a developmental disorder involving craniofacial anomalies, intellectual disability and multiple congenital malformations (Hoischen *et al.,* 2011; Bainbridge *et al.,* 2013; Dinwiddie *et al.,* 2013; Iourov *et al.,* 2013; Hastings *et al.,* 2011; Magini *et al.,* 2012). Both ASXL1 and ASXL2 functionally interact with the histone methyltransferase complex PRC2 and facilitate PRC2 localization to target genes (Abdel-Wahab *et al.,* 2012; Lai and Wang, 2013). PRC2 plays critical roles in the developing heart. Depending on the specific lineage in which PRC2 is inactivated, mutant animals either exhibit an array of congenital heart malformations or develop postnatal cardiac hypertrophy and fibrosis (Delgado-Olguin *et al.,*

2012; He *et al.,* 2012). However, the role of ASXL proteins in heart development is not well understood.

We have previously shown that in the C57BL/6J;129Sv F1 genetic background, *Asxl2* is dispensable for heart morphogenesis but is essential for the preservation of cardiac function during adult life (Baskind *et al.,* 2009; Lai *et al.,* 2012; Lai and Wang, 2013). Here we uncover a role for *Asxl2* in heart development in the inbred C57BL/6J background. C57BL/6J *Asxl2*$^{-/-}$ animals die shortly after birth with cardiac malformations, patent ductus arteriosus (PDA) and consequent lung hemorrhage. We also report evidence that *Asxl1* plays regulatory roles in both cardiac morphogenesis and lung development. The cardiac phenotypes in *Asxl2*$^{-/-}$ and *Asxl1*$^{-/-}$ animals are different from that of PRC2-inactivated mice, suggesting that ASXL proteins and PRC2 have distinct functions in the developing heart. Taken together, these results reveal that normal heart development requires both ASXL2 and ASXL1 and implicate *ASXL* mutations as novel causes for CHD.

3.3 Results

3.3.1 Asxl genes are expressed in the heart

Our prior studies demonstrated strong activity of a *lacZ* reporter inserted downstream of the endogenous *Asxl2* promoter in the developing heart (Baskind *et al.,* 2009). To confirm the results of these reporter assays, we examined the distribution of *Asxl2* transcripts in developing embryos by whole-mount *in situ* hybridization. *Asxl2* is highly expressed in the heart and somites at E9.5-10.5 (Fig. 3a, b). At E9.5, *Asxl2* transcript was detected throughout the heart tube, including the outflow tract, ventricles, and sinus venosus/atria (Fig. 3a). At E10.5, expression was detected in both atria and ventricles (Fig. 3b). These results are consistent with the *lacZ* reporter expression pattern.

Among the three *Asxl* genes, *Asxl2* is the most highly expressed in the adult heart, while *Asxl1* and *Asxl3* are expressed at much lower levels (Lai and Wang, 2013). We found a similar trend is true in the E18.5 heart, in which the transcription levels of *Asxl1* and *Asxl3* are ~16% and ~8% of *Asxl2*, respectively (Fig. 3c). In the *Asxl2*$^{-/-}$ heart, *Asxl2* transcript is reduced to ~10% of wildtype levels, and the loss of *Asxl2* is not compensated by up-regulation of either *Asxl1* or *Asxl3* at the transcript level (Fig. 3c).

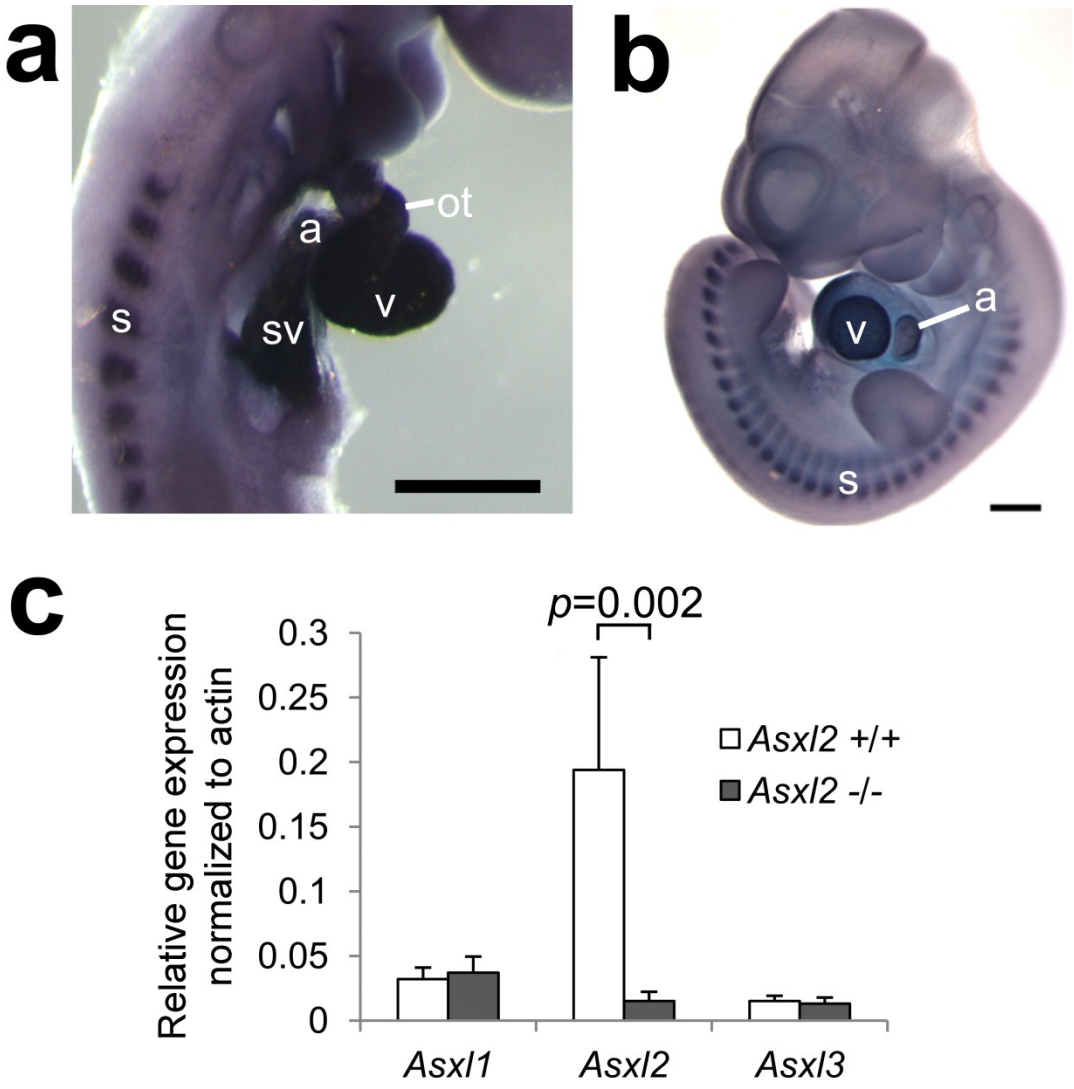

Figure 3: Expression of *Asxl* homologs in the heart.

(a) Whole-mount *in situ* hybridization of *Asxl2* in E9.5 embryo. *Asxl2* transcript is expressed in the outflow tract (ot), ventricles (v), atria (a), and sinus venosus (sv) of the heart, in addition to the somites (s). Scale bar: 250 µm. (b) *In situ* hybridization of *Asxl2* transcript in E10.5 embryo. Scale bar: 500 µm. (c) Quantitative real-time PCR analysis of gene expression levels in E18.5 wildtype and *Asxl2*$^{-/-}$ hearts. *Asxl2* is the most highly expressed *Asxl* homolog in the wildtype heart. In the *Asxl2*$^{-/-}$ heart, *Asxl2* transcript levels are reduced to 10% of wildtype, and neither *Asxl1* nor *Asxl3* are upregulated.

3.3.2 The *Asxl1*^{tm1a} allele causes ablation of *Asxl1* transcript

The expression of *Asxl1* in the fetal heart is evident albeit low, suggesting that *Asxl1* may play a regulatory role in the developing heart, either independent of or in redundancy with *Asxl2*. Additionally, 50% of patients with Bohring-Opitz syndrome, which has been attributed to *de novo ASXL1* mutations, exhibit varied cardiac defects including atrial septal defects, valve abnormalities, and patent ductus arteriosus (Hastings *et al.*, 2011). To explore the potential role for *Asxl1* in the heart we obtained the *Asxl1*^{tm1a} mice (Fig. 4a), generated by the European Conditional Mouse Mutagenesis Program. Transcription across exons 2 and 5 of *Asxl1* was not detected in *Asxl1*$^{tm1a/tm1a}$ hearts by RT-PCR (Fig. 4b). Using the more sensitive quantitative RT-PCR (qRT-PCR) assay, we measured transcript levels across exons 12 and 13. *Asxl1* transcript is reduced to ~2% of wild-type levels in the *Asxl1*$^{tm1a/tm1a}$ heart (Fig. 4c). The loss of *Asxl1* did not induce compensatory up-regulation of *Asxl2* transcription (Fig. 5). Taken together, these results suggest that *Asxl1*^{tm1a} is a strong loss-of-function allele. *Asxl1*^{tm1a} is henceforth referred to as *Asxl1*$^{-/-}$.

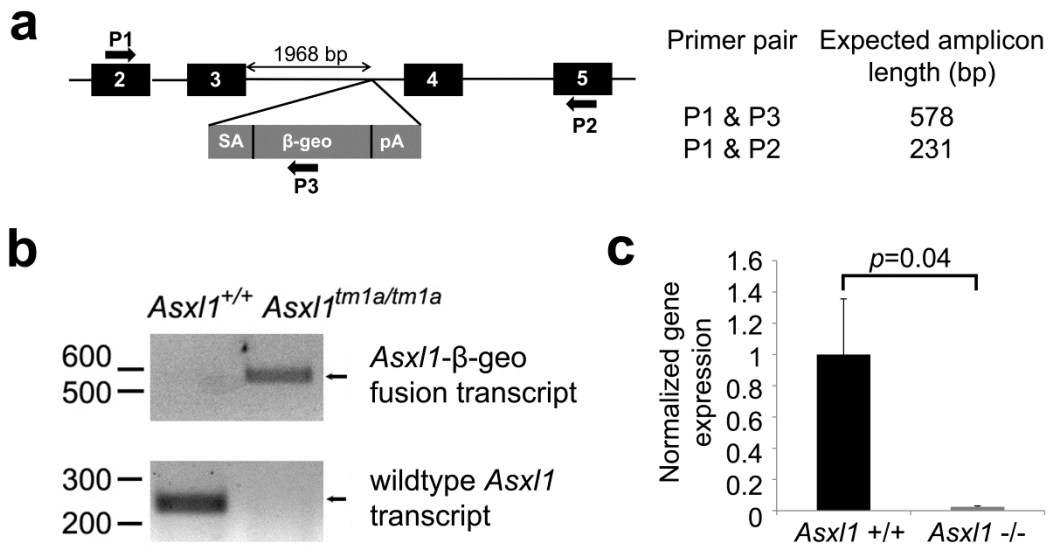

Figure 4: Characterization of the *Asxl1* mutant allele.

(a) Schematic representation of the *Asxl1*^{tm1a} allele (not to scale). The β-geo cassette is inserted 1968 bp downstream of exon 3. P1, P2 and P3: primers used in RT-PCR. SA, splice acceptor site. β-geo, beta-galactosidase/neomycin fusion reporter. pA, poly-adenylation sequence. (b) Gel electrophoresis of RT-PCR product amplified from heart RNA using primers P1 and P3 (upper gel) or P1 and P2 (lower gel). A 578-bp product from the *Asxl1-β-geo* fusion transcript was identified in *Asxl1*$^{tm1a/tm1a}$ samples. The 231-bp product from the wildtype *Asxl1* transcript was absent in *Asxl1*$^{tm1a/tm1a}$ samples. (c) Quantitative real-time PCR analysis of *Asxl1* transcript levels in E17 wildtype and *Asxl1*$^{tm1a/tm1a}$ hearts. *Asxl1* transcript is reduced to 2% of wildtype levels in *Asxl1*$^{tm1a/tm1a}$ hearts. Error bars represent the means ± standard deviations from 3 samples per genotype.

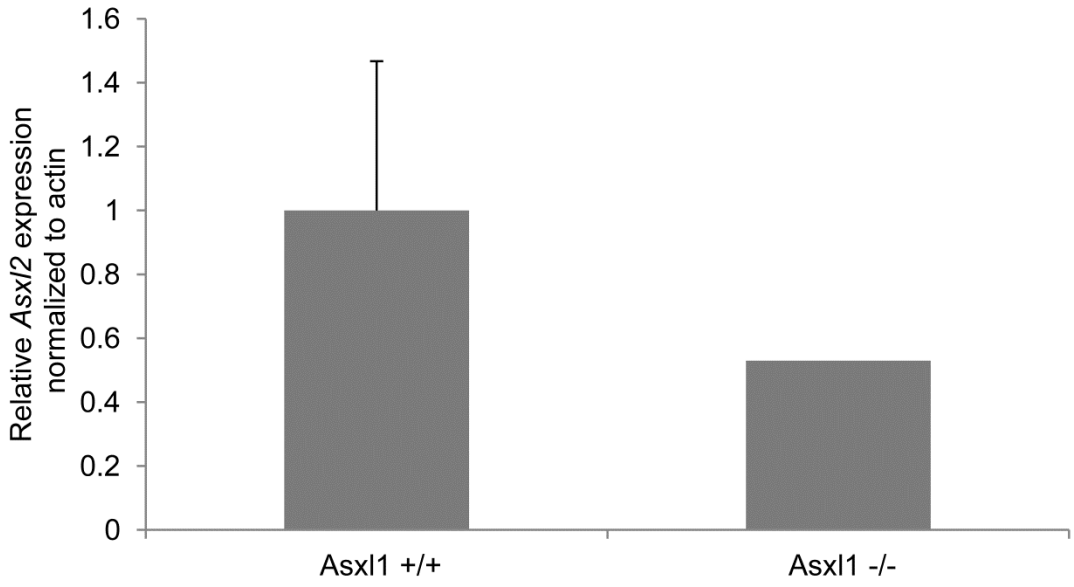

Figure 5: *Asxl2* is not upregulated in the *Asxl1*$^{-/-}$ heart.

Quantitative real-time PCR analysis of *Asxl2* transcript levels in E17 wildtype and *Asxl1*$^{-/-}$ hearts. *Asxl2* is not upregulated in the fetal heart upon loss of *Asxl1*. Insufficient sample size precludes determination of whether *Asxl2* is expressed at lower levels in the *Asxl1*$^{-/-}$ heart; the apparent difference shown is not statistically significant by Student's T-test. N = 2 hearts per genotype. Error bars represent means ± standard deviation.

3.3.3 *Asxl2* and *Asxl1* are required for embryonic development and postnatal survival

We next investigated whether *Asxl2* is required for embryonic development in the C57BL/6J inbred background. Progenies from mating between $Asxl2^{+/-}$ mice were recovered and genotyped at various stages of embryonic and postnatal development. $Asxl2^{-/-}$ embryos were present at Mendelian ratio at E12.5 and close to Mendelian ratio at E18.5 (Table I). In contrast, at postnatal day 1 (P1), only 2 pups out of a total of 44 were $Asxl2^{-/-}$ (Table I). At the time of weaning, P21, only 5 animals out of a total of 271 were $Asxl2^{-/-}$ (Table I). E18.5 $Asxl2^{-/-}$ embryos weighed ~11% less than wildtype littermates (Fig. 6) but exhibited normal gross morphology. The few $Asxl2^{-/-}$ animals that survived to P21 were runts and presented with gray/black fur and smaller eyes (Fig. 25).

While *Asxl2* appears to be dispensable for overall embryonic development, the loss of *Asxl1* has a more severe effect. $Asxl1^{-/-}$ embryos were recovered at less than Mendelian ratio from as early as E12.5, and by E18.5 they represent only 11.1% of all embryos recovered (Table II). Numerous resorping necrosed embryos were observed in the uterine tract during dissection at E18.5. Those $Asxl1^{-/-}$ embryos that survive to E18.5 exhibited ~22% reduction in body weight, cleft lip and palate of varying severity and absent eyes (Fig. 7a, b). The reduced weight and cleft palate of $Asxl1^{-/-}$ embryos are consistent with phenotypes reported in an independently generated *Asxl1* mutant strain (Abdel-Wahab *et al.,* 2013) as well as with symptoms of the human Bohring-Opitz syndrome (Hoischen *et al.,* 2011).

TABLE I: RECOVERED PROGENY OF *ASXL2*$^{+/-}$ TIMED MATINGS AND INTERCROSSES

Stage	N	+/+ (%)	+/- (%)	-/- (%)
E12.5	175	43 (24.6)	88 (50.3)	44 (25.1)
E15.5	117	27 (23.1)	62 (53.0)	28 (23.9)
E18.5	208	55 (26.4)	106 (51.0)	47 (22.6)
P1	44	9 (20.5)	30 (68.2)	2[a] (4.5)
P21	271	88 (32.5)	178 (65.7)	5 (1.8)

[a] Three additional animals were found deceased at this time point.

TABLE II: RECOVERED PROGENY OF *ASXL1*$^{+/-}$ TIMED MATINGS AND INTERCROSSES

Stage	N	+/+ (%)	+/- (%)	-/- (%)
E12.5	14	4 (28.6)	7 (50.0)	3 (21.4)
E18.5	36	10 (27.7)	22 (61.0)	4 (11.1)
P21	98	35 (35.7)	63 (64.3)	0 (0)

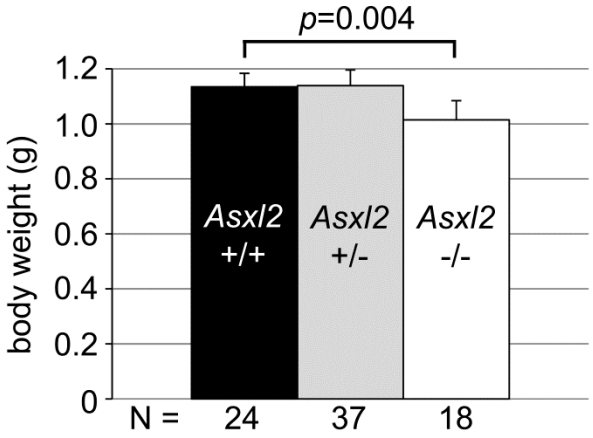

Figure 6: *Asxl2*$^{-/-}$ animals are smaller than wildtype.

The average body weight of E18.5 *Asxl2*$^{-/-}$ embryos is 11% less than that of wildtype littermates. Error bars represent means ± standard deviations.

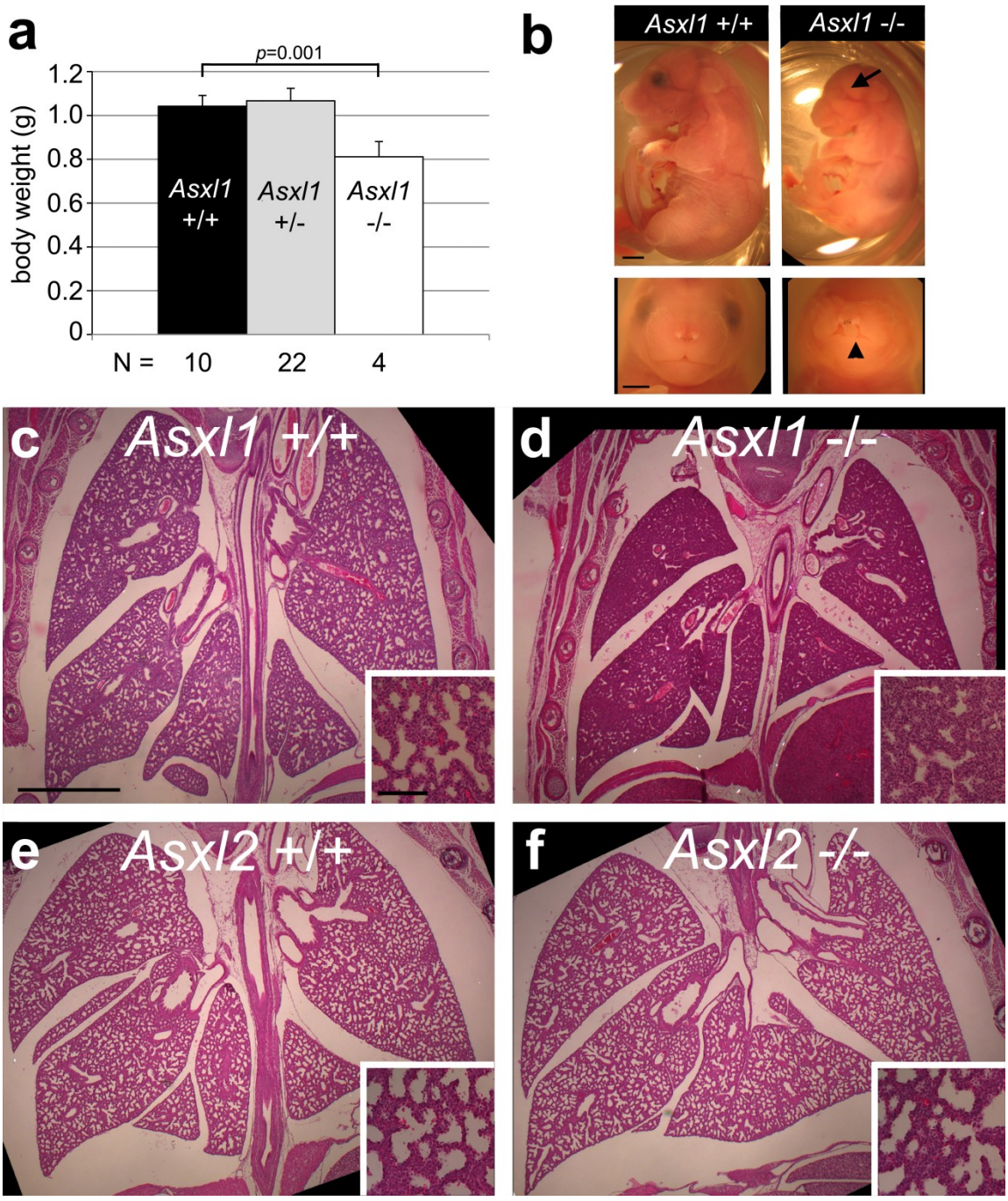

Figure 7: *Asxl1*$^{-/-}$ animals exhibit developmental immaturity at E18.5.

(a) *Asxl1*$^{-/-}$ animals have a 22% reduction in body weight compared to wildtype at E18.5. Error bars represent means ± standard deviations. (b) All *Asxl1*$^{-/-}$ exhibited degenerated eyes (arrow) and some exhibit cleft lip (arrowhead). Scale bar: 1mm (upper), 200µm (lower). (c, d) H&E staining of lung sections in E18.5 wildtype and *Asxl1*$^{-/-}$ embryos. *Asxl1*$^{-/-}$ lungs (d) are immature

with fewer, smaller saccular air spaces and thickened mesenchyme compared to wildtype. (e, f) H&E staining of lung sections in E18.5 wildtype and *Asxl2*$^{-/-}$ embryos. *Asxl2*$^{-/-}$ lungs are comparable to wildtype in both saccular air spaces and mesenchyme thickness. (c-f) Scale bar: 1mm. For each panel, the inset is a higher magnification image of the same lung, showing morphology of the mesenchyme. Inset scale bar: 100 μm.

3.3.4 *Asxl1* is required for fetal lung maturation

Histological examination revealed that E18.5 *Asxl1*$^{-/-}$ embryos displayed a significant defect in lung development. During lung development epithelial-lined airways branch within the lung mesenchyme to generate the respiratory air spaces (Turgeon *et al.*, 2009). Epithelial cells lining the air spaces differentiate into type I pneumocytes, which function in gas exchange, and type II pneumocytes, which produce surfactant (Warburton *et al.*, 2000). The respiratory saccules failed to mature in E18.5 *Asxl1*$^{-/-}$ lungs, which displayed thickened mesenchyme and fewer air spaces (Fig. 7c, d). In contrast, E18.5 *Asxl2*$^{-/-}$ embryos exhibited normal lung morphology (Fig. 7e, f). Consistent with the lung development defect, no *Asxl1*$^{-/-}$ animals were recovered postnatally (Table II).

We investigated the developmental defect in the E18.5 *Asxl1*$^{-/-}$ lung by immunostaining for Clara cell-specific protein (CCSP), a marker of proximal epithelial cell differentiation, as well as T1α and surfactant protein-C (SP-C), markers of distal epithelium type I and type II pneumocytes, respectively (Zhou *et al.*, 1996; Ramirez *et al.*, 2003; Xu *et al.*, 2010; Hsu *et al.*, 2011). CCSP was expressed normally in the bronchioles of *Asxl1*$^{-/-}$ lungs, indicating normal proximal differentiation (Fig. 8a, b). Both T1α and SP-C were found in the *Asxl1*$^{-/-}$ lungs, however fewer air spaces expressing the markers were present (Fig. 8c-f). Proliferation indices normally decline between E15 and E18 in the mouse lung as differentiation advances (Kauffman, 1975). Analysis of phosphorylated-serine 10-histone H3 (pH3) immunostaining at E18.5 revealed the *Asxl1*$^{-/-}$ lung had a significantly higher mitotic index than wildtype lung (Fig. 8g). These results suggest a maturation defect in which the *Asxl1*$^{-/-}$ lung continues to proliferate and delays differentiation. Taken together, these results suggest that *Asxl1* plays essential roles during fetal lung development.

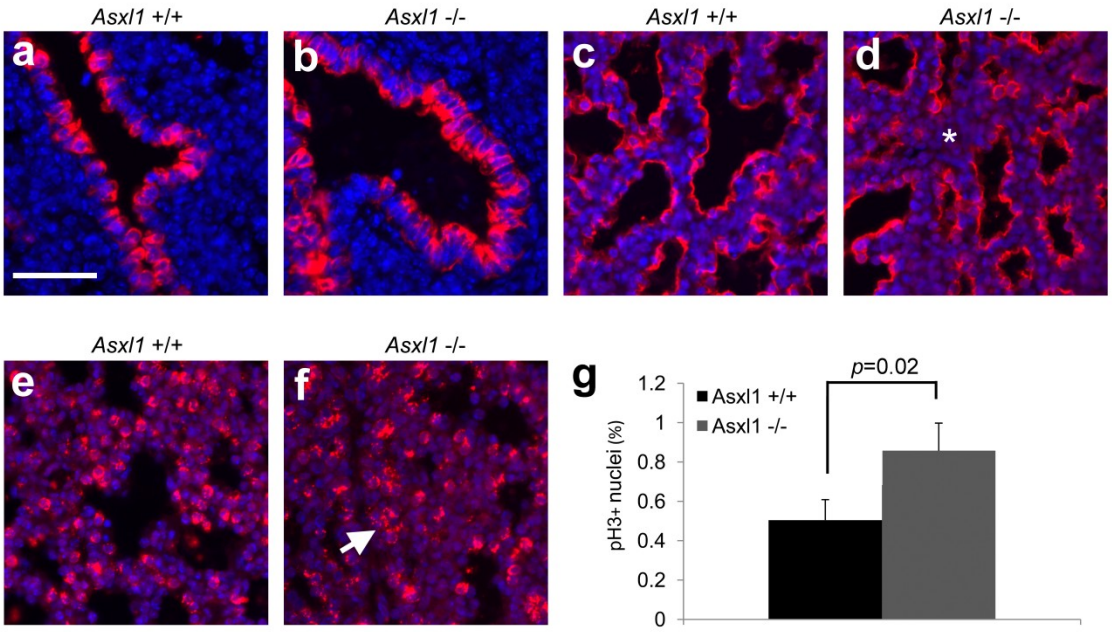

Figure 8: Differentiation and proliferation are abnormal in *Asxl1*$^{-/-}$ lungs at E18.5.

(a, b) Clara cell-specific protein is expressed in the bronchioles of (a) *Asxl1*$^{+/+}$ and (b) *Asxl1*$^{-/-}$ lungs. (c, d) T1α is expressed in the epithelium lining distal airspaces in both genotypes. (d) *Asxl1*$^{-/-}$ lungs displayed fewer T1α^{+} airspaces and thicker mesenchyme (*). (e, f) SP-C is expressed in both (e) *Asxl1*$^{+/+}$ and (f) *Asxl1*$^{-/-}$ lungs. (f) *Asxl1*$^{-/-}$ lungs displayed frequent clustering of SP-C^{+} cells in the mesenchyme (arrow). For (a-f), marker staining is represented in red and DAPI staining in blue. Scale bar: 50 μm. (g) The mitotic index in the distal lung lobes was ~70% higher in *Asxl1*$^{-/-}$ animals compared to wildtype. Error bars represent means ± standard deviations from 3 samples per genotype.

3.3.4 *Asxl2*$^{-/-}$ and *Asxl1*$^{-/-}$ exhibit congenital heart defects

Given the expression of both *Asxl2* and *Asxl1* in the heart and neonatal death observed in both mutant lines, we examined heart morphology at the latest viable time point, E18.5. Serial sections of hearts were examined for proper development of the ventricles, atria, epicardium, atrial and ventricular septa, outflow tract, as well as atrioventricular, aortic, and pulmonary valves. Both *Asxl2*$^{-/-}$ and *Asxl1*$^{-/-}$ animals exhibited various cardiac defects with 78% penetrance (Table III). *Asxl2*$^{-/-}$ exhibited ventricular septal defects (VSD) at low penetrance (22%) that were restricted to the membranous portion of the interventricular septum (IVS), the thinner fibrous region that sits atop the muscular IVS (Table III, Fig. 9a). *Asxl2*$^{-/-}$ animals also displayed thickening of one or both atrioventricular valves resulting in apparent valval stenosis with incomplete penetrance (Table III, Fig. 9b).

In contrast to the minor membranous VSDs observed in the *Asxl2*$^{-/-}$ heart, *Asxl1*$^{-/-}$ animals displayed more severe septal defects. VSDs in the inlet septum, located inferioposterior to the membranous septum, beneath the tricuspid valve, were identified in 44% of *Asxl1*$^{-/-}$ hearts (Table III, Fig. 9b). Inlet VSDs are related to atrioventricular (AV) canal defects in which the entire AV septum is disturbed (Minette and Sahn, 2006). AV canal defects were observed with 33% penetrance in *Asxl1*$^{-/-}$ hearts (Table III, Fig. 9d). Affected hearts displayed a common AV junction and leaflets overriding the muscular septum (Fig. 9d). Additionally, one *Asxl1*$^{-/-}$ animal with an inlet VSD also displayed a large opening in the muscular portion of the IVS and disorganized myocyte arrangement (Fig. 9d).

TABLE III: INCIDENCE OF CARDIAC DEFECTS IN *ASXL2*$^{-/-}$ AND *ASXL1*$^{-/-}$ MICE AT E18.5

	Asxl2$^{+/+}$	*Asxl2*$^{-/-}$	*Asxl1*$^{+/+}$	*Asxl1*$^{-/-}$
Membranous ventricular septal defect[a]	0/5 (0)	2/9 (22)	0/5 (0)	0/9 (0)
Atrioventricular canal type VSD	0/5 (0)	0/9 (0)	0/5 (0)	3/9 (33)
Inlet VSD	0/5 (0)	0/9 (0)	0/5 (0)	4/9 (44)
Muscular ventricular septal defect	0/5 (0)	0/9 (0)	0/5 (0)	1/9 (11)
Thickened septum	0/5 (0)	7/9 (78)	0/5 (0)	0/5 (0)
Thickened left ventricle wall	0/5 (0)	5/9 (56)	0/5 (0)	0/5 (0)
Thickened atrioventricular valve	1/5 (20)	5/9 (56)	0/5 (0)	0/5 (0)
Total with cardiac defects	1/5 (20)	7/9 (78)	0/5 (0)	7/9 (78)

[a] Percentages shown in parentheses.

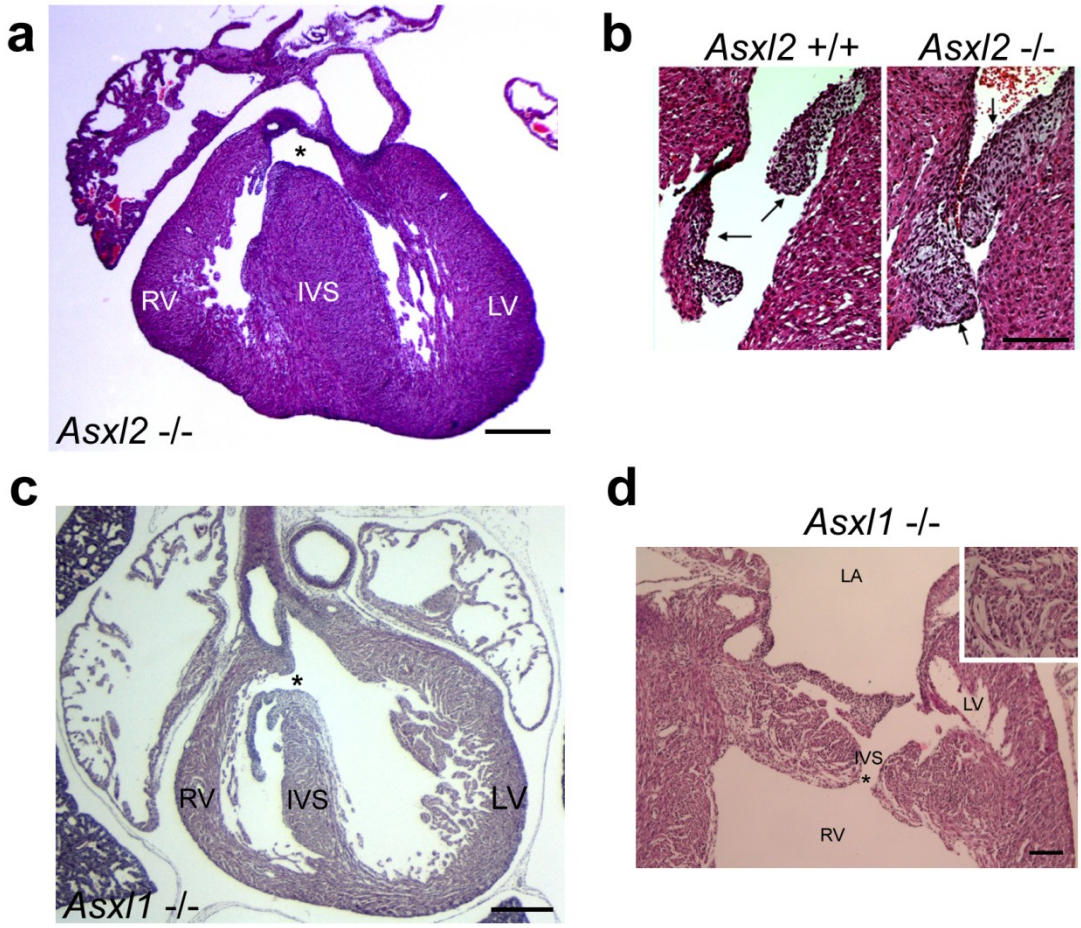

Figure 9: Cardiac defects in *Asxl2*$^{-/-}$ and *Asxl1*$^{-/-}$ at E18.5.

(a) Two of nine *Asxl2*$^{-/-}$ hearts exhibited membranous septal defects (*). Scale bar: 500 µm. (b) Four of nine *Asxl2*$^{-/-}$ hearts exhibited atrioventricular stenosis with thickened valves. Arrows: mitral valve leaflets. Scale bar: 100 µm. (c) Four of nine *Asxl1*$^{-/-}$ hearts exhibited inlet ventricular septal defects (*). Scale bar: 500 µm. (d) One *Asxl1*$^{-/-}$ heart displayed a muscular septal defect (*) with disorganized myocytes (inset at higher magnification). Scale bar: 100 µm.

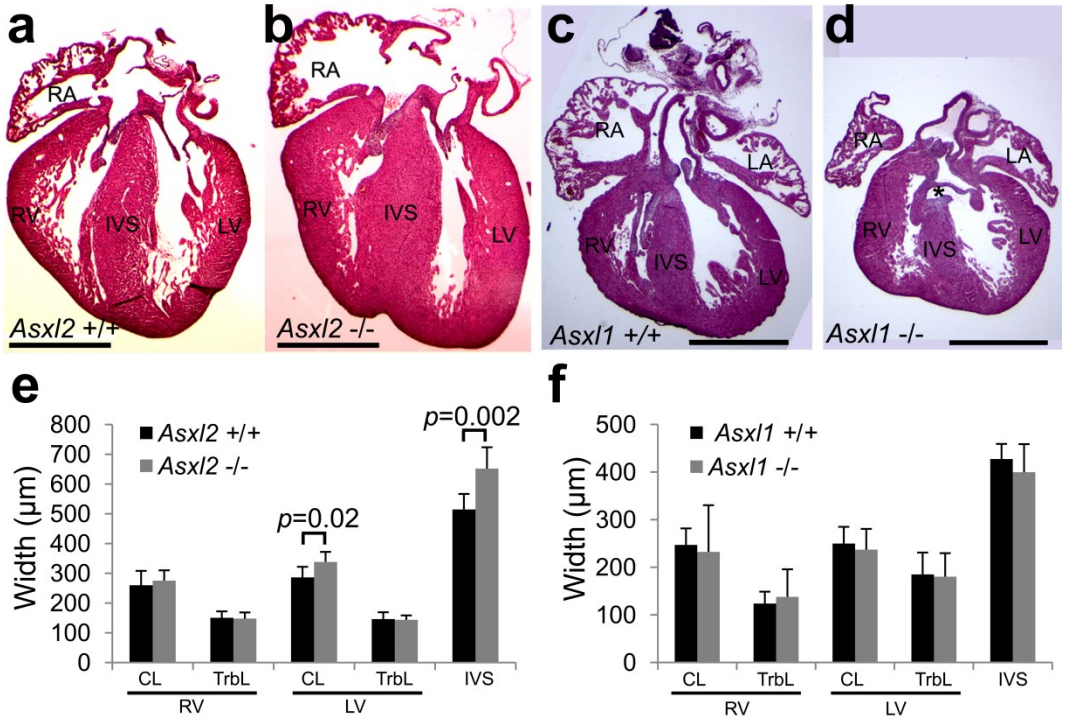

Figure 10: *Asxl2*$^{-/-}$ hearts display thickened LV free wall and thickened IVS.

(a, b) H&E staining of frontal sections of E18.5 wildtype and *Asxl2*$^{-/-}$ hearts. Most *Asxl2*$^{-/-}$ hearts display thickening of the LV free wall and the IVS. RA: right atrium. RV: right ventricle. (c, d) H&E staining of frontal sections of E18.5 wildtype and *Asxl1*$^{-/-}$ hearts. *Asxl1*$^{-/-}$ hearts have normal myocardial wall and valval thickness. Asterisk marks an atrioventricular canal defect with common overriding valve. Scale bar: 1 mm. (e) Quantitative comparison of myocardial thickness in E18.5 *Asxl2*$^{-/-}$ embryos (N = 9) and wildtype embryos (N = 5). CL: compact layer. TrbL: trabeculated layer. (f) Quantitative comparison of myocardial thickness in E18.5 *Asxl1*$^{-/-}$ embryos (N = 4) and wildtype embryos (N = 3).

3.3.5 *Asxl2*$^{-/-}$ hearts have thickened compact myocardium in the left ventricle

In addition to displaying VSD and valval stenosis, *Asxl2*$^{-/-}$, but not *Asxl1*$^{-/-}$, embryos often display thickening in the LV free wall and the muscular IVS at E18.5 (Fig. 10a-d). This phenotype is not observed at E12.5 or E13.5, indicating that it manifests during the fetal maturation of the heart. The overall size of the *Asxl2*$^{-/-}$ heart was not appreciably larger, and the thickening appears to result in smaller LV chamber size, which may limit the blood volume that can be ejected with each pump. As this phenotype is possibly functionally important, we quantified the wall thickness in *Asxl2*$^{-/-}$, *Asxl1*$^{-/-}$ and control hearts by morphometric analyses (Fig. 10e, f). Thickening of the LV free wall and the IVS in *Asxl2*$^{-/-}$ embryos is statistically significant, although the degree of thickening varied between individuals. Thickening of the LV free wall was restricted to the compact layer, with apparent normal development of the trabecular layer.

3.3.7 Fetal Asxl2-/- hearts have normal proliferation rates

Overgrowth of the fetal heart usually occurs by over-proliferation of cardiomyocytes. The fetal ventricles grow by proliferation of cells in the myocardium (Ieda *et al.,* 2009). In the LV free wall, proliferation is much higher within the compact layer myocardium compared to the trabecular myocardium, and the proliferation rate peaks between E11.5-E12.5 before declining gradually during fetal growth of the heart (Ieda *et al.,* 2009; Toyoda *et al.,* 2003). No studies of proliferation rates within the IVS are known to date.

To determine whether thickening of the compact layer of *Asxl2*$^{-/-}$ LV free wall and IVS is due to over-proliferation, we compared the proliferation rates in wildtype and mutant hearts by BrdU labeling at various time points prior to E18.5, when the phenotype manifests. Consistent with previous reports, the BrdU labeling index within the wildtype LV free wall compact layer was highest at E13.5 (~30%), and declined between E15.5 (~20%) and E17.5 (~16%) (Fig. 11a). A similar pattern was observed within the wildtype IVS, with the highest proliferation rates at E13.5 (27%), followed by E15.5 (24%) and E17.5 (15%) (Fig. 11b). However, no significant differences in BrdU labeling indices were observed between *Asxl2*$^{-/-}$ and wildtype samples at any time point examined.

Next we asked whether there is an accumulated increase in proliferation during fetal stages, even though the increase may be too subtle for detection at individual time points. We administered a single pulse of EdU to pregnant females at E15.5 and assayed the accumulative proliferation rate at E18.5. In comparison to BrdU, EdU is detected with higher sensitivity and therefore facilitates the detection of diluted signal after multiple cell divisions during chase experiments (Salic and Mitchison, 2008). Double-labeling of EdU and NKX2.5 allowed us to assay EdU-incorporation rates within the cardiomyocyte lineage (NKX2.5^{+}) versus the non-

cardiomyocyte lineage (NKX2.5^{-}). We observed a higher proliferation rate within NKX2.5^{+} cardiomyocytes compared to NKX2.5^{-} non-cardiomyocytes both in the LV free wall and the IVS (Fig. 11c, d). However, no significant difference in EdU incorporation indices was observed between *Asxl2*$^{-/-}$ and wildtype hearts in either cell population or combined.

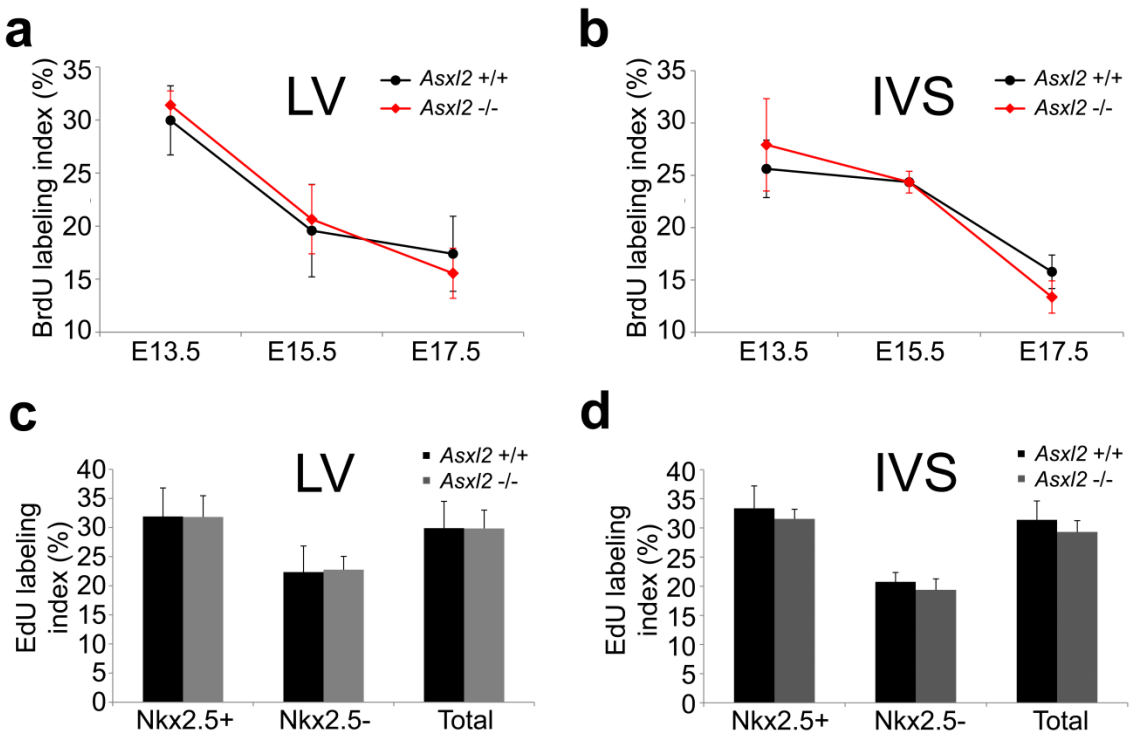

Figure 11: Thickening of the LV free wall and IVS in *Asxl2*$^{-/-}$ embryos is not due to overproliferation of fetal cardiomyocytes.

(a, b) BrdU labeling indices in LV compact layer (a) and IVS (b) at E13.5, E15.5, and E17.5. BrdU incorporation rate in *Asxl2*$^{-/-}$ hearts is not significantly different from wildtype. (c, d) Accumulative EdU labeling indices in LV (c) and IVS (d) at E18.5, following a single pulse of EdU administered at E15.5 and a three-day chase. EdU labeling indices are shown for the NKX2.5^{+} population, the NKX2.5^{-} population, and all cells (total). Error bars represent means ± standard deviations from 3 animals per genotype in (a, b) and 4 animals per genotype in (c, d).

3.3.8 *Asxl2*$^{-/-}$ cardiomyocytes are not hypertrophic

Hypertrophic growth of cardiomyocytes is another mechanism that could result in thicker myocardium, especially in the adult heart (MacLellen and Schneider, 2000; Frey and Olson, 2003). Although this mechanism is not typically utilized in the fetal heart, it has been documented in a mutant model in which PRC2 was inactivated in the second heart field (Delgado-Olguin *et al.,* 2012). To determine whether the *Asxl2*$^{-/-}$ heart is comprised of larger cardiomyocytes, we performed wheat germ agglutinin (WGA) staining of the LV free wall and the IVS at E18.5 (Fig. 12a). WGA labels cell membranes, allowing visualization of cardiomyocyte size. No difference in cell size was observed between wildtype and *Asxl2*$^{-/-}$ samples. We next analyzed the distance between cells by measuring nuclei density (Fig. 12b). No significant difference was observed between wildtype versus *Asxl2*$^{-/-}$ samples. Furthermore, the area occupied by cardiomyocytes relative to non-cardiomyocytes is normal in E18.5 *Asxl2*$^{-/-}$ hearts (Fig. 13), confirming that *Asxl2*$^{-/-}$ cardiomyocytes were not hypertrophic.

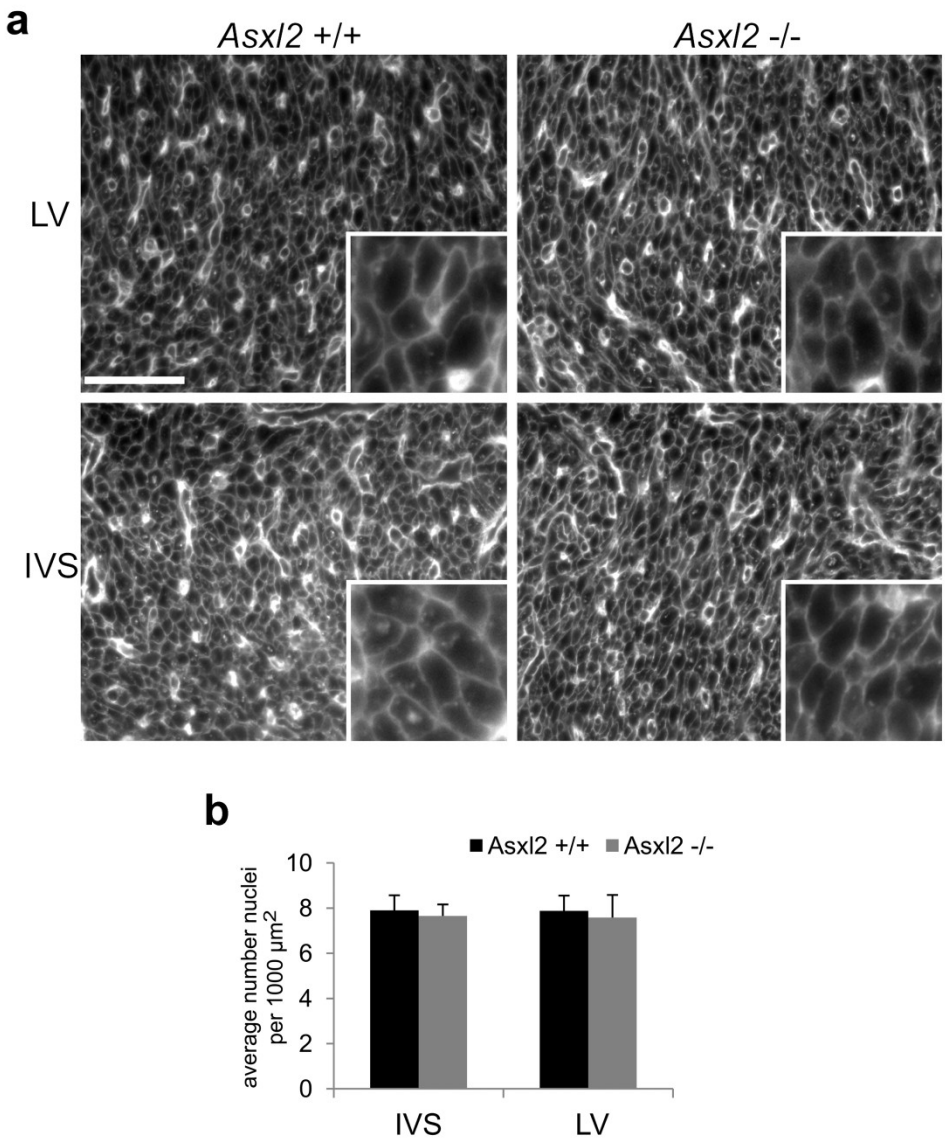

Figure 12: *Asxl2*$^{-/-}$ hearts are not hypertrophic.

(a) WGA staining of wildtype and *Asxl2*$^{-/-}$ hearts revealed comparable cardiomyocyte size. Three randomly selected 40x fields were imaged per region for 6 samples per genotype. Images were qualitatively compared by two observers blinded to sample genotype. Scale bar: 50 µm. (b) Nuclear densities within the LV free wall compact layer and IVS are not significantly different

between wildtype and *Asxl2*$^{-/-}$ hearts. Error bars represent means ± standard deviations from 5 samples per genotype.

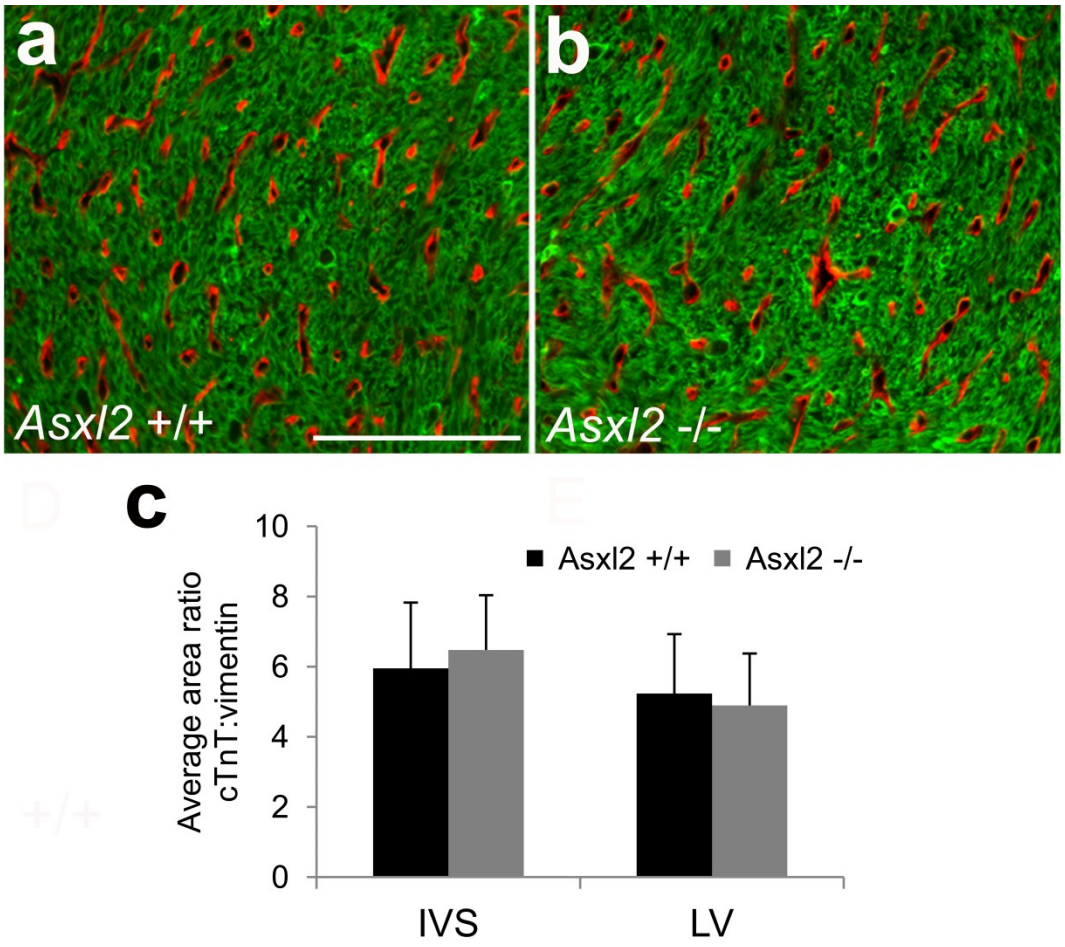

Figure 13: Cardiomyocyte:non-cardiomyocyte area ratio is unchanged in *Asxl2*$^{-/-}$ heart.

(a,b) Immunostaining of E18.5 interventricular septum for cardiac troponin T, a marker of cardiomyocytes (green) and vimentin, which labels fibroblasts and endothelial cells (red). Scale bar: 100 µm. (c) Quantification of average area taken up by cardiomyocytes (cTnT^{+}) versus non-cardiomyocytes (vimentin^{+} cells and intermyocardial spaces) in the IVS and LV compact layer. Error bars represent means ± standard deviations from 3 samples per genotype.

3.3.9 *Asxl2*$^{-/-}$ hearts have normal trabeculation

We next evaluated whether the increase in compact layer thickness in the *Asxl2*$^{-/-}$ heart at E18.5 is associated with abnormal development of the trabeculated layer. The trabeculae consist of finger-like projections of myocardial tissue that extend into the lumen of the ventricles. The sponge-like consistency of the trabecular layer allows oxygenation of the myocardium before the formation of the coronary vasculature. Trabeculae begin forming in the mouse heart at E9.5 (Sedmera and McQuinn, 2008). By E12.5 the trabecular layer is considerably thicker than the compact layer and represents the majority of the ventricular wall (Chen *et al*., 2009). During fetal development the trabeculae undergo remodeling and compaction to rejoin the compact layer. The bulk of trabecular compaction occurs between E13 and E14, and is essential for survival (Sedmera and McQuinn, 2008; Samsa *et al.*, 2013).

Because the compact layer grows both by cardiomyocyte proliferation within this layer and by compaction of the trabeculae, over-growth of the trabecular layer, followed by compaction, could result in a thicker compact layer at E18.5. To determine whether this is the case in *Asxl2*$^{-/-}$ embryos, we qualitatively examined development of the trabecular layer at E13.5, when compaction is at its peak, and at E15.5, a timepoint immediately following the peak of compaction. The trabecular layer exhibited variable thickness in different regions of the same hearts, thus serial sections throughout the heart were photographed and compared. No consistent difference in the density of trabeculae or thickness of the trabeculated layer was found in *Asxl2*$^{-/-}$ versus wildtype hearts at either E13.5 (Fig. 14a-b) or E15.5 (Fig. 14c-d). We conclude that the thickening of the LV compact layer and IVS in the *Asxl2*$^{-/-}$ heart is probably not due to compaction of an over-grown trabeculated layer. However, additional timepoints throughout the course of trabeculation and compaction (E9.5-E15.5) should be examined to definitively rule out

this possibility. Further, quantitative analysis and/or 3-dimensional modeling, such as high-resolution episcopic imaging, may reveal defects in the trabeculae that were not apparent in this qualitative analysis using 2-d sections.

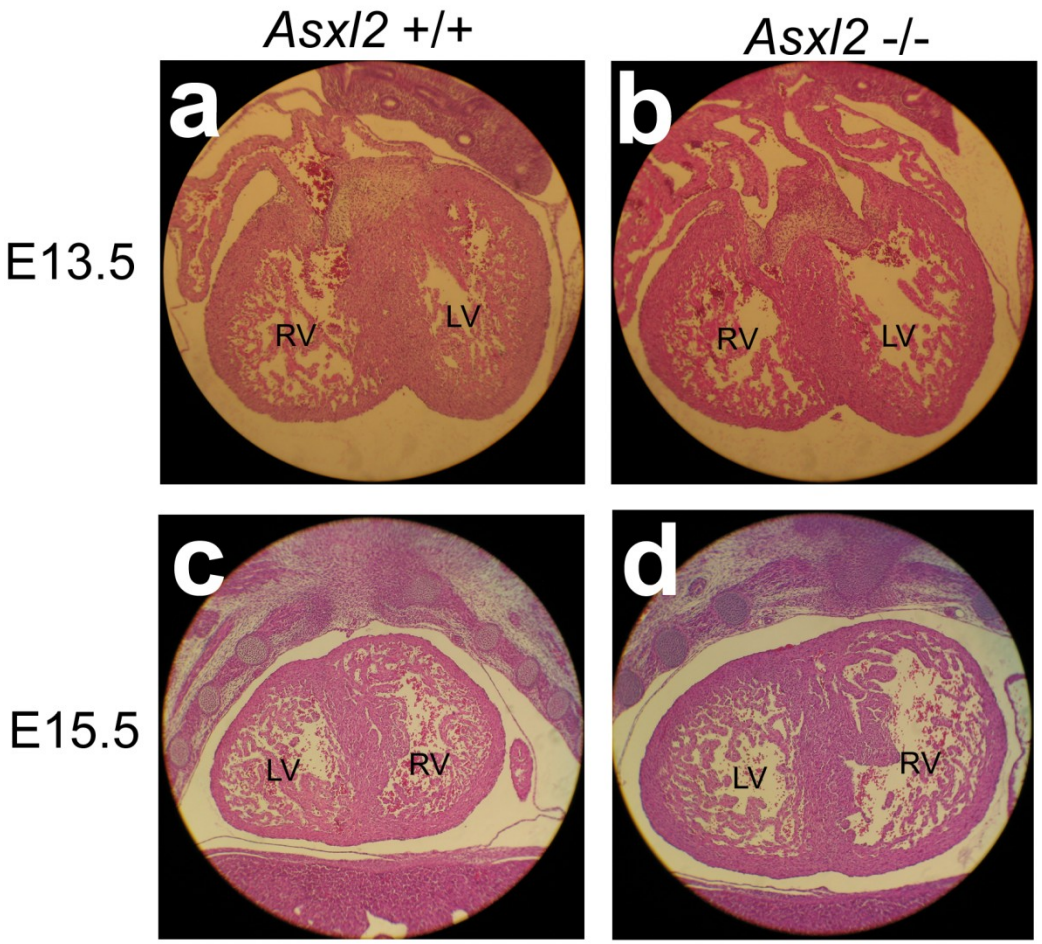

Figure 14: *Asxl2*$^{-/-}$ hearts exhibit normal trabeculation at E13.5 and E15.5.

(a-d) H&E staining of frontal serial sections through wildtype (a, c) and *Asxl2*$^{-/-}$ (b, d) hearts at E13.5 (a-b) and E15.5 (c-d). The *Asxl2*$^{-/-}$ heart exhibits comparable density of trabeculae and thickness of the trabecular layer at both stages. Scale is equal for panels of the same developmental stage. LV: left ventricle. RV: right ventricle.

3.3.10 *Asxl2*$^{-/-}$ neonates display cyanosis, open ductus arteriosus, and lung hemorrhage

While *Asxl2*$^{-/-}$ embryos exhibit congenital heart defects, these defects are not fully penetrant and cannot explain the nearly complete absence of *Asxl2*$^{-/-}$ neonates. Histological examination of E18.5 *Asxl2*$^{-/-}$ embryos did not reveal apparent abnormality or severe developmental delay that may impair the animals' readiness of postnatal survival. To determine the cause of death of *Asxl2*$^{-/-}$ neonates, we delivered pups on E19 by Cesarean section and monitored their behavior for two hours. Wildtype and *Asxl2*$^{+/-}$ animals recovered quickly from the procedure, displaying unassisted breathing and a bright pink skin tone within twenty minutes after delivery. In contrast, four of the five *Asxl2*$^{-/-}$ animals delivered displayed cyanosis (Fig. 15a) and irregular breathing patterns marked by infrequent breaths, gasping, or breathing only when stimulated by touch.

Histological examination of the trunk revealed that all four cyanotic *Asxl2*$^{-/-}$ pups displayed an open ductus arteriosus (DA) lumen (Fig. 15b, c), while the non-cyanotic *Asxl2*$^{-/-}$ pup had a normal closed DA. During fetal development, the DA shunts blood from the pulmonary artery to the aorta, allowing the blood to bypass the fluid-filled lungs (Echtler *et al*., 2010). Shortly after birth, the DA must close to allow normal pulmonary circulation. Failure to close the DA postnatally can allow high-pressure blood from the aorta to flow backwards through the pulmonary artery and into the lungs (Stoller *et al*., 2012); Drayton and Skidmore, 1987). Indeed, all of the *Asxl2*$^{-/-}$ pups with an open DA, but not the one pup with a closed DA, displayed hemorrhage in the alveolar spaces of the lung (Fig. 15d, e). Taken together, we propose that cyanosis and subsequent death in *Asxl2*$^{-/-}$ neonates is due to a failure to close the DA. Interestingly, the morphology of the DA lumen and the histology of the smooth muscle wall

surrounding the lumen were indistinguishable in E18.5 wildtype and *Asxl2*$^{-/-}$ embryos (Fig. 16), suggesting that *Asxl2* regulates the process of DA closure but not the formation of the DA itself.

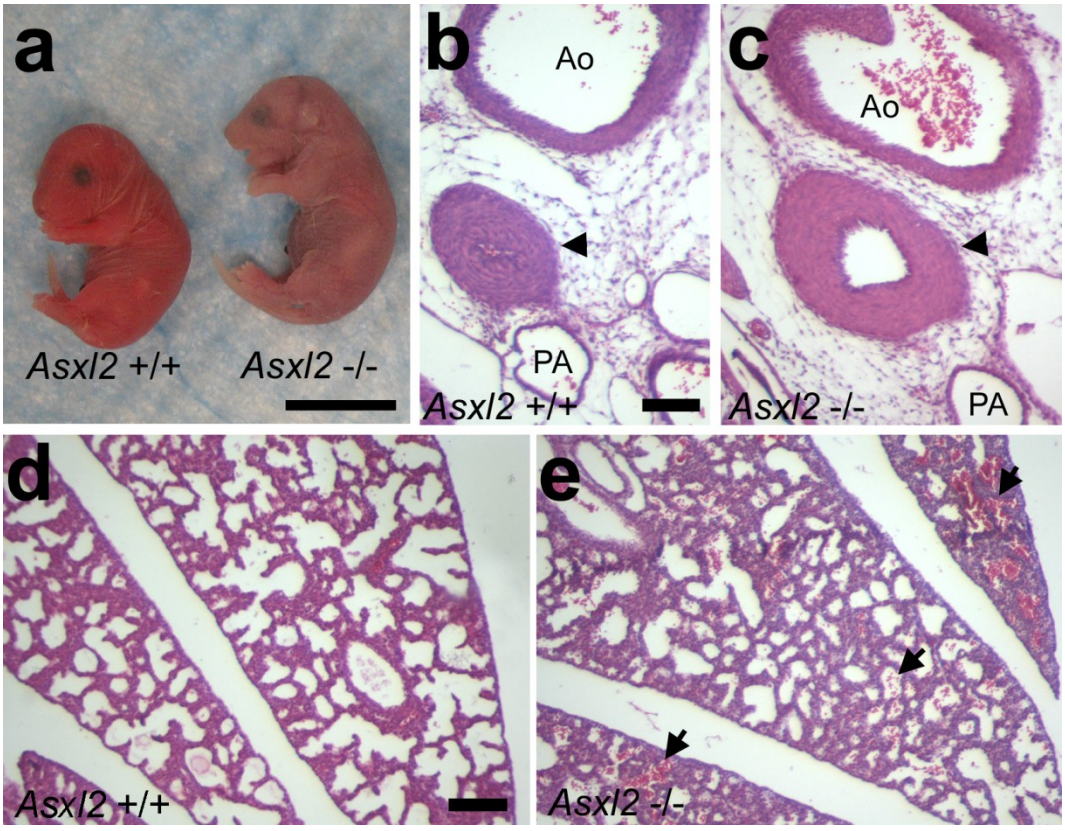

Figure 15: *Asxl2*$^{-/-}$ neonates display cyanosis, failure of ductus arteriosus closure and lung hemorrhage.

(a) Appearance of pups delivered by cesarean section on E19. Four out of five *Asxl2*$^{-/-}$ neonates were cyanosed with difficult breathing. Scale bar: 1 cm. (b, c) H&E staining of frontal sections through pups that were delivered by cesarean section on E19 and sacrificed 2 hours after delivery. The DA (arrowhead) is closed in wildtype pups (b) but displays an open lumen (c) in *Asxl2*$^{-/-}$ pups. PA: pulmonary artery. Ao: aorta. Scale bar: 200 µm. (d, e) H&E staining of lung tissue in wildtype and *Asxl2*$^{-/-}$ pup. The lungs of *Asxl2*$^{-/-}$ pups display hemorrhage into alveolar space (arrows) (e). Scale bar: 200 µm.

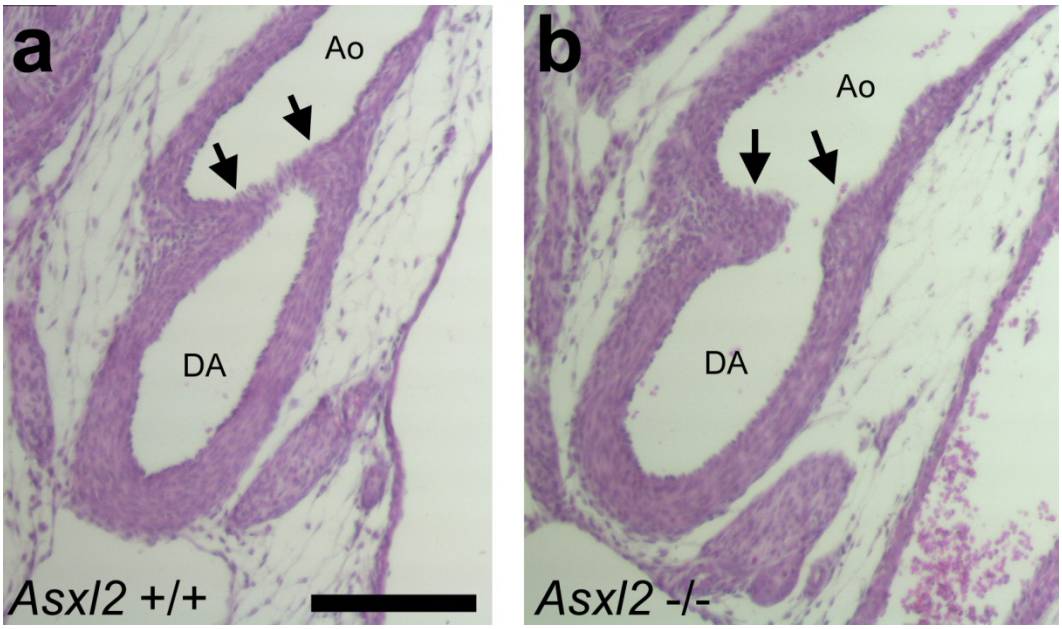

Figure 16: *Asxl2*$^{-/-}$ ductus arteriosus has normal morphology prior to birth.

(a, b) H&E staining of *Asxl2*$^{+/+}$ (a) and *Asxl2*$^{-/-}$ (b) embryos at E18.5. The ductus arteriosus (DA) is connected to the aorta (Ao), has an open lumen, comparable wall thickness and organization, and has developed intimal cushions (arrows) in both *Asxl2*$^{+/+}$ and *Asxl2*$^{-/-}$ animals. Scale bar: 200 μm.

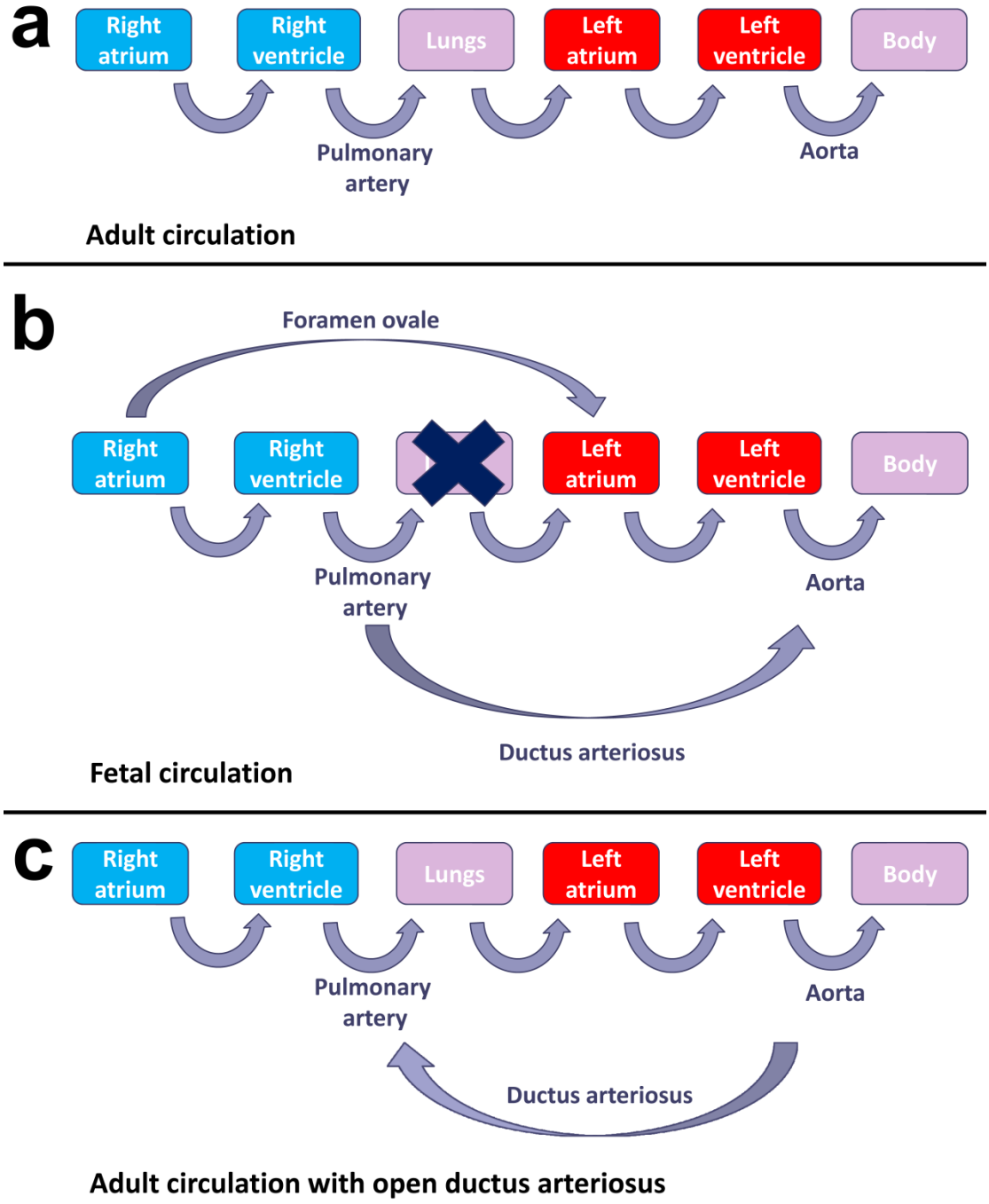

Figure 17: Failure to close the ductus arteriosus after birth allows abnormal blood flow into the lungs.

(a) Normal adult circulation pattern. Deoxygenated blood flows from the right side of the heart to the lungs, where it is reoxygenated, to the left side of the heart and then body. (b) During fetal

circulation the lungs are filled with fluid and most of the blood leaving the right side of the heart is diverted away from the lungs using two shunts: the foramen ovale and ductus arteriosus. Normally, these shunts close immediately after birth. (c) Failure to close the ductus arteriosus allows high-pressure blood from the aorta to flow backwards into the pulmonary artery and lungs. Damage to the pulmonary vasculature and lung hemorrhage can result without intervention, as observed in *Asxl2*$^{-/-}$ pups after birth.

3.4 Discussion

3.4.1 Normal heart development requires both *Asxl2* and *Asxl1*

Among the three *Asxl* genes, *Asxl2* is the most strongly expressed in the heart (Fig. 3c; Lai and Wang, 2013) and is known to play a role in postnatal heart function (Lai *et al.,* 2012). On the other hand, *Asxl1* is only weakly expressed in the heart (Fig. 3c), and previous studies of *Asxl1* mutant models have not reported any cardiac phenotype (Fisher *et al.,* 2010a, Fisher *et al.,* 2010b, Abdel-Wahab *et al.,* 2013; Wang *et al.,* 2014). Interestingly, we found congenital heart defects in both *Asxl2*$^{-/-}$ and *Asxl1*$^{-/-}$ embryos (Table III; Fig. 10a-d; Fig. 9), suggesting that normal heart development requires both *Asxl2* and *Asxl1*. Moreover, the specific defects displayed by *Asxl2*$^{-/-}$ and *Asxl1*$^{-/-}$ animals are different. *Asxl1*$^{-/-}$ animals exhibit a higher incidence and greater severity of VSD. *Asxl2*$^{-/-}$ animals tend to have thickened LV walls, IVS and AV valves, while *Asxl1*$^{-/-}$ animals have normal thickness in both myocardial walls and valves. These results suggest that ASXL2 and ASXL1 regulate different cardiogenic processes.

Due to the lack of antibodies that support immunostaining, the expression patterns of ASXL2 and ASXL1 have not been resolved at the cellular level. However, it is likely that the two homologs are expressed in, and regulate the differentiation of, distinct cell populations within the developing heart. For example, while *Asxl2* is broadly transcribed in the myocardium throughout development, *Asxl1* may be restricted to the endocardial cushions at an earlier time point. The inlet and atrioventricular canal defects observed in the *Asxl1*$^{-/-}$ animals are consistent with a deficiency in the cushion tissue (Marino and Digilio, 2000). The endocardial cushions form at E9, and by E11 have grown to surround the atrioventricular canal (Webb *et al.*, 1998; Gitler *et al.*, 2003). Prior *in situ* hybridization of whole-mount wildtype mouse embryos did not detect *Asxl1* expression in E10.5 or E11 heart (Fisher *et al.*, 2006). However, it is possible that

whole-mount *in situ* was not sensitive enough to detect localized expression of *Asxl1* in the endocardial cushions, especially if the expression is of low levels. Examination of the cellular expression pattern of both ASXL1 and ASXL2 proteins will shed light on these questions.

3.4.2 The effects of *Asxl* mutations on heart development are distinct from PRC2 inactivation

Both ASXL2 and ASXL1 have been shown to interact with the PRC2 histone methyltransferase complex and facilitate the association between PRC2 and target promoters (Abdel-Wahab *et al.,* 2012; Lai and Wang, 2013). PRC2 plays important roles in the developing heart. Using an *Nkx2.5-Cre* line, Pu and colleagues showed that inactivation of PRC2 in the ventricular cardiomyocyte lineage resulted in thinning of the compact myocardium, hypertrabeculation, atrial and ventricular septal defects, and perinatal lethality (He *et al.,* 2012). When PRC2 is inactivated in the secondary heart field (SHF) via *Mef2cAHF-Cre*, the mutant mice were viable with morphologically normal hearts, but developed cardiac hypertrophy and fibrosis in the right ventricles, which is derived from the SHF (Delgado-Olguin *et al.,* 2012). However, neither $Asxl2^{-/-}$ nor $Asxl1^{-/-}$ animals display thin myocardium or hypertrabeculation. Instead, $Asxl2^{-/-}$ hearts often exhibit thickening of the compact myocardium that is not due to hypertrophy. Taken together, these results indicate that ASXL proteins and PRC2 have independent functions during heart development.

In addition to regulating PRC2, ASXL proteins also regulate the histone H2A deubiquitinase BAP1 (Scheuermann *et al.*, 2010; Lai and Wang, 2013). BAP1 alone is inactive in *in vitro* deubiquitination assays, but the addition of recombinant ASXL1 stimulates BAP1 activity (Scheuermann *et al.*, 2010). In the adult heart, the loss of *Asxl2* resulted in significantly decreased BAP1 protein level and an accumulation of ubiquitinated H2A (Lai and Wang, 2013).

BAP1 is essential for early embryonic development, and constitutive *Bap1* mutant animals die by E9.5 (Dey *et al.,* 2012). However, a conditional allele of *Bap1* has been made (Dey *et al.,* 2012), and it would be interesting to ask what role BAP1 plays in heart development and whether it functions together with either ASXL proteins.

3.4.3 *Asxl2* regulates myocardial thickness by an unknown mechanism

Thickening of the LV free wall and IVS is the most penetrant phenotype in *Asxl2*$^{-/-}$ hearts at E18.5, affecting 78% of embryos. Consequently, the size of the LV chamber in *Asxl2*$^{-/-}$ embryos is smaller than that in wildtype animals. The fetal myocardium normally grows by proliferation, and the adult myocardium responds to stress by hypertrophic growth (Ieda *et al.*, 2009; MacLellen and Schneider, 2000). Surprisingly, the thicker myocardium in E18.5 *Asxl2*$^{-/-}$ hearts is not due to overproliferation or hypertrophy of fetal cardiomyocytes. Additionally, the thicker myocardium is not due to abnormalities of the trabecular layer. Given that myocardial thickening was observed in the LV free wall and IVS, but not in the RV, it may be due to a specific defect in cells arising from the first heart field (FHF). A possible explanation is an overabundance of FHF progenitors. Interestingly, hematopoietic-specific deletion of *Asxl1* has been shown to cause an increase in the number of hematopoietic stem/progenitor cells (Abdel-Wahab *et al.,* 2013). It is conceivable that deletion of *Asxl2* has a similar effect on cardiac progenitors, and future studies shall be directed toward answering this question.

Clinically, prominent thickening of the LV walls has been reported in pediatric cardiomyopathy patients (Maron *et al.,* 2006). Although some of these cases are secondary to known syndromes such as Noonan syndrome, the causes of most cases remain unknown (Maron *et al.,* 2006). Therefore, the implication of *Asxl2* in pediatric cardiomyopathy is exciting and intriguing.

3.4.4 *Asxl2* is a novel regulator of ductus arteriosus closure

A failure to close the DA in is a significant health threat for infants. The incidence of patent ductus arteriosus (PDA) is 1 in 500 in full-term infants, 1 in 3 in preterm infants with birth weights <1500 g, and between 50-70% in infants with birth weights <1000 g (Echtler *et al.,* 2010). Infants with PDA are at heightened risk for pulmonary hypertension, bronchopulmonary dysplasia, infections, and congestive heart failure. To date, BRG1, a chromatin remodeling ATPase, is the only epigenetic factor that has been demonstrated to have a role in DA closure. Smooth muscle cell (SMC)-specific knockout of *Brg1* (*smBrg1*$^{-/-}$) produces neonatal cyanosis, death and PDA with incomplete penetrance (33%) (Zhang *et al.,* 2011). While it remains unclear how BRG1 regulates DA closure, *smBrg1*$^{-/-}$ mice exhibit thinner DA walls, disorganized cellular arrangement and increased apoptosis among SMCs (Zhang *et al.,* 2011), suggesting that *Brg1* is required for the development and/or maturation of the smooth muscle layer surrounding the DA. In contrast, *Asxl2*$^{-/-}$ animals did not display any apparent defect in the thickness of the DA wall or in the abundance/arrangement of SMCs, indicating that the mechanism by which ASXL2 regulates DA closure is distinct from that of BRG1.

It is possible that ASXL2 regulates the expression of components of the signaling pathway that triggers DA closure upon birth. Several such components have been identified, including cyclooxygenase 1 and 2, PGT and EP4 (Baragatti *et al.,* 2003; Yokoyama *et al.,* 2006; Chang *et al*., 2010). Alternatively, ASXL2 may regulate the expression of contractile proteins in the smooth muscle layer surrounding the DA. This is the case in a *Myocardin* knockout mouse model, in which selective deletion of *Myocardin* in neural crest-derived SMCs resulted in a failure of these cells to constrict and thereby close the DA (Huang *et al.,* 2008). Taken together,

our studies identify ASXL2 as a novel epigenetic regulator of DA closure and underscore a link between epigenetic derangement and PDA.

3.4.5 Consequences of loss of *Asxl2* are modulated by genetic background

In the present study we report that in the inbred C57BL/6J strain, *Asxl2*$^{-/-}$ causes neonatal lethality. Additionally, no surviving *Asxl2*$^{-/-}$ animals are recovered in the inbred 129Sv strain (McGinley, personal observation). In contrast, in a C57BL/6J;129Sv F1 hybrid background, most *Asxl2*$^{-/-}$ mice survive to beyond 1 year of age. Echocardiography at 1 month and 2 months after birth showed normal cardiac function in these mice. However, they develop late-onset cardiac dysfunction, which appears to be the result of a failure to maintain normal cardiac gene expression patterns (Lai *et al*., 2012; Lai *et al*., 2013). This suggests that the action of ASXL2 is modulated by strain-specific modifiers. Strain-dependent cardiac phenotypes have been previously reported for mutants of CHF1/*Hey2* and heterozygous mutation of *Tbx5*, *Gata4* and *Nkx2.5* (Sakata *et al*., 2006; Bruneau *et al*., 2001; Rajagopal *et al*., 2007; Winston *et al*., 2010). In each case, penetrance of cardiac defects is higher in inbred backgrounds and reduced in F1 hybrid progeny. For example, loss of a single *Nkx2.5* allele causes VSDs at ~37% penetrance in C57BL/6J animals (Winston *et al*., 2010). However, in C57BL/6J;FVB/N F1 progeny, the penetrance is reduced to ~2% (Winston *et al*., 2010). In addition to defect penetrance, strain background also influences which cardiac defects are present. *Gata4*$^{+/-}$ have VSDs at an equal penetrance in the FVB and C57 inbred strains, however severe cushion defects are found at a 20-fold higher incidence in the C57 background (Rajagopal *et al*., 2007).

The identification of genetic modifiers influencing cardiac disease outcomes in mice may yield useful insights for the treatment of human cardiac disorders (Hamilton and Yu, 2012). Recently one such modifier was identified using quantitative trait loci mapping: the cardiac-

specific kinase TNNI3K is highly expressed in the C57BL/6J background, but is not detected in DBA/2J hearts, likely due to an intronic SNP that causes transcript degradation (Wheeler *et al*., 2009; reviewed in Pu, 2009). *Tnni3k* dramatically modifies disease progression in the *Calsequestrin* transgenic (Csq^{Tg}) model of dilated cardiomyopathy (Wheeler *et al*., 2009). The high expression of *Tnni3k* is associated with rapid disease progression in B6 Csq^{Tg} animals. When *Tnni3k* is overexpressed in the DBA/2J background, cardiomyopathy progresses as rapidly as in the B6 strain (Wheeler *et al*., 2009). As with the identification of *Tnni3k*, investigating strain-specific differences in the presentation of cardiac defects may reveal novel regulators of cardiac development and disease. It would be very interesting to determine what modifiers are responsible for the variation in $Asxl2^{-/-}$ phenotype in different mouse genetic backgrounds, and whether these modifiers serve similar functions in humans.

IV. ADDITIONAL SEX COMBS-LIKE 2 REGULATES EPICARDIAL AND MELANOCYTE DEVELOPMENT

4.1 Abstract

Additional sex combs-like 2 regulates functions of the PcG family of epigenetic repressors. PcG proteins regulate cell identity during development via histone modifications that generate repressive chromatin configurations and repress target gene expression. Here we present evidence that *Asxl2* is required for the normal development of two cell populations: epicardial cells and melanocytes. Loss of *Asxl2* may cause delayed or perturbed differentiation in these cells.

4.2 Introduction

PcG proteins are epigenetic regulators of gene expression acting at the level of chromatin (Kohler *et al*., 2008; Pietersen *et al*., 2008; Schwartz and Pirrotta, 2007). Originally identified in Drosophila as regulators of homeotic genes, PcG proteins are now recognized to function in a wide variety of contexts in vertebrates, invertebrates, and plants (Kohler *et al*., 2008). Members of the PcG family work in large multi-protein complexes to establish and maintain histone modifications (Schwartz and Pirrotta, 2007). These modifications generate repressive chromatin configurations that affect gene expression. During development and differentiation, PcG proteins create a system of cellular memory to maintain target genes in a repressed state across many cell divisions, even after the transcriptional signals that initiated their repression are long gone (Sparmann and van Lohuizen, 2006).

Additional sex combs-like 2 (ASXL2) regulates gene expression by working with two PcG complexes: PRC2 and PR-DUB. PRC2 represses target genes by trimethylating histone H3K27 (Margueron and Reinberg, 2011). ASXL2 is required for PRC2 binding at target genes,

and loss of *Asxl2* leads to reduced H3K27me3 and derepression of target genes in the heart (Lai and Wang, 2013). ASXL2 is also a member of the Polycomb repressive deubiquitinase complex (PR-DUB). BAP1 of PR-DUB removes monoubiquitin from histone H2A, a process that is critical for proper repression of *Hox* genes (Scheuermann *et al*., 2010). ASXL2 interacts with BAP1 and is required for its deubiquitinase activity (Lai and Wang, 2013). During development *Asxl2* is required for both morphogenesis and maintenance of cardiac function in adulthood (McGinley *et al*., 2014; Lai *et al*., 2012). However, its role in other tissues is largely unexplored. Here I present roles for *Asxl2* in the regulation of two migratory, multipotent cell populations during development: epicardial cells and melanocytes.

4.2.1 Development of the epicardium and melanocytes

The epicardium of the heart consists of a single layer of epithelial cells that covers the surface of the heart. The epicardium is essential for cardiac development, and has two primary roles: signaling to the underlying myocardium to control growth and generating the cells that form the coronary vasculature system (Olivey and Svensson, 2010; Zhou *et al*., 2011; Chen *et al*., 2002; Bhattacharya *et al*., 2006). Both roles are essential for proper cardiac function.

The epicardium is derived from a transient organ called the proepicardium. The proepicardium is a cluster of splanchnic mesoderm cells that are located ventral to the inflow tract of the tubular heart and sit on the cranial side of the transverse septum. From E9 – E11.5, cells from the proepicardium migrate across the surface of the heart, forming the epicardium (Cossette and Misra, 2011; Mikawa and Brand, 2010). Beginning at E12.5, some of these epicardial cells undergo an epithelial-to-mesenchymal transition (EMT) in which they delaminate from the surface of the heart and migrate into the myocardium (Hill *et al*., 2012; Olivey *et al*., 2006). These cells differentiate into smooth muscle and some endothelial cells that

form the coronary vasculature system, and also give rise to the cardiac fibroblast population (Olivey and Svensson, 2010; Wilting *et al*., 2007; Acharya *et al*., 2012). A small subset of these cells also appears to rarely give rise to cardiomyocytes (Cai *et al*., 2008; Zhou *et al*., 2008). Thus, the epicardium represents a multipotent progenitor population that generates many cell types critical to cardiac function.

The production of melanocytes also involves EMT and cell migration. Melanocytes are a heterogenous population of cells derived from migratory neural crest cells (Goding, 2007). They produce the black pigment melanin, which is stored in melanosomes, specialized cytoplasmic organelles (Cichorek *et al*., 2013). Melanocytes are responsible for pigmentation of the epidermis, hair, and pigmented retina. Small populations also exist in many tissues, including the heart, where they are linked to atrial arrhythmias (Cichorek *et al*., 2013; Levin *et al*., 2009).

Melanoblasts are the migratory progenitor of melanocytes (Wilkie *et al*., 2002). Like epicardial cells, melanoblasts undergo EMT during their development. Neural crest cells along the entire A/P axis delaminate from the neural tube by EMT and become committed to the melanoblast lineage (Ernfors, 2010). Melanoblasts migrate dorsolaterally under the epidermis to populate the skin of the entire body (Ernfors, 2010). They continue to proliferate along their migration route. Differentiation into melanocytes and melanin synthesis begins after migration has ended (Kelsh *et al*., 2009).

Most melanocytes reside in two locations: the epidermis and hair follicles. In the skin individual melanocytes associate with a cluster of 20-40 keratinocytes (Bandarchi *et al*., 2013). The melanocyte distributes pigment through its associated cells. Melanocytes of the skin are slow-dividing and long-lived (Botchkareva *et al*., 2003). In contrast, melanocytes of the hair follicle are continually renewed (Nishimura, 2011). At the end of a hair's lifespan, 3 weeks in

mice, cells within the hair shaft die and must be replaced for the growth of a new hair (Alonso and Fuchs, 2006). New melanocytes are thought to be produced from a progenitor population of amelanotic melanoblasts within the bulge area of the hair follicle (Slominski *et al*., 2005). The melanoblast progenitors found within the hair follicle are also responsible for periodically resupplying the epidermis with new melanocytes (Nishimura, 2011).

4.2.2 Epigenetic regulation of epicardium and melanocytes

To date no known PcG or TrxG complexes are known to regulate epicardial development. However, one chromatin remodeling complex has a major role: BAF180. BAF180 is a member of the SWI/SNF chromatin remodeling complexes and is highly expressed in the proepicardium and epicardium (Huang *et al*., 2008). In *Baf180* mutant mice, the epicardium forms but has impaired EMT. These animals generate only surface-level coronary vessels, and many PECAM-1^{+} nodules are present within the subepicardium (Huang *et al*., 2008). Whether and how other aspects of epicardium development might be regulated epigenetically is an intriguing area requiring more research.

As is the case for epicardial development, little is known about epigenetic factors in melanocyte development. The PcG protein AEBP2 is required for normal neural crest cell migration, including melanoblasts (Kim *et al*., 2011). Mice deficient for AEBP2 have white tail tips and hindlimb toes, a relatively mild melanocyte migration deficit phenotype (Kim *et al*., 2011). Although thorough analyses of the PRC2 repressors EZH1 and EZH2 have demonstrated their role in regulating the cycling of hair follicle stem cells, these studies focused on epidermal-derived stem cells within the follicle, not melanoblasts from the neural crest lineage (Ezhkova *et al*., 2011; Ezhkova *et al*., 2009). Other studies have demonstrated that micropthalmia-associated-transcription-factor (MITF) interacts with BRG1 of the SWI/SNF chromatin remodeling

complex in melanoma cells to alter MITF target gene expression and inhibit apoptosis of melanoma cells after UV radiation (Saladi *et al*., 2013). MITF is a transcription factor and master regulator of the melanocyte cell lineage during development (Ernfors, 2010). It is possible that MITF may function with BRG1 or other epigenetic mechanisms in non-cancer contexts, but this has not yet been established.

Here we present data demonstrating that *Asxl2* is required for normal development of both the epicardium and melanocytes. *Asxl2*$^{-/-}$ animals display deficits in the number of both cell types at specific developmental stages.

4.3 Results

4.3.1 The *Asxl2*$^{-/-}$ embryonic epicardium is deficient at E12.5 and E13.5

We conducted a series of investigations on the *Asxl2*$^{-/-}$ epicardium to determine whether epicardial abnormalities contribute to the thickened left ventricular wall phenotype observed at E18.5. First, histology was used to examine the epicardium at E12.5, shortly after migration from the proepicardium is complete. We found that at E12.5 the *Asxl2*$^{-/-}$ epicardium is composed of fewer cells than the wildtype heart (Fig. 18). Whereas the wildtype epicardium appeared as a tightly associated layer of cells, the *Asxl2*$^{-/-}$ epicardium appeared more sparsely populated, with greater distance between cells. Although this general observation held true across samples, there was great regional variation in the epicardium in each heart. There can be found regions of the wildtype epicardium as sparse as the *Asxl2*$^{-/-}$ epicardium, as well as regions of the *Asxl2*$^{-/-}$ epicardium as densely populated as in the wildtype. Thus we conclude there is a subtle, but consistent, deficiency in the number of cells in the *Asxl2*$^{-/-}$ epicardium at E12.5.

We further investigated the histological appearance of the epicardium by examining serial sections of hearts at E13.5. At this timepoint migration from the proepicardium has ceased

and epicardial cells are undergoing EMT. During EMT cells delaminate from the epicardial epithelium and migrate into the subepicardial space below. This space is rich in hemangioblasts and primitive blood vessels that will become the coronary arteries and veins. At E13.5, the *Asxl2*$^{-/-}$ hearts appeared to have fewer cells in the subepicardial space than in wildtype. The wildtype subepicardial space was 1-3 cell layers thick, with many developed blood vessels visible throughout (Fig. 19a). In contrast, the *Asxl2*$^{-/-}$ was only 1-2 cell layers thick in most places, and fewer blood vessel cells were visible in this region (Fig. 19b). Interestingly, the density of cells in the epicardial epithelium was comparable in both genotypes at E13.5 (Fig. 19). This suggests that the sparse epicardium phenotype observed at E12.5 in the *Asxl2*$^{-/-}$ has largely recovered by E13.5.

We next conducted several studies to determine the activity of the *Asxl2*$^{-/-}$ epicardium. Because the epicardium gives rise to many cell types in the myocardium, we hypothesized that an increase in EMT could contribute to the thickened myocardium phenotype observed at E18.5 in the *Asxl2*$^{-/-}$ heart. We first used an *ex vivo* vital dye labeling assay to label and quantify cells undergoing EMT from the epicardium (Zhou *et al*., 2008). Individual *Asxl2*$^{-/-}$ and wildtype hearts were collected at E12.5, after the epicardium has formed, and incubated in CMFDA. CMFDA is a vital dye that penetrates the cell membrane of the outermost cell layer of the heart (the epicardium) and is then trapped inside the cytoplasm. The dye has low toxicity and can be used to label cells over several days or multiple cell divisions. Hearts were then cultured for 24-48 hours to allow EMT to take place.

We observed that the *Asxl2*$^{-/-}$ heart had numerous labeled migrated cells within the subepicardium and compact myocardium after 24 hours in culture (Fig. 20b). In contrast, the wildtype hearts had few labeled migrated cells (Fig. 20a). However, when we examined hearts

after only 30 minutes post-labeling, we found fluorescent dye had penetrated into the subepicardial space in the *Asxl2*$^{-/-}$, but not wildtype hearts (Fig. 20c-d). Taken together these results suggest that the *Asxl2*$^{-/-}$ epicardium is more dye-permeable than the wildtype epicardium at E12.5. This is consistent with our prior observation that the *Asxl2*$^{-/-}$ epicardium appears sparser by histology at E12.5 (Fig. 18). No conclusions regarding the frequency of EMT can be drawn from this assay as the dye-labeling is not restricted to the epicardial layer in *Asxl2*$^{-/-}$ hearts. It would be interesting to investigate whether the increased dye permeability is due to more widely spaced epicardial cells, or to defects in the cell adherens junctions that maintain the epithelial sheet.

We next used immunostaining assays to determine whether increased EMT is occurring in the *Asxl2*$^{-/-}$ heart. Vimentin is a flexible cytoskeletal protein expressed in mesenchymal-derived cells. It is found in epicardial cells at basal levels, and is upregulated upon EMT (Acharya *et al*., 2012; Song *et al*., 2009; Fig. 21a). We immunostained hearts for vimentin at E13.5, a timepoint when EMT activity is high. Because the epicardium exhibits regional differences in its development, with the dorsal surface of the heart developing ahead of the ventral surface, we analyzed these regions independently. We found comparable expression of vimentin in *Asxl2*$^{-/-}$ and wildtype samples in both dorsal and ventral surfaces of the heart (Fig. 21b-c).

We further examined the activity of the *Asxl2*$^{-/-}$ epicardium by quantifying the proliferation rate of the epicardium at E13.5 (Fig. 22). We used immunostaining of WT1, a transcription factor highly expressed in developing epicardial cells, to label the epicardium. Proliferative activity was marked by BrdU labeling, a thymine analog that is incorporated during S phase of the cell cycle, administered to pregnant females 2 hours before embryo collection.

Proliferation was quantified independently for the dorsal and ventral sides. Approximately 9% of the $Wt1^{+}$ epicardial cells were $BrdU^{+}$, on both the dorsal and ventral surfaces (Fig. 22c). No significant difference was detected between *Asxl2*$^{-/-}$ and wildtype samples, indicating that proliferation is not perturbed at this timepoint.

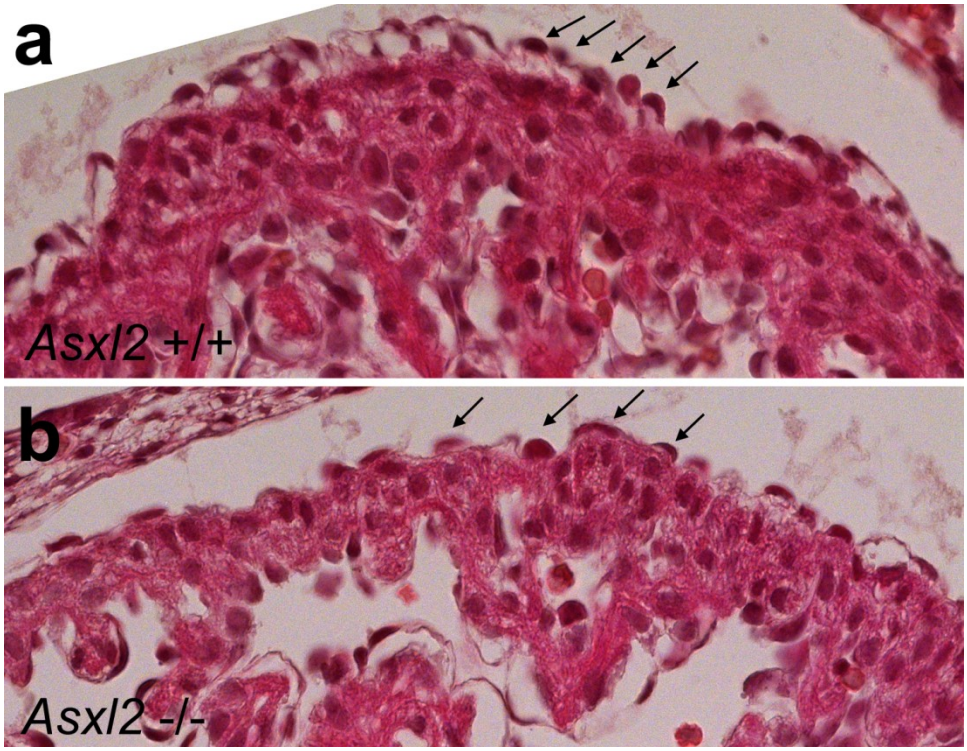

Figure 18: *Asxl2*$^{-/-}$ epicardium has regions of fewer cells at E12.5.

(a-b) H&E staining of serial sections through E12.5 hearts revealed that the *Asxl2*$^{-/-}$ epicardium (b) consists of less densely spaced cells. Arrows: epicardial cell nuclei. The apparent difference in myocardial thickness is due to regional variations in thickness, and is not representative of all *Asxl2*$^{-/-}$ hearts at this stage.

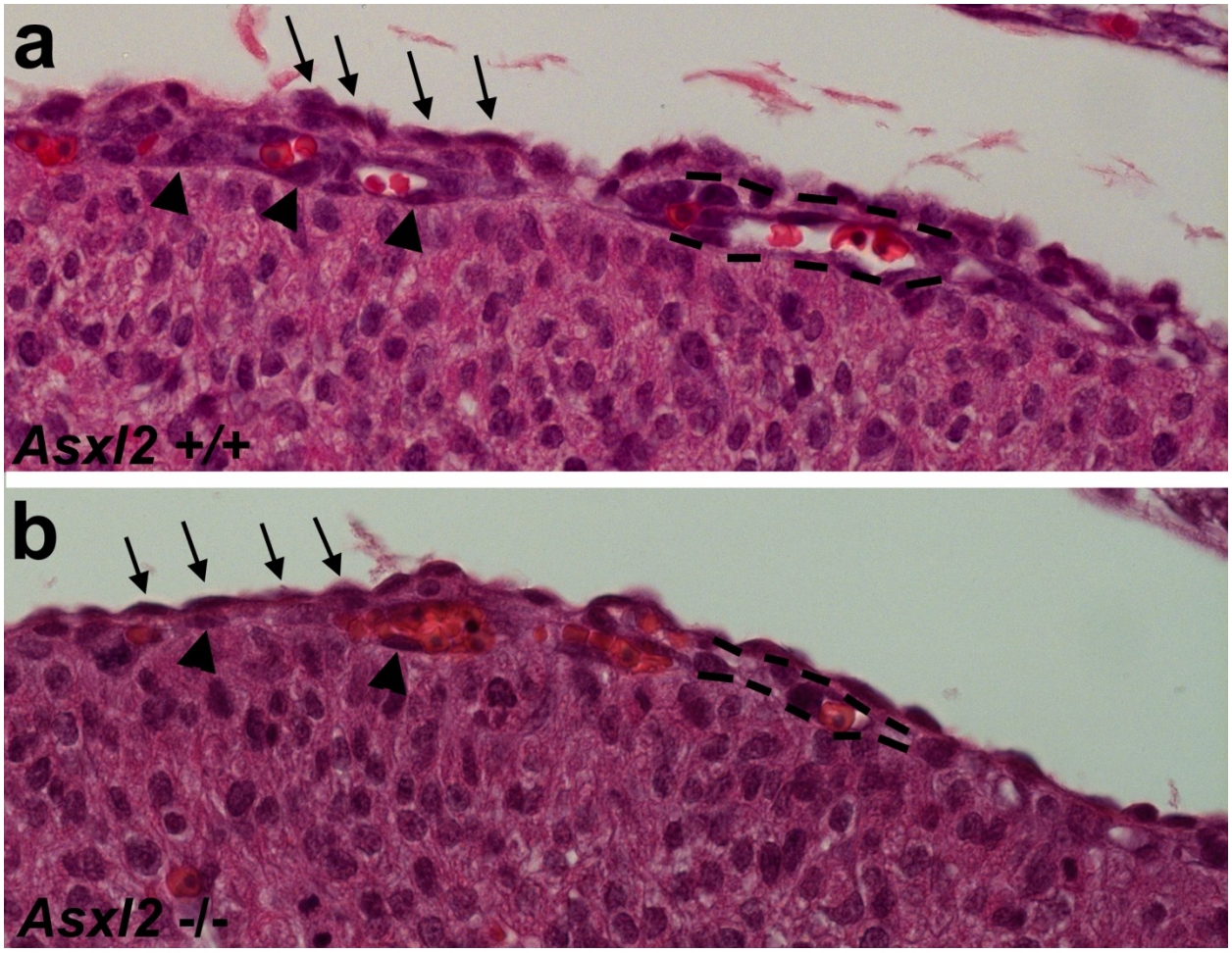

Figure 19: *Asxl2*$^{-/-}$ subepicardium has fewer cells at E13.5.

(a-b) H&E staining of serial sections through E13.5 hearts revealed that the *Asxl2*$^{-/-}$ heart (b) has a thinner subepicardium at this stage with fewer blood vessels. Arrowheads: nuclei of subepicardial cells. Dashed lines outline a portion of the subepicardial space. The density of epicardial cells (arrows) is comparable in both genotypes, in contrast to the fewer cells observed in *Asxl2*$^{-/-}$ at E12.5.

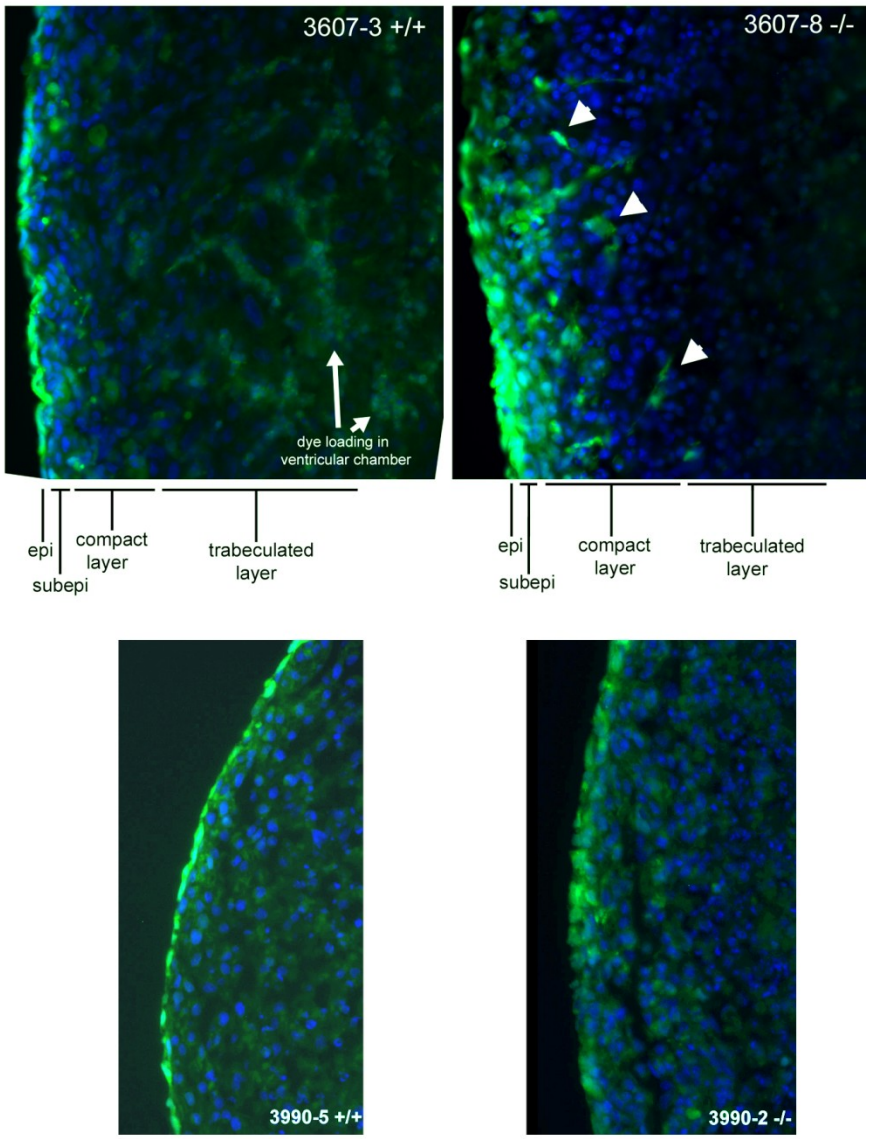

Figure 20: The *Asxl2*$^{-/-}$ epicardium is more permeable to the dye CMFDA at E12.5.

(a-d) Vital dye labeling of the epicardium in hearts isolated from E12.5 *Asxl2*$^{+/+}$ (a,c) and *Asxl2*$^{-/-}$ (b,d) embryos. Hearts were exposed to CMFDA (green) for 30 minutes, then cultured for 24 hours (a-b) or 30 minutes (c-d). Numerous migrated labeled cells (arrowheads) were observed in the *Asxl2*$^{-/-}$ heart after 24 hours of culture (b). However, control experiments revealed that CMFDA labels both the epicardium and subepicardium in *Asxl2*$^{-/-}$ hearts (d), whereas labeling is

restricted to the epicardium in wildtype hearts (c). Epi: epicardium. Subepi: subepicardium. DAPI counterstain is shown in blue.

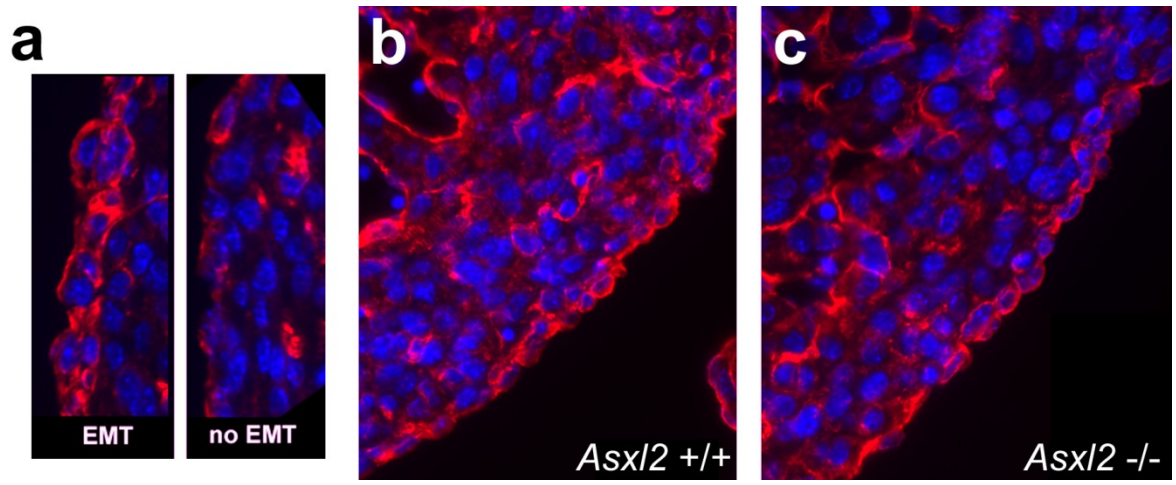

Figure 21: EMT is unperturbed in the *Asxl2*$^{-/-}$ epicardium at E13.5.

(a-c) Immunostaining of vimentin (red) in *Asxl2*$^{+/+}$ (a-b) and *Asxl2*$^{-/-}$ (c) E13.5 hearts. (a) Vimentin is upregulated upon EMT. Comparable levels of vimentin staining were observed in matched sections of wildtype (b) and *Asxl2*$^{-/-}$ (c) epicardium. DAPI counterstain is shown in blue.

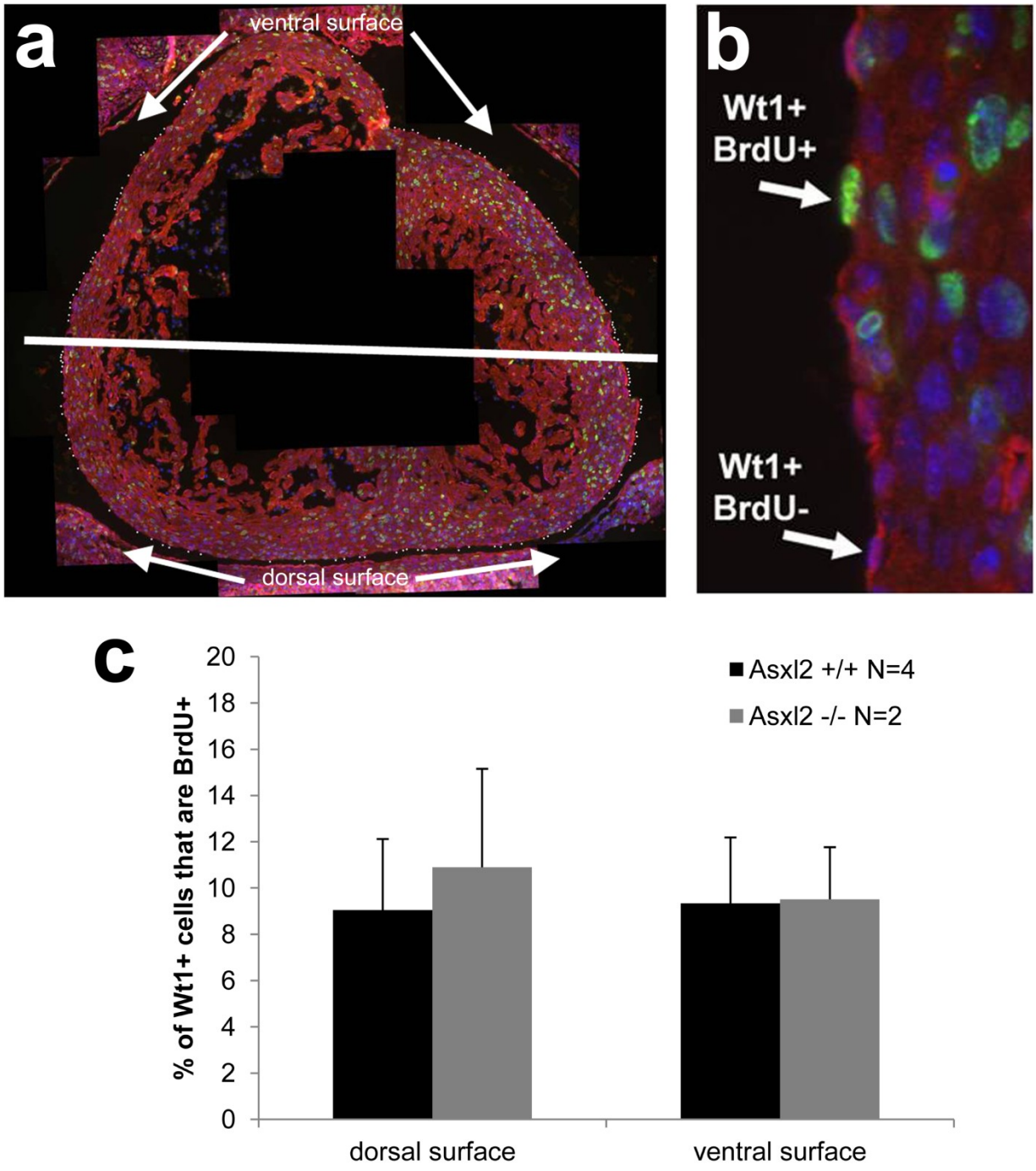

Figure 22: Epicardial proliferation in the *Asxl2*$^{-/-}$ heart is normal at E13.5.

(a-b) Immunostaining of WT1 (red) and BrdU (green) was used to determine proliferation rates of the epicardium in wildtype and *Asxl2*$^{-/-}$ hearts at E13.5. (a) Representative composite image assembled from 20X images of the epicardial surface. Proliferation on the ventral and dorsal

surfaces of the heart was calculated independently. (b) Higher magnification of epicardium showing $BrdU^+$ and $BrdU^-$ nuclei. (c) Quantification of proliferation rates. *Asxl2*$^{+/+}$ N=4, *Asxl2*$^{-/-}$. N=2. No statistically significant difference was found by Student's t-test. Error bars represent means ± standard deviation. DAPI counterstain is shown in blue.

4.3.2 A population of blood island cells exists on the ventral surface of the *Asxl2*$^{-/-}$ heart at E16.5, but not E18.5.

The myocardium of the heart is supplied with oxygenated blood by the coronary arteries and veins. These vessels include both endothelial cells and smooth muscle cells. Both cell types are derived partially from epicardial cells that undergo EMT and migrate into the subepicardial space, then into the myocardium. Other sources for these cells include sprouting vessels from the sinus venosus (endothelial cells) and migratory neural crest cells (smooth muscle cells proximal to the aorta) (Red-Horse *et al*., 2010; Riley and Smart, 2011). Among the cells that migrate into the subepicardial space, a subpopulation forms hemangioblast cells that are arranged in clusters termed blood islands (Olivey and Svensson, 2010). These hemangioblast-containing blood islands are observable on the surface of the heart by E12.5, and express CD45, SCA1, and SCL, markers of blood lineage progenitors, as well as PECAM-1 (Lavine *et al*., 2008). Nucleated red blood cells are observable within the blood islands at E12.5, providing further evidence that these clusters give rise to *de novo* blood cells, as at this time the clusters are not connected to any other vessels in the heart (Tomanek *et al*., 2006).

We performed PECAM-1 immunostaining on whole embryo hearts at E16.5 to observe the distribution of the coronary vessels. By this timepoint the major coronary arteries and veins have formed, and surface vessels can be visualized by PECAM-1 staining. Although we did not identify any differences in the formation or distribution of vessels in the *Asxl2*$^{-/-}$ heart, we did identify multiple abnormal clusters of PECAM-1^{+} cells on the ventral surface of the *Asxl2*$^{-/-}$ heart over the interventricular septum (Fig. 23a-b). These clusters resemble the appearance of blood islands, although further marker expression characterization is required to confirm this.

We also performed whole-mount PECAM-1 immunostaining at E13.5 and E18.5 to determine the time course of the blood islands' appearance. At E13.5 blood islands were observed in the same region in wildtype samples (Fig. 23c). At E18.5 no blood islands were observed in wildtype or *Asxl2*$^{-/-}$ hearts (Fig. 23d). Taken together, these data suggest the *Asxl2*$^{-/-}$ likely has a persistent or ectopic population of blood island cells on the ventral surface of the heart at E16.5.

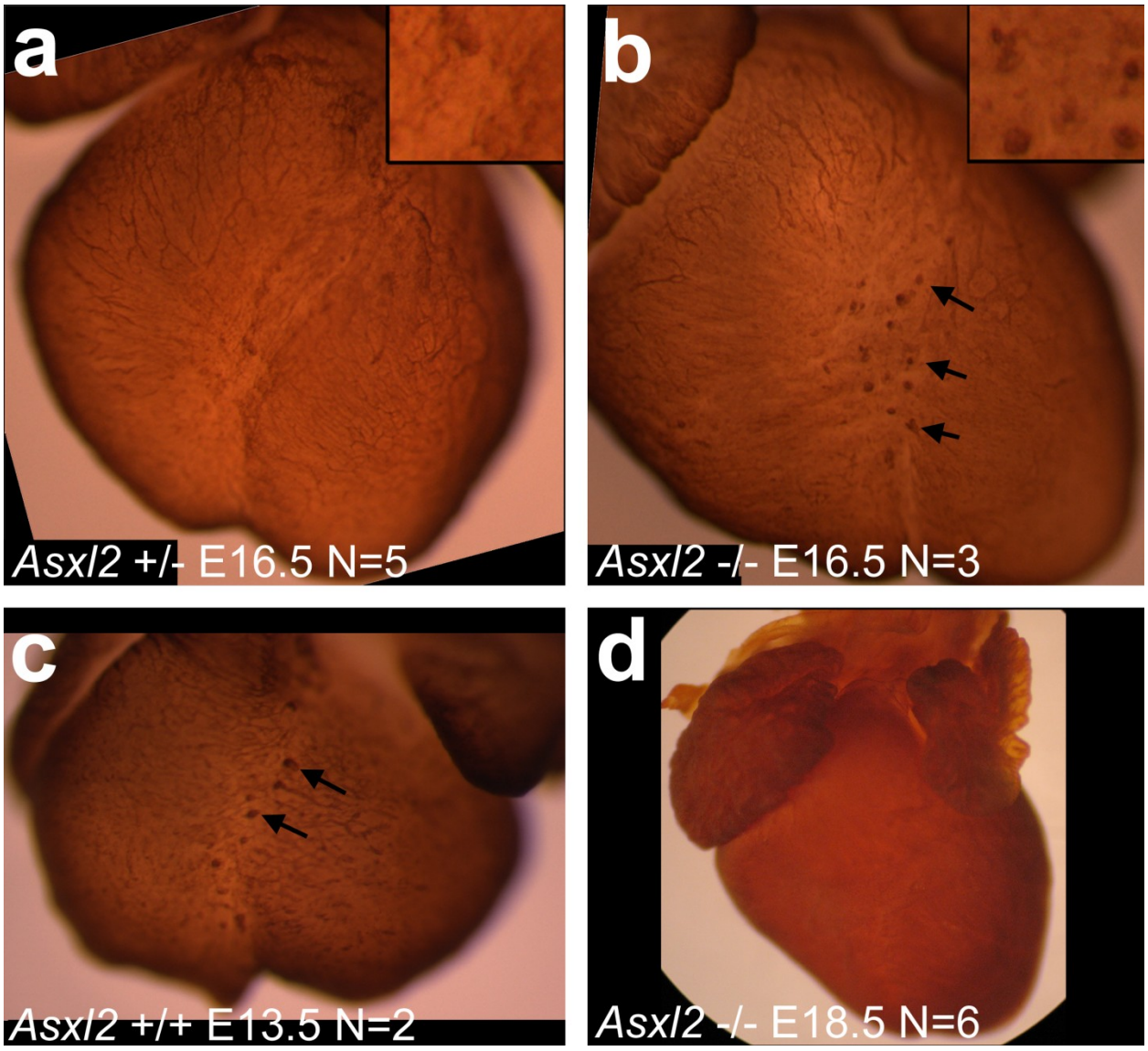

Figure 23: *Asxl2*$^{-/-}$ hearts have abnormal PECAM-1^{+} blood islands on the ventral surface at E16.5.

(a-d) Whole-mount immunostaining of PECAM-1 on control (a,c) and *Asxl2*$^{-/-}$ hearts (b,d). (a-b) At E16.5 clusters of blood islands (arrows) are visible on the surface of *Asxl2*$^{-/-}$ (b) but not control (a) hearts. These clusters are found on wildtype hearts at E13.5 (c), but on neither wildtype nor *Asxl2*$^{-/-}$ (d) hearts at E18.5. Panels a-b shown at same scale.

4.3.3 *Asxl2*$^{-/-}$ fetuses have deficiencies in a population of nose melanocytes

While collecting *Asxl2*$^{-/-}$ embryos we noted that these animals have a deficiency in a population of melanocytes on the tip of the nose. To investigate this phenotype we collected embryos at E15.5 and E18.5 and imaged their noses (Fig. 24). Melanocytes are visible within the thin epidermis due to their endogenous black pigmentation. At E15.5 the number of visible melanocytes in this region is dramatically reduced in *Asxl2*$^{-/-}$ embryos (Fig. 24). At E18.5 the phenotype is more dramatic than at E15.5: the *Asxl2*$^{-/-}$ has a greatly reduced number of visible pigmented melanocytes on the nose compared to wildtype (Fig. 24). We conclude from this data that the *Asxl2*$^{-/-}$ embryo may have impaired numbers or migration of melanoblast progenitors. Because melanocytes do not begin producing pigment until their post-migration terminal differentiation, it is also possible that a normal number of melanocytes are present, but not visible due to delayed differentiation or impaired melanin synthesis (Goding, 2007).

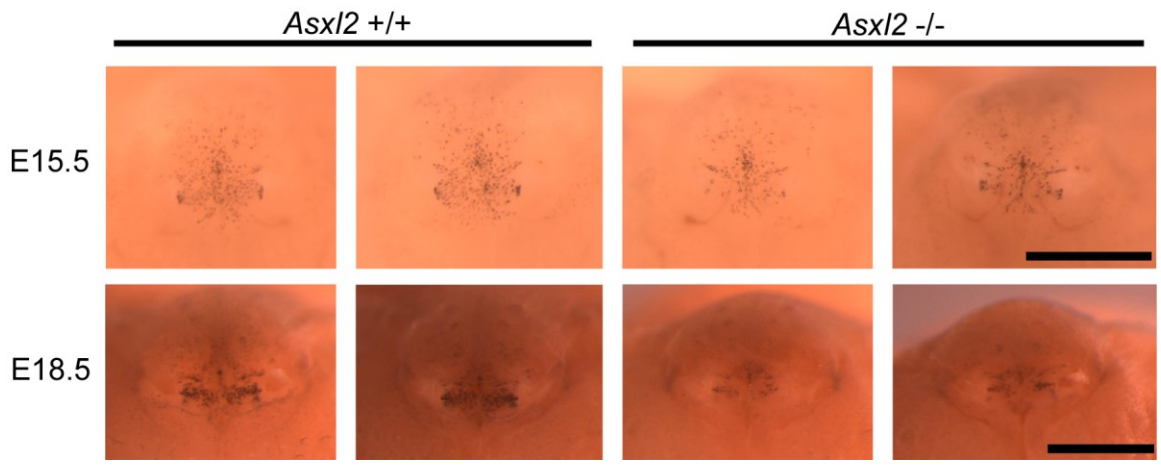

Figure 24: *Asxl2*$^{-/-}$ embryos have a melanocyte deficiency.

Whole-mount embryo noses were photographed. A population of black pigmented melanocytes are visible within the epidermis of the nose. This population is reduced in size in *Asxl2*$^{-/-}$ embryos at both E15.5 and E18.5. Scale bar: 1 mm.

4.3.4 Surviving *Asxl2*$^{-/-}$ B6 animals have abnormal fur color

Although most *Asxl2*$^{-/-}$ animals do not survive beyond birth in the C57BL/6J inbred background, some survivors are recovered sporadically (Table I). These surviving mutants are small runts; whereas wildtype and *Asxl2*$^{+/-}$ animals can be weaned at 3 weeks of age, surviving *Asxl2*$^{-/-}$ animals cannot be safely weaned until they are 5-6 weeks old (McGinley, personal observation). In adulthood the *Asxl2*$^{-/-}$ animals display a lighter black fur color than their wildtype and *Asxl2*$^{+/-}$ littermates (Fig. 25). The grayed fur phenotype is subtle, but significant enough that *Asxl2*$^{-/-}$ animals can be readily distinguished from littermates by fur color alone. The lighter coat color is consistent across the entire coat. No white spots or lighter patches have been observed on the belly of these animals or elsewhere. Taken together with the melanocyte deficiency observed in *Asxl2*$^{-/-}$ embryo noses (Fig. 24), we hypothesize that *Asxl2* may be required for the survival or differentiation of melanocytes, or may regulate their synthesis of melanin.

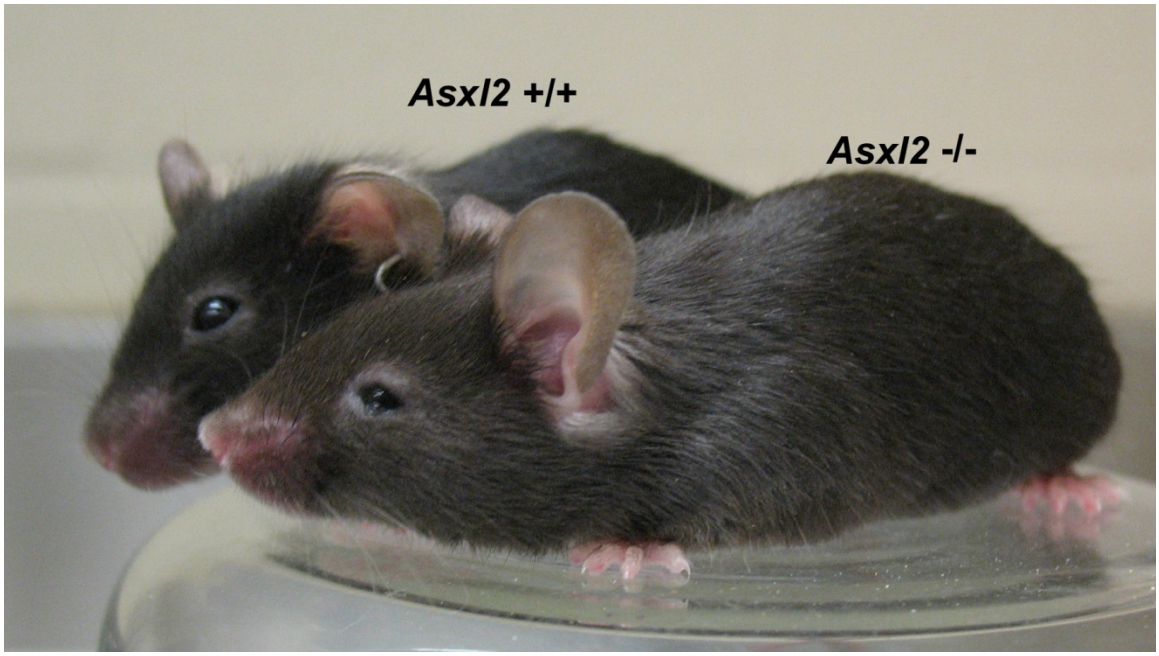

Figure 25: Surviving *Asxl2*$^{-/-}$ C57BL/6J animals have lighter fur color.

Photograph of *Asxl2*$^{+/+}$ (left) and *Asxl2*$^{-/-}$ (right) female littermates at 2 months of age. *Asxl2*$^{-/-}$ animals have a gray/light black coat, in contrast to the dark black coat of wildtype animals. The coloration is consistent across the entire coat of these animals. *Asxl2*$^{-/-}$ survivors also present with micropthalmia and a thickened ring of skin around the eyes.

4.4 Discussion

4.4.1 Function of *Asxl2* in epicardial cells

We report here that *Asxl2* is required for the normal development of epicardial cells. *Asxl2*$^{-/-}$ animals exhibited fewer epicardial cells shortly after migration is complete at E12.5 (Fig. 18), and fewer epicardially-derived cells in the subepicardium at E13.5 (Fig. 19). We also noted a population of cells resembling blood islands on the surface of the heart that is present at E16.5, but not E18.5 in mutant animals (Fig. 23). Because these phenotypes manifest at specific developmental timepoints, but later are resolved, these phenotypes are suggestive of a delay in epicardial differentiation.

The blood island phenotype observed at E16.5 is particularly interesting given the thickened interventricular septum that is observed in *Asxl2*$^{-/-}$ hearts at E18.5. What is the source and fate of these cells? As they are not found by E18.5, do they differentiate and contribute to the greater bulk within the septum? This seems unlikely, considering the small quantity of blood island-like cells present. However, the cells might be responsible for supplying some pro-growth signal to the underlying myocardium.

Do the blood islands represent an ectopic population that appears as a result of abnormal differentiation, or are they simply normal cells with delayed differentiation? A more careful analysis of the time course of their appearance, and the markers they express may yield answer to these questions. The formation of PECAM-1+ nodules was also observed in *Baf180*$^{-/-}$ embryo hearts (Huang *et al*., 2008). However, these nodules are accompanied by abnormal coronary formation, which was not observed in *Asxl2*$^{-/-}$ animals. In *Baf180*$^{-/-}$ nodules, thick layers of endothelial and smooth muscle cells accumulate, suggesting aberrant differentiation. It would be interesting to characterize the expression within the *Asxl2*$^{-/-}$ blood island-like clusters for

endothelial, smooth muscle, fibroblast, and hematopoetic markers. Lineage tracing of epicardially-derived cells may reveal the origin and fate of these cells. Multiple reporters are available for this purpose, most notably a $Wt1^{CreERT2}$ line that can be used to label Wt1-expressing epicardial cells (Zhou *et al*., 2008).

4.4.2 Function of *Asxl2* in melanocytes

In our analysis of *Asxl2*$^{-/-}$ animals we also noted two phenotypes suggestive of abnormal development of melanocytes. *Asxl2*$^{-/-}$ embryos have fewer pigmented melanocytes visible on their nose at both E15.5 and E18.5 (Fig. 24). Unlike the epicardial phenotypes, which resolve at later stages of development, pigmentation of the fur does not recover before 6 months of age, the longest B6 *Asxl2*$^{-/-}$ were observed. Several possible explanations exist for this phenotype: *Asxl2* may regulate 1) the migration of melanoblasts, 2) their proliferation, 3) their survival, or 4) their terminal differentiation and synthesis of melanin.

Mutant mouse models with defective melanocyte migration typically present with white patches of fur on the belly, limbs, or tail (Liakath-Ali *et al*., 2014). These regions are furthest in distance from the neural tube, the source of neural crest cells that become the melanoblasts. Given that the light fur color in surviving adult *Asxl2*$^{-/-}$ animals manifests evenly across the entire coat (Fig. 25), the defect is probably not due to an error of migration.

The proliferation of melanocytes within the hair follicle is tightly regulated and coincides with the life cycle of the hair follicle. Melanoblasts reside in the bulge region of the follicle. As keratinocytes generate the hair shaft, melanoblasts migrate to the bottom of the follicle, differentiate into melanocytes, and begin synthesizing melanin, transferring it to the hair as it grows. When the hair follicle regresses, the melanocytes undergo apoptosis. Resident melanoblasts proliferate and repopulate the hair follicle at the beginning of the next cycle

(Nishimura, 2011). Proper coat color requires proliferation of melanoblasts. Fewer melanocyte progeny result in grayed fur phenotypes in B6 animals, such as in the bcat^{sta} mutant model where activated β-catenin induces MITF over-expression (Delmas *et al*., 2007; Yajima and Larue, 2008). This phenotype is reminiscent of B6 *Asxl2*$^{-/-}$ animals, suggesting that the number of melanoblasts may be affected. To determine whether this is the case, tissue sections of skin could be immunostained for proliferation in the melanoblast niche, the bulge region of hair follicles.

The survival of melanoblasts progenitors is essential for proper pigmentation. Melanocytes normally undergo apoptosis at the end of each hair cycle. If the apoptotic pathways are disregulated and activate prematurely, a reduced pool of melanocytes results (Wakamatsu *et al*., 1998). Apoptosis of melanoblasts at any point along their migration path or within the hair bulge region would also reduce the population of melanocytes. To distinguish whether apoptosis is misregulated in the *Asxl2*$^{-/-}$ animals, TUNEL staining for cell death could be performed on skin sections, examining melanoblasts in the bulge region and melanocytes in the follicle root. Additionally, TUNEL staining of migrating melanoblasts from E9.5-12.5 can be used to determine whether cell death occurs during migration. Immunostaining of DCT can be used to visualize melanocytes throughout their lifespan, and an antibody is available that performs well for this purpose (Santa Cruz 10451; Dr. Ian Jackson, personal communication 2012).

Finally, the hypopigmentation in B6 *Asxl2*$^{-/-}$ animals could be produced by a defect in melanin synthesis. Melanin is generated in differentiating melanocytes. Could ASXL2 regulate the differentiation of melanoblasts? Melanoblast primary cultures could be isolated from wildtype and *Asxl2*$^{-/-}$ neonatal mouse skin to test this hypothesis (Sviderskaya *et al*., 1997). These cells differentiate gradually over a period of 2-3 weeks, and distinct marker expressions are known at each step of differentiation. The accumulation of melanin can be observed in

culture and assayed biochemically (Hu, 2008). These cultures can also be used to directly test the proliferation abilities of melanoblasts.

V. ADDITIONAL SEX COMBS-LIKE 1 IS REQUIRED FOR NORMAL EYE AND PALATE DEVELOPMENT

5.1 Abstract

Additional sex combs-like 1 (ASXL1) is a chromatin factor that functions with multiple Polycomb Group (PcG) members. PcG proteins regulate many important developmental processes, including those in the eye and palate, by altering chromatin states. We found that *Asxl1* is required for normal development of both tissues. The phenotypes observed in *Asxl1*^{tm1a} mice bear similarities to those observed for other *Asxl1* mutant mice strains as well as human Bohring-Opitz Syndrome.

5.2 Introduction

Additional sex combs-like 1 (*Asxl1*) interacts with multiple members of the PcG epigenetic regulators. Most PcG proteins regulate gene expression at the level of chromatin via posttranslational modifications to histone tails (reviewed in Steffen and Ringrose, 2014). These modifications alter the chromatin configuration into repressive states, thereby affecting transcriptional activity of target genes. One PcG complex, PRC1, can induce chromatin compaction independently of histone modifications (Eskeland *et al*., 2010). ASXL1 belongs to the PcG PR-DUB complex, where it is required for the removal of monoubiquitin from histone H2AK119 by BAP1 (Scheuermann *et al*., 2010). PR-DUB antagonizes H2A ubquitination generated by PRC1. Although PRC1's ubiquitinase activity is required for gene repression, the removal of this same mark by PR-DUB is also required for repression (Endoh *et al*., 2012; Scheuermann *et al*., 2012). Thus the proper balance of H2AK119ub1 versus H2AK119 is critical for proper repression. In addition to its function in H2A deubiquitination, ASXL1 also interacts with EZH2 and SUZ12 of the PRC2 complex, and is required for PRC2 to generate the repressive histone H3K27me3 mark (Gelsi-Boyer *et al*., 2012).

Asxl1 is expressed broadly during development (Fisher *et al*., 2006). It is highly expressed in hematopoietic cells and has numerous roles there (Fisher *et al*., 2006; Abdel-Wahab *et al*., 2013; Wang *et al*., 2013). Loss of *Asxl1* in mice is associated with impairment of differentiation in both the lymphoid and myeloid blood cell lineages (Fisher *et al*., 2010b; Wang *et al*., 2013; Abdel-Wahab *et al*., 2012). Mutations to human *ASXL1* are frequently found in cancers of the myeloid lineages, and are predictive of aggressive cancers with poor prognosis (Gelsi-Boyer *et al*., 2012). Germline mutations of *ASXL1* cause the congenital disorder Bohring-Opitz syndrome (BOS). Individuals with BOS have severe psychomotor and intellectual disability, craniofacial abnormalities, and most die during early childhood (Hoischen *et al*., 2011).

To date four different mutant mouse strains have been reported for *Asx1l,* described in Table IV (Fisher *et al*., 2010b; Abdel-Wahab *et al*., 2013; Wang *et al*., 2014; McGinley *et al*., 2014). All four alleles cause late fetal or early postnatal lethality for most animals, with reduction in body weight. Hematopoietic defects were found in all 3 strains examined for them. *Asxl1*$^{\Delta/\Delta}$ and *Asxl1:nlacZ* have severe myelodysplasia due to impaired differentiation of myeloid progenitors. Both show changes to hematopoietic stem cell (HSC) populations with impaired self-renewal. In contrast, *Asxl1*^{tm1Bc} animals exhibit mild lymphoid differentiation defects, but not changes to the myeloid lineage or HSC progenitors. In addition to hematopoietic defects, all *Asxl1*$^{-/-}$ strains exhibit anopthalmia, a severe early defect in eye development. Homeotic skeletal transformations, cardiac, lung, and craniofacial defects have also been reported in some strains. Here we report data showing that *Asxl1*$^{tm1a/tm1a}$ animals exhibit the absence of eyes and cleft lip/palate, as reported for other *Asxl1*$^{-}$ alleles.

5.2.1 Major events and epigenetic factors in eye development

The mammalian eye is a complex organ that begins developing at E8 in the mouse (reviewed in Graw, 2010). Two lateral bulges form on the right and left side of the diencephalon at E8, becoming the optic vesicles. The optic vesicles grow towards the surface ectoderm between E8 and E9 (Chow and Lang, 2001). The optic vesicles then induce the formation of the lens placode from surface ectoderm on E9. The lens placode invaginates beginning at E10, pushing the optic vesicle inward to form a two-layered optic cup (Graw, 2010). The inner layer of the cup becomes the sensory retina, generating the light-sensing cells of the eye, whereas the outer layer becomes the retinal pigmented epithelium (Martinez-Morales *et al*., 2004). The lens placode separates from the surface ectoderm and becomes the lens and cornea. The eye also receives contributions from migratory neural crest cells around E12, which become the stroma of the cornea (Shaham *et al*., 2012).

During eye development the transcription factor (TF) PAX6 plays critical roles. PAX6 operates near the top of a hierarchy of eye-determining TFs, including RX, SIX3, LHX2, and OPTX2 (Zuber *et al*., 2003). The expression of *Pax6*'s homolog is sufficient to drive formation of ectopic eyes in Drosophila imaginal discs (Kumar and Moses, 1997). Early eye TFs are expressed broadly throughout the entire eye domain of the forebrain. Sonic hedgehog signaling from the underlying prechordal plate mesoderm causes the repression of Pax6 and other downstream factors in the medial ventral forebrain (Fuhrmann, 2008; Shaham *et al*., 2012). As differentiation proceeds the early eye TFs become partitioned in their expression and regulate different processes. Morphogenesis of the optic cup is controlled by RX. Three lineages of progenitors arise, which are regulated primarily by one or more of the early eye TFs: optic stalk progenitors, PAX2, VAX1, and VAX2; pigmented retina, MITF; sensory retina, VSX2 (Shaham

et al., 2012). PAX6 regulates the proliferation versus differentiation of eye progenitors (Philips *et al*., 2005).

PcG and TrxG proteins have critical functions in the developing eye. In Drosophila, *Ubx*, *sine oculis* (*so*), *twin of eyeless* (*toy*), *rbf1*, *hth*, and *tsh* are all PcG targets in the developing eye (Schuettengruber *et al*., 2007; Collins and Moon, 2013; Janody *et al*., 2004). In a screen for genes needed for Drosophila photoreceptor differentiation, multiple PcG and TrxG members were found: *kohtalo*, *skuld*, *brahma*, *trithorax*, *Enhancer of zeste*, and *Polycomb* (Janody *et al*., 2004).

Pax6 appears to be a PcG target gene in eye and non-eye tissues. In Drosophila PcG proteins repress the homologs of *Pax6* before eye development commences and in haltere/third leg imaginal discs (Schuettengruber *et al*., 2009). Upon the inactivation of the PRC2 component EZH2 in mouse hearts, *Pax6* is upregulated 49-fold (He *et al*., 2012). Further, mice mutant for *Rybp,* which encodes a PcG-associated protein, exhibit altered *Pax6* expression in the eye (Pirity *et al*., 2007).

Interestingly, RYBP interacts with RING1 (Garcia *et al*., 1999), the PcG protein that catalyzes H2A ubiquitination, as well as with H2Aub1 (Arrigoni, *et al*., 2006). Additionally, Both *Ring1*, and *Rybp* mutant mice exhibit abnormal anterior eye formation (Lorente *et al*., 2006; Pirity *et al*., 2007). *Rybp* mutant mice exhibit retinal coloboma and abnormal cornea and lens development (Pirity *et al*., 2007). These proteins regulate H2A ubiquitination, along with ASXL1. Thus both histone methylation and ubiquitination activities are essential for eye development.

5.2.2 Major events and epigenetic factors in palatogenesis

The palate is located in the roof of the mouth, separating the oral and nasal cavities. The palate is a compound tissue that forms in two stages: primary and secondary palatogenesis (reviewed in Bush and Jiang, 2012). During primary palatogenesis the medial frontonasal prominence fuses with the maxillary processes on the left and right side of the face at E10.5 (Lane and Kaartinen, 2014; Smith *et al*., 2012). These prominences are bulges of ectodermally-lined head mesenchyme derived from mesoderm and neural crest cells.

Secondary palatogenesis begins around E11 when primordia form on the inner surface of the maxillary processes (Gritli-Linde, 2007). These primordia are derived from neural crest cells and become the palatal shelves, which generate both the bony hard palate and muscular soft palate. The palatal shelves proliferate and lengthen vertically within the oral cavity between E12.5-E14 (Gritli-Linde, 2007). From E14.5-E15.5 the palate shelves undergo elevation and move upwards away from the tongue (Bush and Jiang, 2012). The shelves continue growing horizontally towards the midline and fuse between E15 and E16 (Dixon *et al*., 2011). Failure of the palate shelves to grow, elevate, or fuse during secondary palatogenesis results in cleft palate. Cleft lip and anterior cleft palate are generally linked to defects in primary palatogenesis, although cleft lip and palate of all types co-occur frequently with each other and are relatively heterogeneous conditions (Dixon *et al*., 2011).

Anterior-posterior patterning of the palate plays important roles in its development. All processes of palatogenesis generally begin in the anteromedial region of the palate, then move towards the anterior and posterior ends simultaneously. A network of transcription factors controls these processes and is expressed in unique domains along the A/P axis (Smith *et al*., 2012). Two major TFs are MSX1 and TBX22. MSX1 is restricted to anterior domains by Hoxa2

expression, whereas TBX22 is restricted to the posterior palate by BMP4 (Fuchs *et al*., 2010). Wnt5a is required to generate an A/P gradient of BMP4 that is highest in the anterior palate and patterns the expression of several TFs in addition to TBX22 (He *et al*., 2008). Perturbations of the A/P identity of palate tissues results in cleft palate defects.

A variety of PcG factors have been implicated in palate development. Cleft palate has been reported in *Phc1*, *Mel18*, and *Bmi1* mutant mice, although their specific role in the palate has not yet been investigated (Isono *et al*., 2005; Akasaka *et al*., 2001). Each of these components belong to PRC1, which generates the H2AK119ub1 mark antagonized by ASXL1. *Jarid2* is expressed strongly in epithelial cells lining the palatal shelves before their fusion (Scapoli *et al*., 2010). Upon fusion, expression of *Jarid2* is lost, suggesting a specific role in regulating the fusion process (Scapoli *et al*., 2010). PHF8 is a demethylase of histone H4K20me1, H3K9me1/2, and H3K27me2 (Laumonnier, 2005). Truncating mutations of *PHF8* lead to cleft lip/palate and X-linked mental retardation in humans (Laumonnier, 2005). MSX1 is a homeoprotein expressed in many developing tissues including the palate and is downregulated upon differentiation. A critical function of MSX1 is the recruitment of PcG complexes to target genes (Wang *et al*., 2011). *Msx1*$^{-/-}$ animals exhibit cleft palate with high penetrance (Wang *et al*., 2011).

Finally, one PcG target gene has been shown to regulate palate development. MEIS2 is homeobox TF and cofactor of other homeotic TFs (Kondo *et al*., 2014). Mutation to *Meis2* results in cleft lip and palate among other craniofacial defects (Crowley, 2010). The tissue-specific expression of *Meis2* in the developing forebrain is tightly regulated by PcG proteins, and its functions in palate may be as well (Kondo *et al*., 2014).

Here we present data that adds to the existing literature on the role of *Asxl1* in eye and palate development. We find that *Asxl1*$^{-/-}$ animals have abnormal eyes with 100% penetrance, and have cleft palate and/or lip with partial penetrance.

Table IV: EYE AND PALATE DEFECTS REPORTED IN *ASXL1* MUTANTS

Asxl1 mutant	Nature of allele	Genetic background	Eye phenotype reported	Palate phenotype reported	Reference
Asxl1^{tm1Bc}	Insertion of PGK-neomycin cassette into exon 5. Premature stop codons at AA 90 predicted to induce nonsense decay or produce truncated protein.	129; C57BL/6J hybrid, backcrossing to B6/J.	2/2 have reduced or absent eyes at E12.5. Surviving adults missing one or both eyes with incomplete penetrance.	Not reported.	Fisher *et al*., 2010a. Fisher *et al*., 2010b. Fisher, 2004.
Asxl1^{fl} Germline *Asxl1*$^{\Delta/\Delta}$ generated by crossing to EIIa-Cre mice.	Conditional allele. LoxP sites flanking exons 5-10. FRT sites flanking neomycin cassette inserted upstream of exon 5.	129/SvEv;C57BL/6 hybrid. Backcrossed to C57BL/6 for 6 generations.	12/12 *Asxl1*$^{\Delta/\Delta}$ have microphtlamia /anophthalmia at E19.5.	5/12 *Asxl1*$^{\Delta/\Delta}$ have cleft palate.	Abdel-Wahab *et al*., 2013.
Asxl1:nlacZ/nGFP	Knock-in of nlacZ/nGFP cassette into exon 1, removing *Asxl1* start codon.	129/Sv; C57BL/6 hybrid.	Absent eyes in adult animals, E15.5 and E18.5 fetuses.	Not reported.	Wang *et al*., 2014.
Asxl1^{tm1a}	Insertion of lacZ/neomycin cassette between exons 3 and 4. Splice acceptor and polyadenylation sequence predicted to produce fusion transcript of exons 1-3 and cassette only.	C57BL/6 NTac; C57BL/6J hybrid, bred to C57BL/6 NTac.	3/3 have reduced or absent eyes at E12.5.	2/5 cleft lip, 4/5 cleft palate at E18.5.	McGinley *et al*., 2014. EUCOMM strain 03996.

5.3 Results

5.3.1 *Asxl1* is required for eye development

During our studies of the *Asxl1*$^{-/-}$ heart, we noted that mutant embryos had abnormal or missing eyes at E18.5 (Fig. 7b). We examined *Asxl1*$^{-/-}$ embryos at E12.5 to determine whether eye development was perturbed at this timepoint. By E12.5 the wildtype eye has formed a bilayered optic cup attached by the optic stalk to the brain. The lens has formed and detached from the overlying surface ectoderm, and neural crest cells are migrating into the anterior eye. All *Asxl1*$^{-/-}$ eyes we observed were abnormal at E12.5. Embryos were either missing visible eyes entirely (Fig. 26d, Fig. 27) or had small malformed eyes (Fig. 26e-f, Fig. 27). Three of six *Asxl1*$^{-/-}$ eyes had a small optic cup. In these eyes the sensory retina layer is particularly thin in comparison to wildtype (Fig. 27). In 2/6 *Asxl1*$^{-/-}$ eyes, no discernible eye tissue could be identified, and no bulge indicative of an optic stalk was found on the diencephalon. It appears that in these eyes early induction of the eye has failed. Where present the optic stalk is thinner and shorter in *Asxl1*$^{-/-}$ eyes, causing some eyes to be located more medially away from the surface ectoderm than is normal (Fig. 27).

We also examined *Asxl2*$^{-/-}$ eyes to determine whether ASXL2 may also regulate eye development. Analysis of histological sections of 3 wildtype and 4 *Asxl2*$^{-/-}$ E18.5 fetuses revealed the *Asxl2*$^{-/-}$ eyes were either comparable to wildtype or have subtly smaller lens and retinal layers. The rare surviving B6 *Asxl2*$^{-/-}$ have smaller eyes at P21 and 2 months of age (Fig. 25).

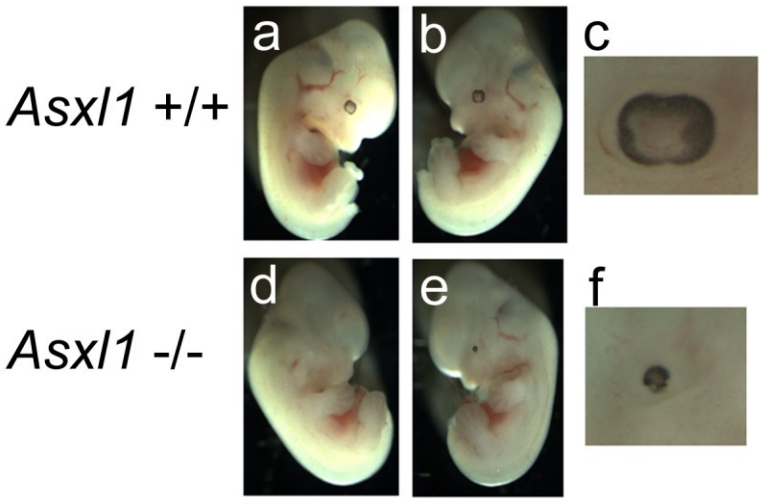

Figure 26: *Asxl1*$^{-/-}$ embryos have abnormal eyes at E12.5.

(a-f) Whole mount *Asxl1*$^{+/+}$ (a-c) and *Asxl1*$^{-/-}$ (d-f) E12.5 embryos. Right and left side of same embryo shown. Wildtype embryos have large eyes with 4-lobed retinal pigmented epithelium visible (a-b). (c) Higher magnification of eye shown in (b). *Asxl1*$^{-/-}$ embryos have either no visible eye tissue (d) or small misshapen eyes (e). (f) Higher magnification of eye shown in (e). Photographs: Zane Deliu.

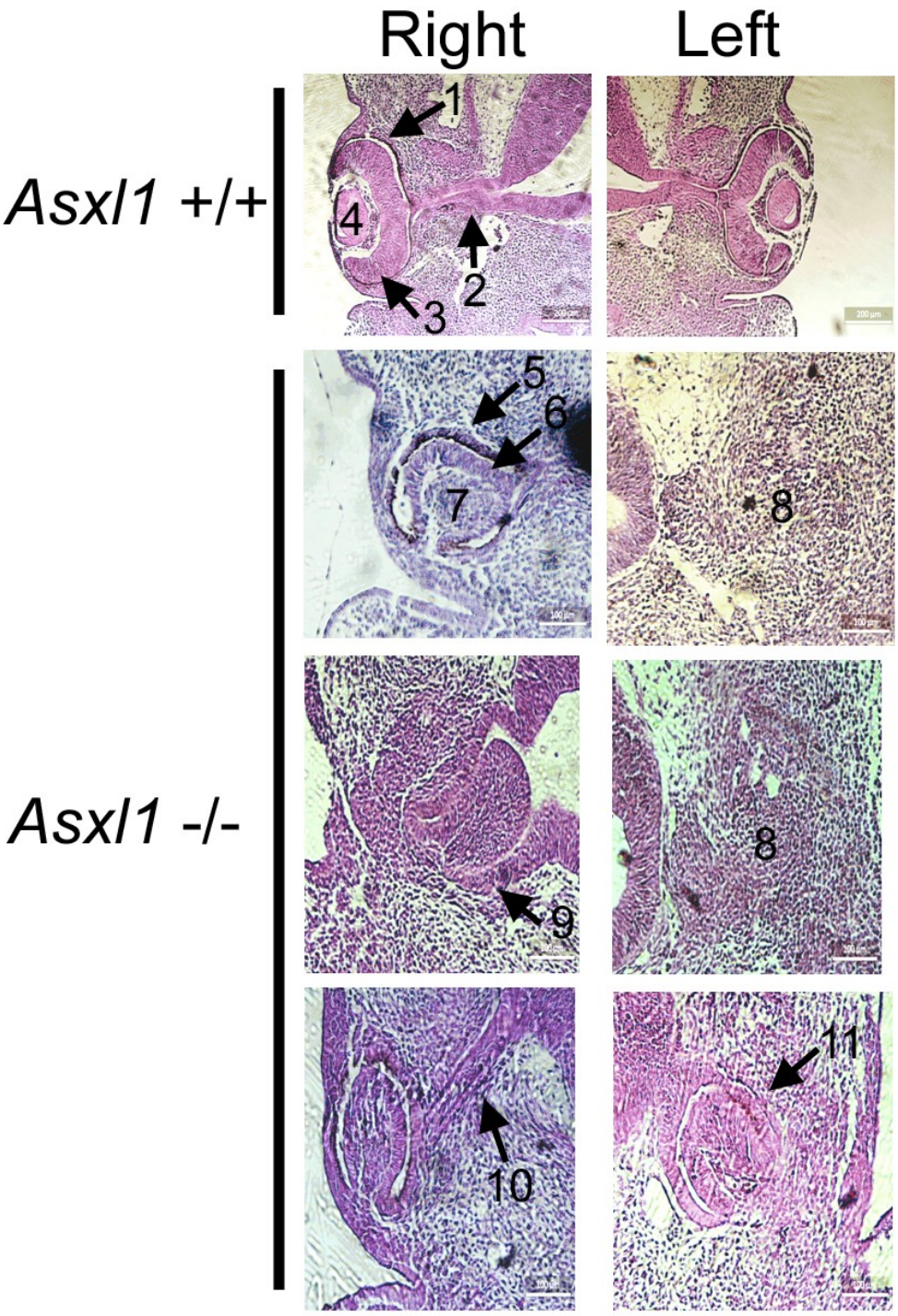

Figure 27: *Asxl1*$^{-/-}$ embryos have abnormal or missing eyes at E12.5.

H&E staining of frontal sections through eyes of 1 *Asxl1*$^{+/+}$ and 3 *Asxl1*$^{-/-}$ littermate embryos at E12.5. *Asxl1*$^{+/+}$ have normal pigmented retinal epithelium (1), optic stalk (2), sensory retina (3),

and lens (4). *Asxl1*$^{-/-}$ eyes had variable abnormal morphology. 3/6 *Asxl1*$^{-/-}$ eyes consisted of a small optic cup with pigmented retinal epithelium (5), sensory retina (6), and lens (7) present. The sensory retina (6) in these animals was notably thinner than in wildtype and the lens was misshapen and composed of loose mesenchymal-appearing cells (7). 2/6 *Asxl1*$^{-/-}$ eyes examined had no discernible eye tissue (8) nor optic stalk. 1/6 *Asxl1*$^{-/-}$ eyes had no optic stalk and misshapen optic cup with no lens (9). When present the optic stalk was thinner than wildtype (10) or very short, resulting in a small optic cup far from the surface ectoderm (11). Histology and photographs: Zane Deliu.

5.3.2 *Asxl1*$^{-/-}$ fetuses display cleft lip and palate with incomplete penetrance

Cleft palate is a frequent finding in Bohring-Opitz Syndrome and has been reported in one other *Asxl1*$^{-/-}$ mouse strain (Table IV). We examined *Asxl1*$^{-/-}$ animals to determine whether they are also deficient in palatogenesis.

Primary and secondary palatogenesis are complete by E16.5. We examined fetuses at E18.5 and found cleft lip in 2/5 *Asxl1*$^{-/-}$ animals (Fig. 28b, Fig. 7b). One animal had a deep bifurcation in the medial upper lip (Fig. 28b), and another had a bilateral cleft with misshapen frontomedial nasal prominence (Fig. 7b). We also identified 1/5 *Asxl1*$^{-/-}$ animals with an elongated proboscis-like nose and central single eye, resembling cyclopia (Fig. 28a-b).

To determine whether the palate had normally closed in these animals, we examined serial sections through the head of 5 *Asxl1*$^{-/-}$ at E18.5. *Asxl1*$^{+/-}$ and wildtype animals had normal elevation of the palatal shelves away from the tongue, and fusion at the midline throughout the anterior-posterior extent of the palate (Fig. 29a). In contrast, 4/5 *Asxl1*$^{-/-}$ had failure of the palate shelves to elevate and/or fuse (Fig. 29b).

We also evaluated palate development in *Asxl2*$^{-/-}$ fetuses at E18.5 to ascertain whether ASXL1 and ASXL2 have overlapping roles in this tissue. Three *Asxl2*$^{-/-}$ and three wildtype E18.5 heads were examined using frontal serial sections. Unlike *Asxl1*$^{-/-}$ fetuses, *Asxl2*$^{-/-}$ have no major defects in elevation or fusion of the palate shelves along the anteroposterior extent of the palate. However, processing artifacts in these samples prevented the analysis of whether subtle fusion defects might be present.

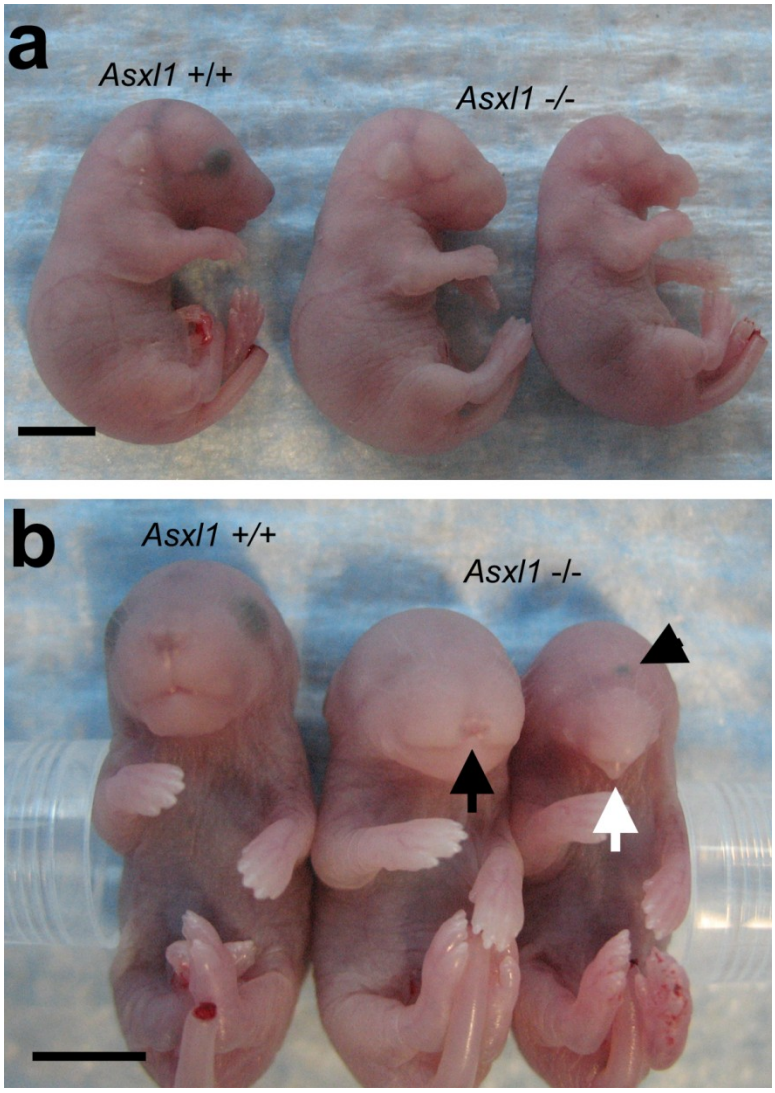

Figure 28: *Asxl1*$^{-/-}$ exhibit cleft lip and craniofacial abnormalities at E18.5.

(a-b) Wildtype and *Asxl1*$^{-/-}$ littermates recovered at E18.5. The same embryos are shown in both panels. 2/5 *Asxl1*$^{-/-}$ animals had cleft lip (black arrow). 1/5 *Asxl1*$^{-/-}$ had a misshapen proboscis-like nose (white arrow) with a single small eye in the center of the face above the nose (arrowhead). Scale bar: 5 mm.

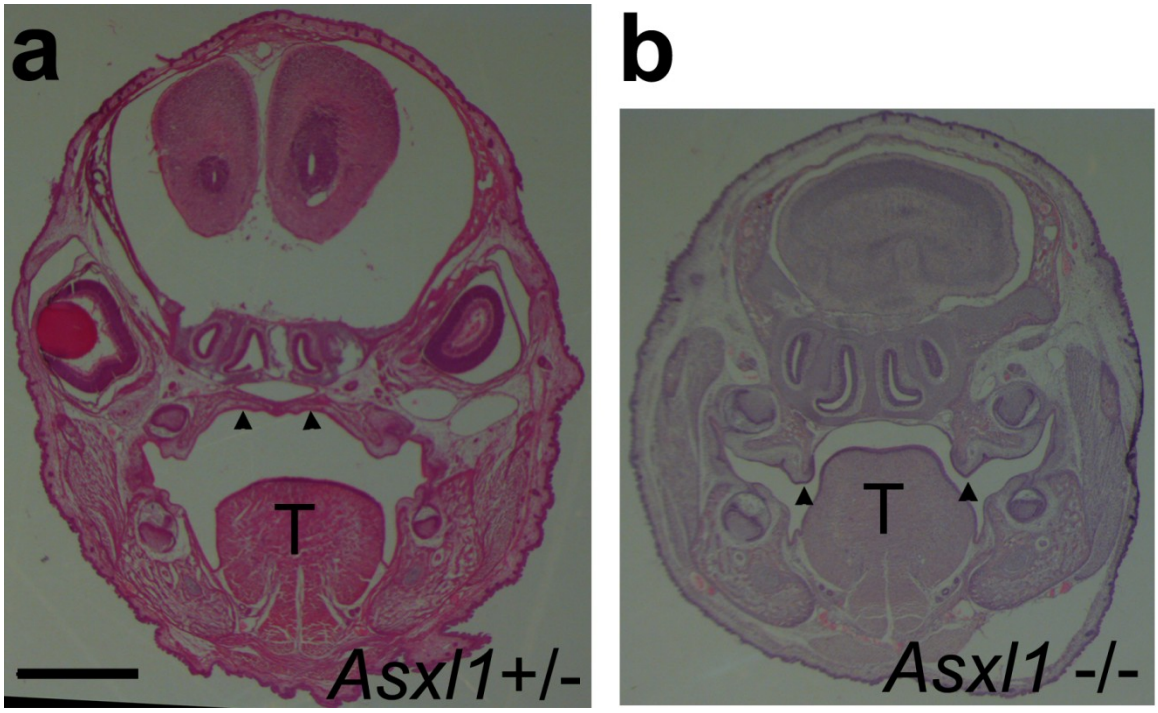

Figure 29: *Asxl1*$^{-/-}$ exhibit cleft palate at E18.5.

(a-b) H&E staining of frontal sections through *Asxl1*$^{+/-}$ (a) and *Asxl1*$^{-/-}$ (b) heads at E18.5. (a) *Asxl1*$^{+/-}$ and wildtype animals had normal fused palatal shelves (arrowheads). (b) 4/5 *Asxl1*$^{-/-}$ fetuses had cleft palate defects ranging from failure to elevate the palatal shelves (shown, arrowheads) to failure to fuse. T: tongue.

5.4 Discussion

5.4.1 Function of *Asxl1* in the developing eye

We find that *Asxl1* is a critical early regulator of mouse eye development. *Asxl1*$^{-/-}$ embryos exhibit variable eye phenotypes ranging from complete failure of the optic cup to form to a small misshapen optic cup with lens. Clinically these conditions are known as anopthalmia or micropthalmia. In the most severe cases, these defects may be caused by failure of the optic vesicles to be induced from the diencephalon. In the milder, yet still severely affected embryos, the smaller optic cup and stalk may be caused by a failure of these structures to proliferate or be maintained. To distinguish between these possibilities histological analyses of embryos during eye induction between E8-E9 should be performed. If eye structures are found to be induced, but fail to grow, a defect in proliferation may be present.

The observation of cyclopia in one *Asxl1*$^{-/-}$ animal highlights a potential role for ASXL1 in regulation of *Pax6* expression. Cyclopia is caused by an early defect in patterning the forebrain into a bilateral structure. This process requires the repression of *Pax6* and other early eye TFs in the midline of the forebrain. *Pax6* is a PcG target and is regulated by histone methylation and ubiquitination activities that ASXL1 regulates. Thus, it would be particularly interesting to determine whether *Pax6* is misregulated in *Asxl1*$^{-/-}$ eyes.

In contrast to the severe eye defect caused by loss of *Asxl1*, we found B6 *Asxl2*$^{-/-}$ animals to have mostly normal eyes at E18.5. Surviving adults have micropthalmia with a thickened ring of skin around the eyes (Fig. 25). Thus, ASXL1, but not ASXL2 is required for early eye formation.

5.4.2 Function of *Asxl1* in palatogenesis

In addition to eye defects, we found cleft lip and/or palate defects in 80% of *Asxl1*$^{-/-}$ mice. Cleft palate was also reported in 42% of *Asxl1*$^{\Delta/\Delta}$ fetuses (Abdel-Wahab *et al*., 2013). These

defects were not reported in two other *Asxl1* mutant alleles, possibly because those animals were maintained on a mixed genetic background (Fisher, 2004; Wang *et al*., 2014). Another possibility is that these alleles have some residual transcript or alternative splicing that escapes the effect of the insertional cassettes used to disrupt transcription. Defects in both the eye and palate have been reported for other mutant alleles of *Asxl1* (Table IV). Severe eye defects were found at nearly 100% penetrance in animals carrying any of the four mutant alleles. Palate defects were found in animals bearing two of the four mutant alleles with 42-80% penetrance (Abdel-Wahab *et al*., 2013; McGinley *et al*., 2014). It is intriguing that the *Asxl1*$^{-/-}$ lines reporting palate defects were both in an inbred C57BL/6 genetic background, whereas the two lines without palate defects are in C57BL/6;129 mixed genetic backgrounds (Table IV). This may be an effect of genetic background on phenotype presentation, as mouse mutants in inbred backgrounds typically have more severe disease phenotypes than in mixed genetic backgrounds (Hamilton and Yu, 2012).

The palate defects observed range from mild failure to fuse at the midline of the secondary palate to severe failure to elevate the palate shelves (Fig. 29). The failure of shelf elevation may be related to general craniofacial defects also observed in these mice, as elevation is driven by morphogenetic movements of the entire face and jaw (Moxham, 2003). The failure of fusion may reflect a role for ASXL1 in maintaining JARID2-mediated PRC2 target gene repression, as JARID2 is highly expressed in palatal epithelial seam cells and regulates their fusion (Scapoli *et al*., 2010).

Our examination of *Asxl2*$^{-/-}$ fetuses suggests that ASXL2 is not required for palate elevation or fusion. Regulation of palate elevation and closure is not shared between ASXL1 and

ASXL2. This divergence might be due to differential expression of the two homologs in the palate, or different interacting partners.

5.4.3 Comparison of mouse *Asxl1* mutant phenotypes and Bohring-Opitz syndrome

Bohring-Opitz syndrome (BOS) is a rare developmental disorder caused by *de novo* mutation to *ASXL1* or *ASXL3* (Hoischen *et al*., 2011; Bainbridge *et al*., 2013). BOS causes early childhood lethality, intrauterine growth retardation and failure to thrive, brain abnormalities, craniofacial defects, and a characteristic posture caused by psychomotor defects (Russell and Graham, 2013). Several of the phenotypes observed in BOS patients have also been found in *Asxl1*$^{-/-}$ mice. *Asxl1*$^{-/-}$ mice have severe early eye defects that result in small degraded or missing eyes with nearly 100% penetrance. BOS patients have less severe eye phenotypes: prominent bulging eyes (100%), myopia (87%), retina/optic nerve defects (62%), strabismus (50%), and ocular hypertelorism (55%) (Russell and Graham, 2013). It is possible that the relatively milder phenotypes in BOS may indicate that one copy of *ASXL1* is sufficient to perform its duty in the eye, or may be due to functional redundancy between *ASXL1*, *ASXL2*, and *ASXL3*. Alternatively, *ASXL1* may be dispensable for early eye development in humans.

Cleft palate and cleft lip are also reported in 33-62% of BOS patients (Russell and Graham, 2013; Oudesluijs *et al*., 2006). Most individuals with BOS have abnormal structure of the palate, including broad alveolar ridges and a high narrow palate (87%), which is a mild, asymptomatic version of cleft palate (Russell and Graham, 2013). Micrognathia/mandibular hypoplasia is found in 89-100% of BOS patients and 33% of one *Asxl1*$^{-/-}$ mouse line (Russell and Graham, 2013; Oudesluijs *et al*., 2006; Abdel-Wahab *et al*., 2013). Taken together, these data indicate that *Asxl1*$^{-/-}$ mice recapitulate at least some of the phenotypes observed in BOS, and may be useful as an experimental model of the disorder. Generating mouse models that mimic the

mutations identified in BOS may help us dissect the function of *ASXL1* in different developmental processes, and perhaps better predict the disease outcomes of *ASXL1* mutations in BOS patients.

VI. GENERAL DISCUSSION

6.1 ASXL proteins play divergent roles in developing tissues

6.1.1 Divergent functions of ASXL1 and ASXL2

This work describes some of the developmental functions of the epigenetic regulators ASXL1 and ASXL2. After examining the development of *Asxl1*$^{-/-}$ and *Asxl2*$^{-/-}$ embryos, I conclude that ASXL family proteins play divergent roles in development. *Asxl1*$^{-/-}$ embryos have growth restriction, failure of eye development, craniofacial anomalies, immature lungs, and endocardial cushion defects of the heart. In contrast, *Asxl2*$^{-/-}$ embryos have only mild growth restriction, melanocyte defects, and defects in the myocardium and epicardium of the heart. Both mutant strains were analyzed in a C57BL/6 inbred genetic background, therefore I propose these phenotypic differences are due to true divergent functions of ASXL1 and ASXL2 in different developmental contexts, not the effects of strain-specific modifiers.

What is the origin of such different functions among homologs sharing the same functional domains? The three mammalian *ASXL* homologs likely arose by gene duplication. Gene duplication is an essential force during the evolution of multicellular organisms (Raes and Van de Peer, 2003). Duplication allows genes to evolve new functions, since having one or more backup copies allows otherwise harmful mutations to be retained (VanderSluis *et al*., 2010). New functions may evolve that only occur in specific tissues or contexts, allowing for the evolution of a great diversity of cellular types and functions.

Often the functions of duplicate genes become restricted to specific tissues or contexts during evolution, termed subfunctionalization (Force *et al*., 1999). This is due to the greater likelihood of neutral or loss of function mutations, either in the regulatory elements or coding regions, which then generate tissue-restricted expression patterns or different protein

interactions, respectively (Eckardt, 2006). Specialization is an important force in developmental biology: tissue-specific expression patterns and functions among developmental gene family members occur frequently.

The expression patterns of ASXL1 and ASXL2 are divergent and correspond to tissues affected in mutants thereof. *Asxl1* is highly expressed in the hematopoietic system, where it is a critical regulator of hematopoietic progenitor proliferation and differentiation. *Asxl2* is highly expressed in the heart, where it regulates left ventricle size and contractile function (McGinley *et al*., 2014; Lai *et al*., 2012). The divergent roles among ASXL1 and ASXL2 may therefore represent restriction of the more ancestral functions of Asx to specific tissue lineages, namely the hematopoietic and myocardial lineages. I propose duplication of *Asxl* genes allowed *Asxl1* and *Asxl2* to undergo specialization, serving roles in these lineages independently. During heart development both myocardial and hematopoietic cells come from a common $BRY^{+}/FLK1^{+}$ progenitor which later diverges (Kattman *et al*., 2006; Milgrom-Hoffman *et al*., 2011). The ancestral *Asx-like* gene may have functioned in this common progenitor population, then later the duplicated *Asx-like* genes evolved through subfunctionalization to specialize in derivative lineages. Evolution of either the coding sequence of *Asxl* genes or evolution of the regulatory elements controlling their expression could contribute to the specialized functions of *Asxl* genes. Substituting one homolog for another in different developmental contexts would reveal whether changes to regulatory elements or protein structure are responsible for the divergent functions of ASXL proteins. For example, if *Asxl1* were expressed in the myocardium of *Asxl2*-deficient animals, could ASXL1 substitute for ASXL2 and prevent the overgrowth of the left ventricle observed in $Asxl2^{-/-}$ embryos? If so, this would suggest that the divergent functions are due to differential expression of *Asxl1* and *Asxl2*. If compensation is not found, this would suggest the

divergent functions are due to evolution of the coding sequence and protein conformation between ASXL1 and ASXL2, generating the ability to bind different protein partners.

6.1.2 Conserved functions of ASXL1 and ASXL2

One important aspect of ASXL proteins has been conserved between the homologs: regulation of anteroposterior patterning. In Drosophila *Asx* regulates both activation and repression of *Hox* genes which determine anteroposterior patterning. These functions are conserved in mammalian ASXL proteins, and appear to be non-divergent between *Asxl1* and *Asxl2* as well. Mutation of either gene causes similar anteroposterior patterning defects. Both *Asxl1*$^{-/-}$ and *Asxl2*$^{-/-}$ mice exhibit TrxG-type homeotic transformations in the anterior vertebrae, and PcG-type transformations in the posterior vertebrae (Fisher *et al*., 2010a; Baskind *et al*., 2009). This is suggestive of a role in activating anterior *Hox* genes and repressing posterior *Hox* genes in the paraxial mesoderm, which gives rise to the vertebrae. Therefore, the functions of ASXL1 and ASXL2 in paraxial mesoderm patterning have been mostly conserved.

6.1.3 Conservation and divergence of functional mechanism between ASXL proteins

Studies of the mechanistic functions of ASXL1 and ASXL2 have found a number of overlapping mechanistic functions. Both proteins are required for binding of the PRC2 complex and it's repression of target genes (Abdel-Wahab *et al*., 2013; Lai and Wang, 2013). They are both necessary for maintaining bulk levels of H3K27me3 on chromatin (Abdel-Wahab *et al*., 2013; Lai and Wang, 2013). This effect was observed in the tissues in which ASXL1 and ASXL2 are most highly expressed: hematopoietic cells and the heart, respectively. ASXL2 is specifically required for conversion of H3K27me2 to H3K27me3 broadly in the heart; whether this is the case for ASXL1 in the blood has not been examined (Lai and Wang, 2013). Both

ASXL1 and ASXL2 partner with BAP1 and participate in the PR-DUB complex, which removes monoubiquitin from H2AK119 (Scheuermann *et al*., 2010; Lai and Wang, 2013).

To date few TrxG-interactive roles have been identified for either ASXL1 or ASXL2, despite being members of the Enhancers of trithorax and Polycomb (ETP) group. TrxG-type anterior transformations are found at low penetrance in *Asxl1*$^{-/-}$ and *Asxl2*$^{-/-}$ animals. Additionally, loss of ASXL1 or ASXL2 does not disrupt bulk H3K4me3, the hallmark of TrxG activity, in hematopoietic stem cells or the heart, respectively (Levine *et al*., 2012; Baskind *et al*., 2009; Lai and Wang, 2013). This suggests ASXL's major functions do not involve the TrxG complexes responsible for methylation of H3K4. Whether ASXL regulates other aspects of TrxG activity is not known.

How do ASXL proteins achieve divergent functions? I propose conservation of functional domains has preserved ASXL's interactions with PRC2 and PR-DUB for both ASXL1 and ASXL2, while sequence divergence outside of these domains has allows interaction with different binding partners in different contexts. One sequence divergence between *Asxl1* and *Asxl2* has been shown to effect functional differences in the behavior of these two homologs. ASXL1 contains a heterochromatin protein 1 (HP1) binding domain, but ASXL2 does not (Park *et al*., 2011). In developing adipocytes ASXL1 binds with HP1α and represses lipogenic target genes. In contrast, ASXL2 localizes with activating histone marks to lipogenic target genes and facilitates adipogenesis. Removal of the HP1 binding domain from ASXL1 causes it to enhance adipogenesis as ASXL2 does. Thus, the loss of the HP1 binding domain in ASXL2 appears to have facilitated the divergent and opposing functions of ASXL1 and ASXL2 in adipocytes, perhaps allowing fine-tuning of the regulation of differentiation in these cells.

In addition to different binding partners, it also appears that evolution of the cis-regulatory elements controlling *Asxl1* and *Asxl2* expression contributes to their divergent functions. Being expressed in different tissues allows ASXL1 and ASXL2 to have novel functions therein.

6.2 How does ASXL2 regulate myocardial size?

In the C57BL/6 inbred genetic background, *Asxl2*$^{-/-}$ hearts have thickened interventricular septum and left ventricle wall with high penetrance at the end of fetal development. To determine the cause of this thickening various hypotheses were tested: 1) increased proliferation within the fetal compact myocardium, 2) hypertrophy of cardiomyocytes, 3) skewed proportions of cardiomyocytes versus non-cardiomyocytes, 4) abnormal trabeculation, and 5) increased contribution from the epicardium. Each of these lines of analyses revealed normal development comparable to wildtype animals. Thus, the source of this increase in size remains an unanswered question.

6.2.1 Do migratory cells contribute to increased *Asxl2*$^{-/-}$ LV size?

How to account for this increase in LV size in *Asxl2*$^{-/-}$ hearts? I will address two formal possibilities that may account for this phenotype without changes to fetal proliferation, cell size, or proportions of cell types. First, as no increase in proliferation rates was detected in the enlarged regions, it is conceivable that a population of cells proliferating outside the heart migrates into the *Asxl2*$^{-/-}$ heart and contributes to its greater size. Three migratory cell populations contribute to the heart: epicardium, cardiac neural crest (CNC), and the second heart field (SHF). I argue that contribution from any of these sources is possible but unlikely.

Epicardial cells give rise to mostly fibroblasts and blood vessel cells in the myocardium, however no increases in these cells were observed in the *Asxl2*$^{-/-}$ heart. Epicardial cells rarely

give rise to cardiomyocytes, yet cardiomyocytes and non-cardiomyocytes were found in normal proportions to one another in the *Asxl2*$^{-/-}$. CNC cells are an unlikely source, as they contribute to the outflow tract of the heart and some small nerves of the myocardium, which could not account for the increase in size observed in the LV. One report described a small CNC-derived stem cell population present in the heart, but how these cells contribute to development is not understood (Tamura *et al*., 2011; Tomita *et al*., 2005).

The SHF is multipotent progenitor population that migrates into the heart from E8.5-E12. The SHF joins the cells of the primary heart tube and adds cells of the right ventricular chamber, outflow tract, and small portions of the atria and IVS – not the LV or bulk of the IVS, where the size increase was observed. SHF progenitors could conceivably migrate into the normally FHF-derived LV upon loss of *Asxl2*. If this were the case, it would suggest an over-proliferative or expanded SHF is migrating into the LV. However, when the SHF progenitor pool is expanded by activating Wnt signaling, the OFT and RV enlarge, but not the LV (Rochais *et al*., 2009). This suggests there are repressive signals in the LV myocardium that normally excludes SHF entry into these regions. It is difficult to imagine a scenario in which an expanded SHF could contribute to larger LV, but not RV and outflow tract, which were normal in *Asxl2*$^{-/-}$ hearts.

6.2.2 Does an expanded FHF progenitor pool contribute to *Asxl2*$^{-/-}$ heart?

A second formal possibility that fits with our understanding of the *Asxl2*$^{-/-}$ heart is that an expanded pool of first heart field (FHF) progenitor cells contributes to the greater LV size apparent during fetal development. The FHF is an early-differentiating field of cardiac progenitors that forms the primitive heart tube. As the heart is remodeled by looping and SHF migration, FHF cells contribute primarily to the LV and IVS. These are the same regions found

enlarged in the *Asxl2*$^{-/-}$ heart. I discuss a model here whereby ASXL2 may regulate the pool of FHF progenitors by via interaction with retinoic acid signaling components and/or regulating *Hox* gene expression.

6.2.3 Does ASXL2 regulate FHF or SHF progenitors via RA signaling?

Retinoic acid (RA) is important for limiting the lateral and posterior boundaries of the FHF and SHF (Evans *et al*., 2010). *Raldh2* is expressed in the lateral plate mesoderm along the posterior extent of the cardiac crescent (Hochgreb *et al*., 2003). RA synthesized by RALDH2 in lateral plate mesoderm cells diffuses throughout the cardiac mesoderm in a posterior-to-anterior gradient. Loss of RALDH2 in mouse and zebrafish embryos causes an expansion of the ISL1^{+} cardiac progenitor pool and enlarged hearts (Ryckebusch *et al*., 2008; Sirbu *et al*., 2008). RA signaling inhibits ISL1^{+} progenitor's posterior expansion by repression of FGF8 (Sirbu *et al*., 2008). RA also exerts positive effects on the FHF progenitors by upregulating TBX5 expression in posterior and lateral cardiac mesoderm. TBX5 is required for the normal size of the LV and atria derived from these regions, as *Tbx5* null animals have hypoplastic LV and atria (Bruneau *et al*., 2001). This suggests a dual role for RA: limiting the addition of mesodermal progenitors to the late-migrating SHF pool, and enhancing the growth of FHF progenitors via TBX5. RA signaling may therefore integrate and balance the size of these two types of cardiac progenitors.

These findings demonstrate RA is an important regulator of anteroposterior regionalization and identity in the heart fields, and misregulation of RA can lead to enlargement of structures derived from the FHF. Is there a role for ASXL2 in the regulation of RA signaling? All mammalian ASXL homologs contain a nuclear hormone receptor binding module, used to bind retinoic acid receptors RARα and RARβ (Katoh, 2013). In human cells ASXL1 binds RAR and acts as a coactivator or corepressor in different contexts (Cho *et al*., 2006; Lee *et al*., 2010).

A mouse ASXL2 protein fragment interacts with RA and activates a retinoic acid response element (RARE) luciferase reporter as a coactivator (F. Khan, submitted). Interestingly, full-length ASXL2 does not activate RA signaling, suggesting that ASXL2 may function as either a coactivator or corepressor, depending on its binding partners and conformation in a given cellular context. It is conceivable that ASXL2 acts as a coactivator for RA in the FHF and/or SHF. Loss of *Asxl2* could induce failure of RA signaling to repress FGF8 and thereby limit the number of the posterior cardiac mesoderm progenitors, which then contribute to the enlarged heart observed in fetal stages. Examination of ISL1, FGF8, and TBX5 expression patterns in the hearts of E8-E8.5 *Asxl2*$^{-/-}$ embryos for an expansion of ISL1^{+} SHF or TBX5^{+} FHF cells would reveal whether this hypothesis is supported.

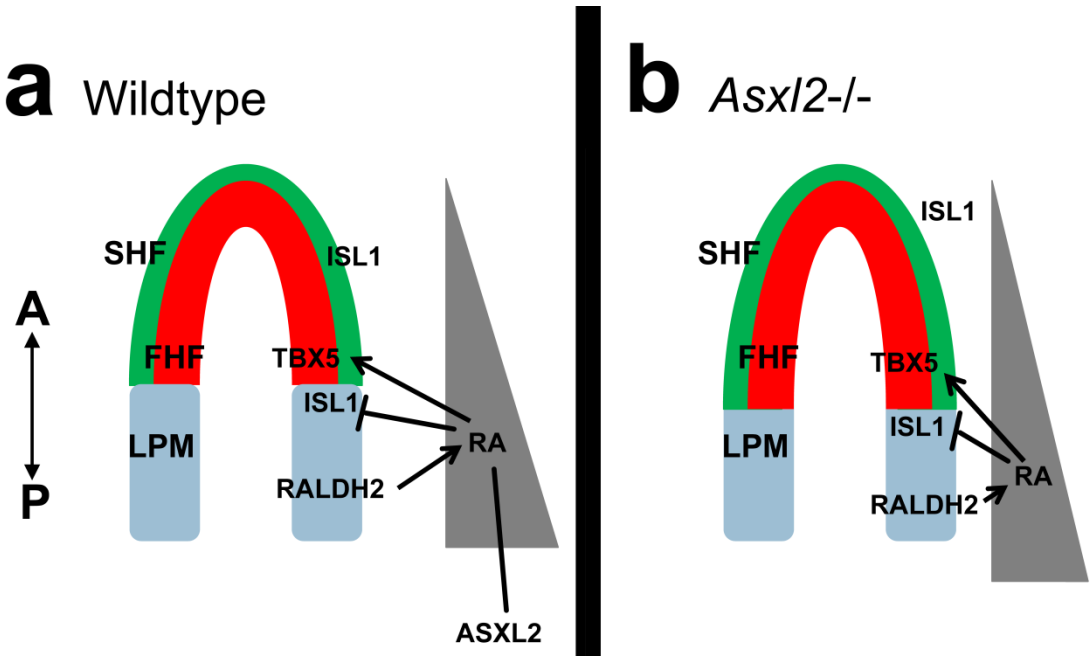

Figure 30: ASXL2 may regulate cardiac progenitor field size by altering retinoic acid signaling gradient.

(a-b) Retinoic acid (RA) signaling gradient patterns the first and second heart fields. $ISL1^{+}$ progenitors are repressed by high levels of RA at the posterior boundary of the cardiac fields. TBX5 in the FHF is positively regulated by moderate RA levels. (b) Loss of *Asxl2* may shift the RA signaling gradient along the A/P axis. A posterior shift in the RA gradient may increase the size of the FHF by extending the TBX5 expression domain posteriorly, converting some lateral plate mesoderm (LPM) into cardiac progenitors via relief of ISL1 repression. SHF: Second heart field.

6.2.4 Does ASXL2 regulate FHF or SHF via *Hox* genes?

ASXL2 might utilize another mechanism for patterning the cardiac progenitor fields with or without RA. *Hox* genes encode homeotic transcription factors that are expressed in specific domains along the anteroposterior axis. RA gradients in the embryo are critical for proper spatiotemporal expression of *Hox* genes (Deschamps and van Nes, 2005). For example, the SHF is patterned by RA-dependent *Hoxb1*, *Hoxa1*, and *Hoxa3* expression in mouse (Bertrand *et al*., 2011). *Hoxb1* is the major *Hox* gene responsive to RA in the SHF. RALDH2 or RA receptor deficient mutants have a loss of $HOXB1^{+}$ cells and the derivative OFT is smaller (Bertrand *et al*., 2011; Ryckebusch *et al*., 2008). *Hoxa3* appears to regulate the FHF progenitor pool. $Hoxa3^{-/-}$ mice exhibit thickening of the left ventricle wall at postnatal day 1 with high penetrance, suggesting a role for *Hoxa3* in regulating the FHF in addition to the SHF (Chisaka and Capecchi, 1991).

Loss of *Asxl2* causes defects in anteroposterior patterning of the somites that are associated with changes in *Hox* gene expression boundaries. Is cardiac mesoderm *Hox* expression, such as *Hoxa3*, perturbed as well? If the expression domain of *Hoxa3* is altered between E7-8, when the FHF is present, an expansion of the $TBX5^{+}/ISL1^{+}$ progenitor region field normally delimited by *Hoxa3* may occur (Bertrand *et al*., 2011). Descendants of $TBX5^{+}$ progenitors are found restricted to the left ventricle and left-facing interventricular septum, and may thereby contribute to the size increases observed therein in the $Asxl2^{-/-}$ heart. *Tbx5* has multiple Hox binding sites, and is regulated by Hox factors during limb development (Nishimoto *et al*., 2014). ASXL2 could be upstream of TBX5 in the FHF by regulating *Hoxa3* gene expression in the heart as a coactivator of RARs, or by recruitment via other factors. *Hoxa3* is a PcG target whose repression requires H3K27me3, a mark maintained by ASXL2 (Lai and Wang,

2013). An examination of the expression of *Hoxa3* and other *Hox* genes in the cardiac mesoderm of *Asxl2*$^{-/-}$ embryos may open interesting avenues of study.

VII. APPENDICES

APPENDIX A. PRIMERS USED FOR GENOTYPING

TABLE V: PRIMERS USED IN GENOTYPING

Genotyping	Primer	Sequence (5'-3')
Asxl2^{-}	wtAQ250	CAAATCTGCCTCATCCTCTC
Asxl2^{-}	AQ480	CTCTCCCATCCACTACTCAG
Asxl2^{-}	In1-11	CCAACCCAACAGTCAGTATG
Asxl1^{tm1a}	gt_ASXL1_for2	AGACCAATATGGCCTGGAACTGAC
Asxl1^{tm1a}	gt_ASXL1_rev	CAGCCTGACCTACAGAGTGAAGAA
Asxl1^{tm1a}	gt_FTR_rev	CCTTCCTCCTACATAGTTGGCAGT
Immortomouse	WT_f	GATCTGCCTGAGGTGTTACTTG
Immortomouse	WT_r	GGATGGCATCACTAGTCATGAC
Immortomouse	tsA_f	AGTCCTCACAGTCTGTTCATGATC

APPENDIX B. PRIMERS USED FOR QUANTITATIVE REAL-TIME PCR ANALYSIS

TABLE VI: PRIMERS USED IN QUANTITATIVE REAL-TIME PCR

Primer	Sequence (5'-3')
β-actin Forward	TCACCCACACTGTGCCCATCTACGA
β-actin Reverse	TGGTGAAGCTGTAGCCACGCT
Asxl1 Forward	TAAAGAGGAGCCCAAAGTCCCG
Asxl1 Reverse	GGCAGGAGGACTCCGTGATG
Asxl2 Forward	CTCCTGAAATGCAGGTGAGA
Asxl2 Reverse	TTGCTTTGGGATCACTTGAG
Asxl3 Forward	CTTCAAAATCCCTGGAAAGTCG
Asxl3 Reverse	ATCTCAGCGCCATCCAGGTC

APPENDIX C. IMMUNOSTAINING CONDITIONS

TABLE VII: IMMUNOSTAINING CONDITIONS

Tissue	Processing	Fixation	Primary antibody	Secondary antibody	Tertiary antibody	Result
Mouse neonate myocytes	ICC	5% formalin 20’	M α cTnT 2 ug/ml NeoMarkers MS-295-PO	H α M IgG-biotin 15 ug/ml	SA-Oregon Green 488 1:200	Cytoplasmic.
E12.5-15.5 heart	IF-P Na-Cit HIER	PFA	Rb α pH3 1:50 Cell Signaling 06-570	D α Rb Texas Red 1:200	--	Nuclear. S phase moderate staining; M phase strong.
E18.5 heart	IF-F	--	WGA-594 1:200 Biotium 29023	--	--	Cell membrane.
E12.5-18.5 heart	IF-P Na-Cit HIER	PFA	Rt α BrdU 1:200	G α Rt FITC 1:200	--	Nuclear.
E17.5 heart	IF-P	PFA	Rb α GATA4 1:50 Santa Cruz sc-9053	D α Rb Texas Red 1:200	--	Nuclear.
E14.5 isolated myocytes	ICC	MeOH:acetone 10’	M α α-actinin 1:100	G α M 488 1:1000	--	Cytoplasmic.
E17.5 heart	IF-P	PFA	G α NKX2.5 1:100	D α G biotin 1:200	SA-DTAF 1:200	Nuclear.
E12.5-E18.5 heart	IHC Whole-mount	PFA Dehydrated in MeOH	Rt α PECAM-1 1:200	G α Rt biotin 1:200	ABC-DAB	Cytoplasmic.
Adult heart	IHC-P No HIER	PFA	M α α-SMA 1:200	G α M biotin 1:400	ABC-DAB	Cytoplasmic. HIER causes nonspecific nuclear signal.

APPENDIX C (continued)

Tissue	Processing	Fixation	Primary antibody	Secondary antibody	Tertiary antibody	Result
E13.5 heart	IF-P TE HIER	PFA	Rb α WT1 1:400	G α Rb biotin 1:200	SA-Cy3 1:200	Nuclear.
E13.5-E17.5 heart	IF-P TE HIER	PFA	Rb α vimentin 1:500	G α Rb biotin 1:200	SA-Cy3 1:200	Cytoplasmic.
E18.5 heart	IF-F	PFA	M α cTnT 1:50	G α M Cy3 1:200	--	Cytoplasmic.
E18.5 heart	IF-F	PFA	Rb α vimentin 1:250	G α Rb 647 1:200	--	Cytoplasmic.
AREC, MEC	ICC	PFA 10’	Rb α WT1 1:400	D α Rb 647 1:200	--	Nuclear.
AREC, MEC	ICC	PFA 10’	Rb α vimentin 1:200	D α Rb 647 1:200	--	Cytoplasmic.
AREC, MEC	ICC	PFA 10’	Rb α PECAM-1 1:500	D α Rb 647 1:200	--	Cytoplasmic.
AREC, MEC	ICC	PFA 10’	Rb α ZO-1 1:200	D α Rb 647 1:200	--	Membrane.
AREC, MEC	ICC	PFA 10’	G α SM22α 1:200	D α G Texas Red 1:200	--	Cytoplasmic.
AREC, MEC	ICC	PFA 10’	M α αSMA 1:500	G α M 488 1:200	--	Cytoplasmic.
AREC, MEC	ICC	PFA 10’	Phalloidin-rhodamine 1:50 Cytoskeleton PHDR1	--	--	Cytoskeletal.
AREC	ICC	PFA 10’	M α β-catenin 1:200	G α M 488 1:200	--	Membrane.
AREC	ICC	PFA 10’	Rb α H3K27me3 1:500	G α Rb biotin 1:200	SA-Cy5 1:200	Nuclear.
E18.5 lung	IF-P Na-Cit HIER	PFA	Rb α SP-C 1:50	G α Rb biotin 1:200	SA-Cy3 1:200	Cytoplasmic.
E18.5 lung	IF-P Na-Cit HIER	PFA	Rb α podoplanin 1:50	G α Rb biotin 1:200	SA-Cy3 1:200	Cytoplasmic.
E18.5 lung	IF-P TE HIER	PFA	Rb α CCSP 1:200	G α Rb biotin 1:200	SA-Cy3 1:200	Cytoplasmic.

Abbreviations: AREC: adult rat epicardial cell line. MEC: Immortalized mouse epicardial cell line. ICC: Immunocytochemistry. IF-P: Immunofluorescence – paraffin sections. IF-F: Immunofluorescence – frozen sections. IHC: Immunohistochemistry. HIER: Heat-induced epitope retrieval 20' at 95°C. Na-Cit: 10mM Sodium-citrate pH 6, 0.05% Tween-20. TE: 10 mM Tris-EDTA pH 9, 0.05% Tween-20. PFA: 4% paraformaldehyde 4°C 8-24 hrs. MeOH: methanol. H: horse. M: mouse. G: goat. Rb: rabbit. D: donkey. SA: streptavidin.

APPENDIX D. CULTURE AND IMMUNOSTAINING OF EPICARDIAL CELL LINES

D.1 Purpose and objective

The culture of epicardial cells is desirable to investigate the role of *Asxl2* and PcG proteins in epicardial cells. Culturing methods for two cell lines were established: immortalized mouse epicardial cells (MEC) and an adult rat epicardial cell line (AREC).

D.2 Materials and methods

For MEC: Immortalized epicardial cells were a generous gift from Dr. Robert Dettman (Northwestern University). MEC were derived from embryonic epicardium from the Immortomouse (Charles River 238 HE) expressing the simian virus 40 (SV40) large tumor T-antigen (TAg). A temperature-sensitive variant of TAg (tsA58) was used that is active at 33°C and unstable at 37°C, under control of the ubiquitous mouse major histocompatability complex *H-2K*^{b} promoter (Jat *et al*., 1991). Interferon-γ (IFNγ) activates the *H-2K*^{b} promoter and is used in culture to induce its activity. MEC were maintained at 33°C in immorto-media (5% FBS (Sigma F6178), 1X insulin-transferrin-selenium (ITS-G, Invitrogen 41400045), 10 U/ml IFNγ (Pepprotech 315-05)). Cells were plated on collagen-coated plastic cell culture dishes (1.5 mg/ml collagen I (BD 354236) in 0.02 N acetic acid), and passaged at 1:6 dilution after 1 minute digestion in 0.05% trypsin.

For AREC: Cells were a generous gift from Dr. David Bader (Vanderbilt University). AREC cells were derived from an epicardial mesothelioma from adult rat (Wada *et al*., 2003; Eid *et al*., 1992). Cells were cultured in DMEM (5% FBS), plated on 1.5 mg/ml collagen, and passaged at 80-90% confluency 1:5 using 1-2 minutes digestion in 0.05% trypsin.

Immunostaining of MEC/AREC was performed as described in Appendix C.

D.3 Results and conclusions

MEC immortalized cells were cultured from passage 11 vial. Cells appeared epithelial in culture and generated a monolayer (Fig. 31a). Rare multi-nucleated cells or cells with vacuoles were observed in passage 11 cells (Fig. 31b). Beginning at passage 14-15 the proportion of cells with abnormal morphology increases to be greater than epithelial-type cells, limiting the usage of this cell line. Varying concentrations of IFNγ were tested from 0-200 U/ml to determine whether greater concentrations of IFNγ could limit the appearance of abnormal/senescent cells. No positive effects were observed. MEC treated with 100-200 U/ml IFNγ appeared unhealthy; 10 U/ml was used for routine culturing. Immunostaining of MEC cells revealed that they express the epicardial transcription factor WT1; vimentin, a general mesenchymal marker; smooth muscle actinin-α (SMAα) and SM22α, two markers of smooth muscle cells; and ZO-1, a marker of epithelial tight junctions (Fig. 31c-g). MEC do not express the endothelial marker PECAM-1 above background (Fig. 31h). These data suggest MEC have an intermediate epithelial phenotype, expressing markers of both epithelial and mesenchymal cells.

AREC cells were cultured from a vial of passage 1 cells. Cells formed epithelial patches at low density (Fig. 32a) and tight epithelial sheets at high density (Fig. 32b). Cultures exhibited epithelial morphology through passage 12, but began accumulating cells with large cytoplasm or mesenchymal morphology beyond this passage number (Fig. 32c). Immunostaining of AREC revealed that they express WT1, vimentin, SMAα, SM22α, and ZO-1, but not PECAM-1 (Fig. 32d-i). Compared to MEC cells, AREC express lower levels of WT1 (Fig. 32c). The cytoskeletal proteins vimentin, SMAα, and SM22α were expressed at higher levels and were arranged in stress-fiber like bundles (Fig. 32e-g). Some AREC did not express SM22α, suggesting there may be heterogeneity of differentiation status in these cultures (Fig. 32g).

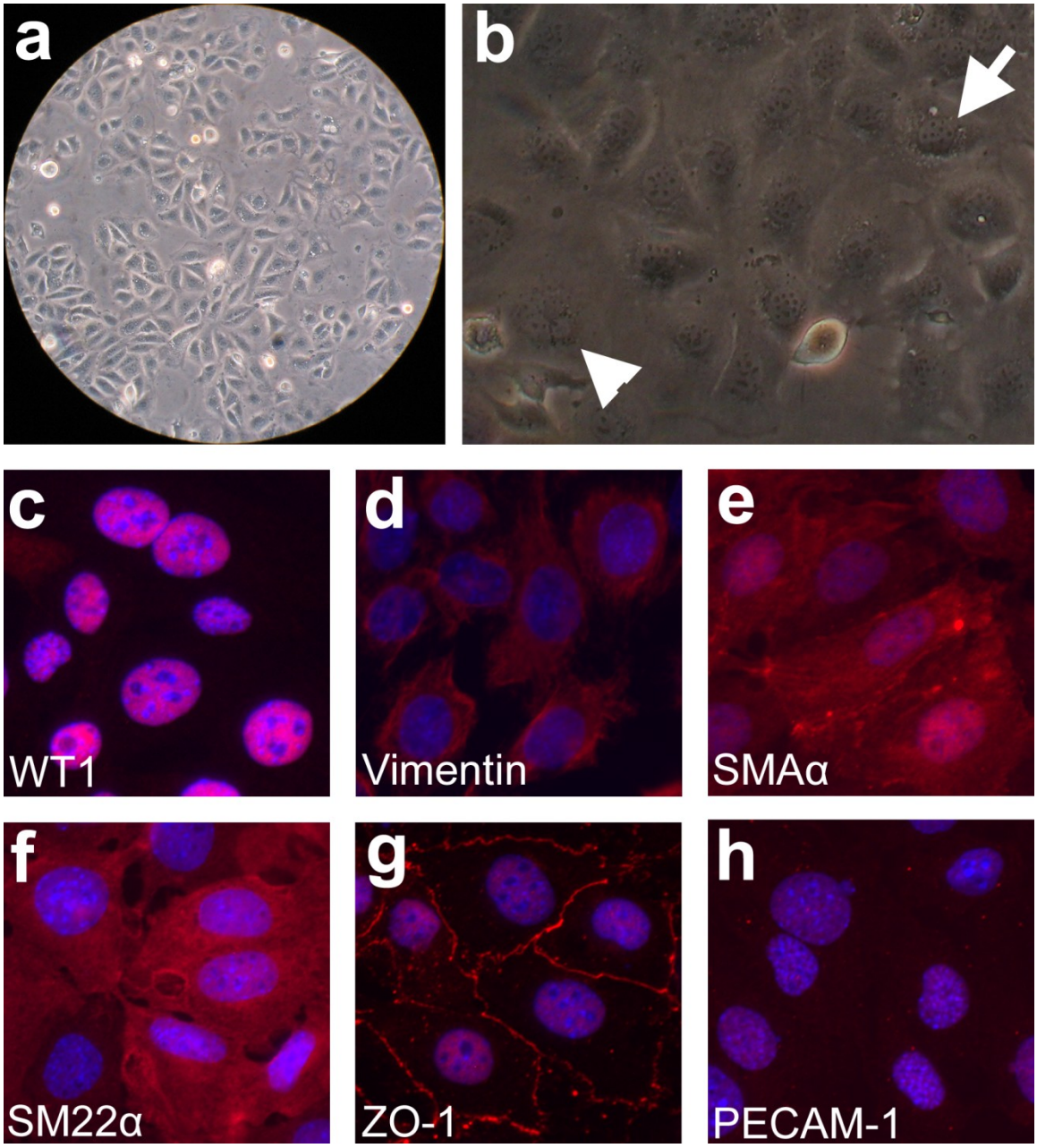

Figure 31: Culture and immunostaining of MEC cells.

(a) Appearance of MEC 24 hours after plating. MEC form epithelial clusters. (b) Higher magnification of MEC. Multinucleated (arrowhead) and vacuole-filled cells (arrow) accumulate after passage 14. (c-h) Immunostaining of epithelial and mesenchymal markers. MEC express WT1, vimentin, SMAα, SM22α, and ZO-1, but not PECAM-1 (red). DAPI: blue.

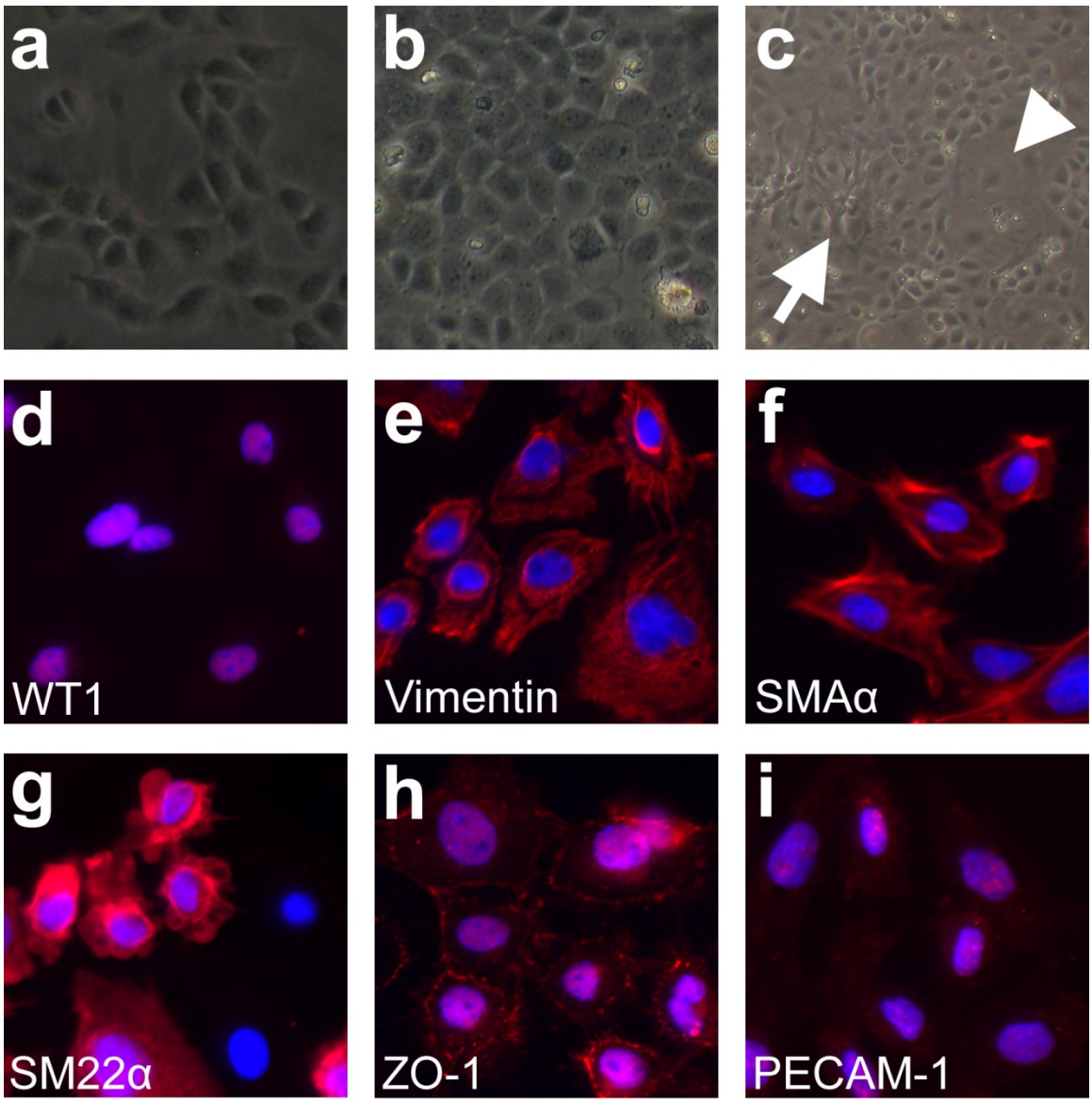

Figure 32: Culture and immunostaining of AREC cells.

(a) Appearance of AREC 24 hours after plating. AREC form epithelial clusters (a) and monolayer epithelial sheets (b). (c) Beyond passage 12 AREC accumulate cells with large cytoplasm (arrowhead) or mesenchymal shape (arrow). (d-i) Immunostaining of epithelial and mesenchymal markers. AREC express WT1, vimentin, SMAα, SM22α, and ZO-1, but not PECAM-1 (red). DAPI: blue.

APPENDIX E. ISOLATION OF FETAL CARDIOMYOCYTES FOR SIZE DETERMINATION

E.1 Purpose and objective

The B6 *Asxl2*$^{-/-}$ heart has an enlarged left ventricle wall and interventricular septum at E18.5. I investigated whether this is due to cellular hypertrophy. Inferring the size and shape of individual heart cells from tissue sections of a 3-dimensional tissue is difficult due to the varied orientation of cells in the heart. Therefore, a protocol for the primary culture of isolated mouse fetal heart cells was established. Individual cardiomyocytes were isolated, plated and then measured.

E.2 Materials and Methods

For E13.5-15.5 hearts: Timed pregnant *Asxl2*$^{+/-}$ female mice were sacrificed using CO_2 and cervical dislocation. Embryos were collected in cold PBS in a 12-well plate using sterile instruments and solutions. Embryos were dissected individually to isolate the heart ventricles. Tissue was rinsed in PBS, then minced with razor blades into 15-20 pieces in a drop of Hank's Balanced Salt Solution (HBSS; Sigma H4891). Minced pieces were transferred into 1.5 ml microcentrifuge tubes containing 1 ml digestion buffer (DB; 2 mg/ml collagenase-2 (Worthington 4176); 110 U of DNase I (Fermentas); HBSS). Hearts were incubated on a nutating platform at 37°C for ~60 minutes until tissue digested. Minced pieces were gently passed through a cut P1000 tip pre-wetted with DB 5 times to break up cell clumps at 0, 10, 20, 40, and 60 minutes. Cells were spun 5 minutes at 800 g and DB was aspirated. Cells were resuspended in 2 ml DMEM + 10% FCS (Hyclone) and plated on 0.1% gelatin-coated dishes. After allowing cells to attach 2 hours, dishes were rocked gently and unadhered cells were transferred to coated glass chamber-well dishes (10 μg/ml laminin; 0.1% gelatin). Pre-plating

step removes mostly fibroblast cells and enriches for cardiomyocytes in final plating; it is omitted for assays of mixed cultures. Cells were cultured 6-24 hours at 37°C 5% CO_2 before fixation for downstream assays.

For E18.5 hearts: Digestion performed in 1 ml DB (4 mg/ml collagenase-2; 110 U DNase I; HBSS) in 1.5 ml microcentrifuge tubes held at 35°C on hot plate under laminar flow hood. Heart pieces were continuously passed through pre-wetted sterile transfer pipettes for 40-60 minutes until digested. Pre-plating step omitted to improve cardiomyocyte health. Culture dishes coated with 10 μg/ml laminin, 50 μg/ml collagen.

Analysis of cell size was performed on cells from E18.5 hearts. Cells were fixed and immunostained for cTnT and vimentin to label cardiomyocytes and fibroblasts, respectively. Images were collected and processed to exclude unhealthy cells from analysis. A cut-out filter (Levels = 8; Edge simplicity = 1; Edge fidelity = 3) was used to find $cTnT^+$ cell edges and remove background (Adobe Photoshop 6.0). Images were thresholded, converted to binary images, and the area of individual cardiomyocytes was measured (NIH ImageJ, MBF plugin set).

E.3 Results and conclusions

Average cardiomyocyte area was calculated for cells isolated from 5 *Asxl2*$^{+/+}$ and *Asxl2*$^{-/-}$ hearts (Fig. 33). For each heart 200-450 cells were measured. The average size of cardiomyocytes ranged from 650-715 μm^2 for wildtype and 540-1000 μm^2 for *Asxl2*$^{-/-}$ hearts. *Asxl2*$^{-/-}$ cells exhibited more variation in size, however no statistically significant difference in average size compared to wildtype was found by Student's T-test. The variation may be due to true size variations in the cell population, or different digestion efficiency for *Asxl2*$^{-/-}$ hearts. Therefore, other methods were used to estimate cardiomyocyte size from tissue sections. These assays also found no consistent differences between E18.5 wildtype and *Asxl2*$^{-/-}$ samples: WGA

staining of cell membranes (Fig. 12), nuclear density (Fig. 12), and ratio of cardiomyocyte:non-cardiomyocyte area (Fig. 13). From these, I conclude loss of *Asxl2* does not cause cellular hypertrophy in the fetal heart.

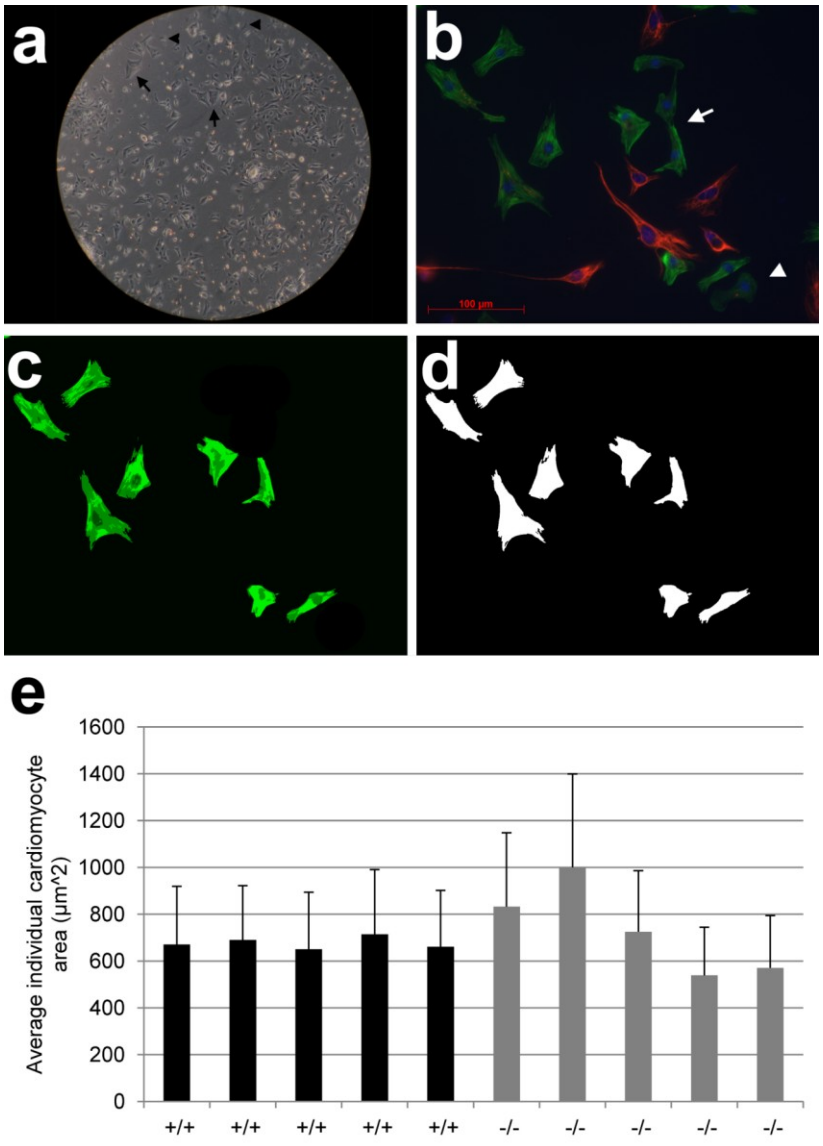

Figure 33: *Asxl2*$^{-/-}$ cardiomyocytes are not larger at E18.5 as determined by cell isolation and size measurement.

(a) Appearance of isolated cells after 16 hours culture. Large cardiomyocytes (arrows) and smaller fibroblasts (arrowhead) are present. (b) Immunofluorescence staining for cTnT (green) or vimentin (red). Cells with abnormal structure (arrowhead) were excluded and touching cells (arrow) were separated. (c) Adobe Photoshop was used to generate outlines of cTnT^{+} cardiomyocytes to be measured. (d) Images were converted to binary and cell area measured in

ImageJ. (e) Average area of measured cells from 5 wildtype and *Asxl2*$^{-/-}$ hearts. Error bars: standard deviation from mean.

APPENDIX F. THE KC17 ANTIBODY DOES NOT DETECT ENDOGENOUS ASXL2 IN IMMUNOSTAINING

F.1 Purpose and objective

We generated a rabbit polyclonal antibody against mouse ASXL2 (KC17). I tested various immunostaining conditions and found KC17 recognizes overexpressed, but not endogenous, levels of ASXL2 by immunostaining.

F.2 Materials and methods

Immunostainings of endogenous ASXL2 were performed on primary cultures of E13.5-E15.5 mouse cardiomyocytes, isolated as described in Appendix E. Fetal cardiomyocytes from *Asxl2*$^{-/-}$ hearts were stained as a negative control in each experiment. Immunostainings of overexpressed ASXL2 was performed on HEK293 cells transfected with pCAG-ASXL2-fl-FLAG (0.45 µg DNA, 7 ul polyethylenimine (PEI) transfection reagent/chamber of 8-well chamber slide).

F.3 Results and conclusions

The KC17 antibody generated against mouse ASXL2 was able to detect over-expressed ASXL2-FLAG in HEK293 cells (Fig. 34). KC17 staining overlapped FLAG staining in transfected cells and was comparable to staining with another ASXL2 antibody generated by a collaborator (Helin Lab, University of Copenhagen) (Fig. 34). However, when KC17 antibody was used to stain fetal cardiomyocytes, a tissue expressing ASXL2, no positive staining above background was detected (Fig. 35). A summary of tested conditions is presented in Table VIII. I conclude that, under these conditions, KC17 is not sensitive enough to detect endogenous levels of ASXL2 by immunostaining. However, KC17 is suitable for detecting endogenous ASXL2 by ChIP (Lai and Wang, 2013) and perhaps other assays.

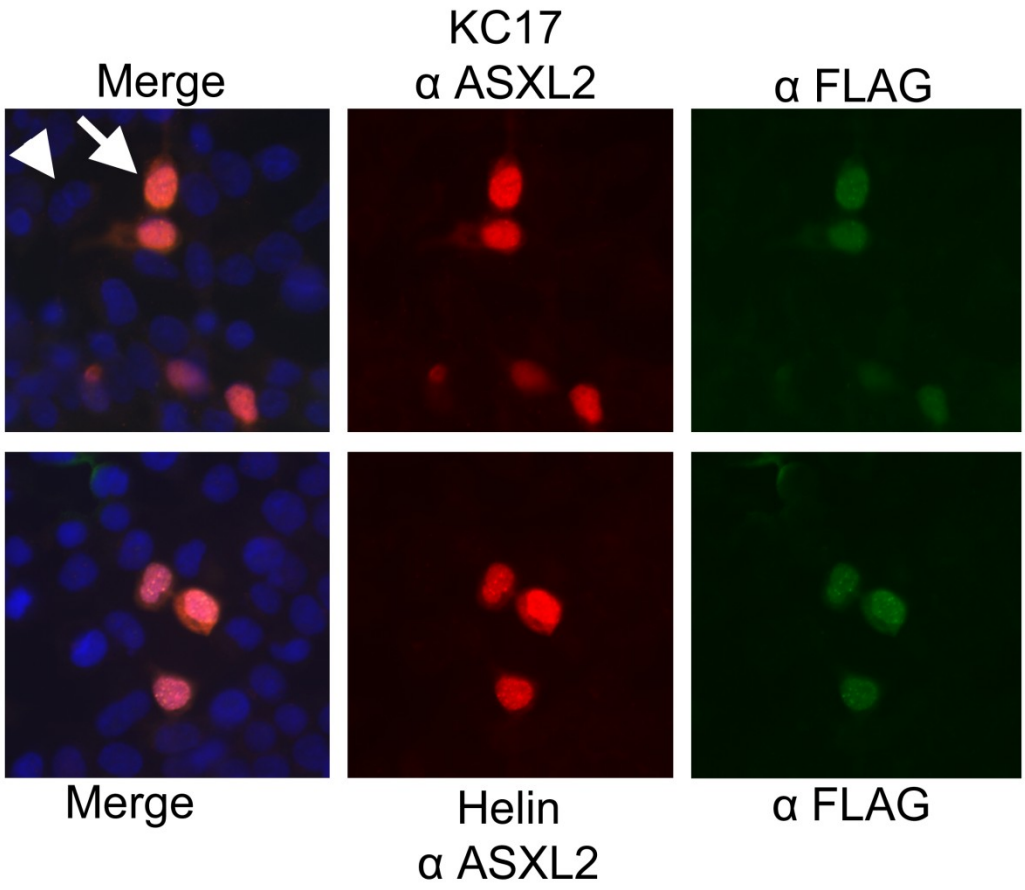

Figure 34: KC17 antibody detects overexpressed ASXL2.

HEK293 cells were transfected with FLAG-tagged full length ASXL2. KC17 antibody (top panels) detected ASXL2 in the nucleus and cytoplasm of transfected cells (arrow) and overlaps with FLAG staining. No signal was observed in untransfected cells (arrowhead). Similar staining patterns were obtained using an anti-ASXL2 antibody from collaborator (lower panels) (Helin Lab).

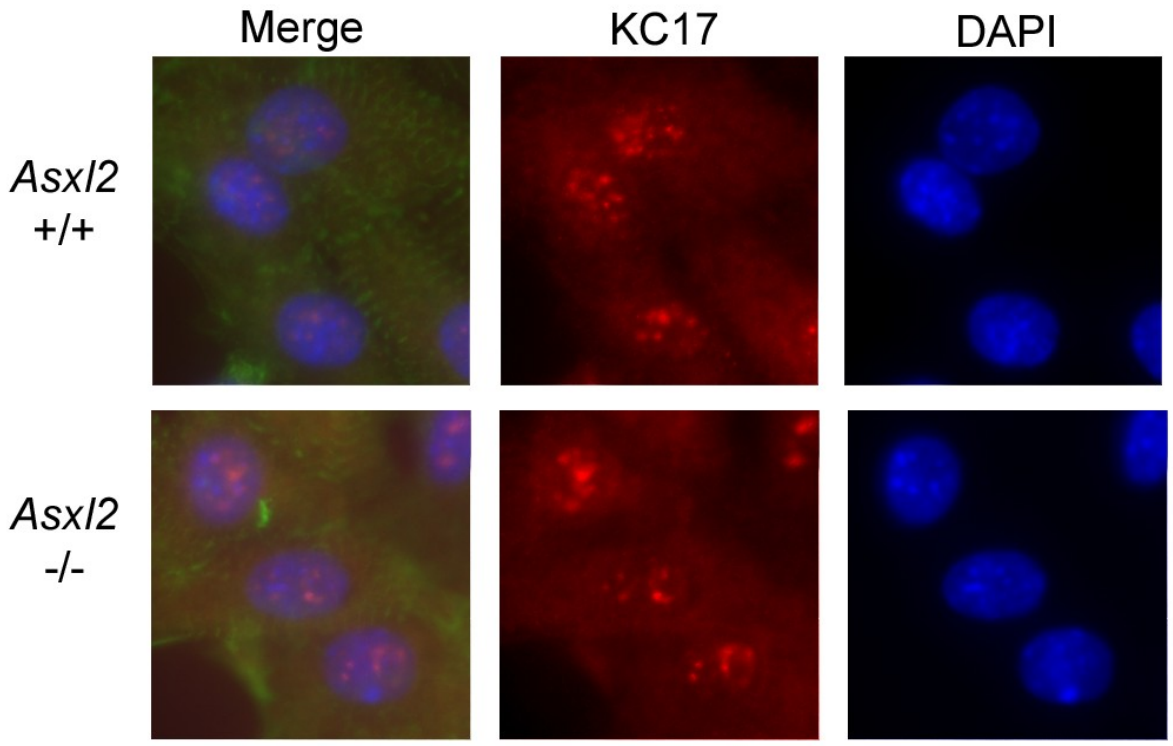

Figure 35: KC17 does not detect endogenous ASXL2 in immunostaining.

Wildtype (upper panels) and *Asxl2*$^{-/-}$ (lower panels) fetal cardiomyocytes were stained with KC17 antibody using various conditions described in Table VIII. Green: α-actinin. Red: KC17. Blue: DAPI stain. KC17 shows nuclear puncta staining that does not overlap with DAPI-dense regions, but these puncta are nonspecific: they are equally prominent in wildtype and mutant cells.

TABLE VIII: IMMUNOSTAINING CONDITIONS TESTED

FOR KC17 ANTI-ASXL2 ANTIBODY

Variable	Conditions tested
Fixation	MeOH:acetone 10’
	MeOH 10’
	5% acetic acid in MeOH 10’
	Acetone 10’
	4% PFA 5-10’
Blocking	1-10% NDS
	5% NDS + 5% NGS
	2.5% NDS + 2.5% NGS
KC17 antibody concentration	1:25-1:3200
Secondary antibody	1:1000 DαRb-TR
	1:1000 GαM-FITC
Preadsorption of antibody	Preabsorped 1:50 KC17 to MeOH-fixed HEK293 cells overnight
Washes	PBS
	PBST (0.05-1% Tween-20)
	TBS
	TBST (0.05% Tween-20)

APPENDIX G. THE ADULT B6;129 ASXL2$^{-/-}$ HEART EXHIBITS MILD FIBROSIS

G.1 Purpose and objective

Asxl2$^{-/-}$ animals in the hybrid B6;129 background survive to adulthood and develop an enlarged heart to body weight ratio at 2 months of age. I investigated whether fibrosis was present in these hearts, perhaps contributing to the increased heart mass. Fibrosis is the deposition of collagen and other extracellular matrix proteins by activated fibroblasts. It can be triggered by pressure overload or injury of the heart and frequently accompanies hypertrophic growth.

G.2 Materials and methods

Adult mice were sacrificed by CO_2 inhalation and cervical dislocation. Hearts were quickly excised and incubated in 1 M KCl in PBS for 5 minutes while still beating. Hearts were fixed in formalin, dehydrated in a graded series of ethanol, cleared with xylene, and embedded in paraffin wax. Frontal serial sections were prepared at 8 μm. Masson's Trichrome staining was performed using standard protocols.

G.3 Results and conclusions

Masson's Trichrome staining was used to visualize collagen deposits in wildtype and *Asxl2*$^{-/-}$ hearts. Fibrosis was found in both genotypes, but *Asxl2*$^{-/-}$ hearts tended to exhibit mild increases in fibrosis in multiple areas (Fig. 36). Areas of collagen fibrosis were classified as intramuscular deposits in the ventricle walls or septum, invasion from adjacent coronary vessels, invasion from the cardiac skeleton near atrioventricular (A/V) junction, expansion of the base of the membranous septum, and invasion from cardiac skeleton near A/V valves. These areas have normal deposition of collagen in wildtype animals, but expanded regions of fibrosis in most *Asxl2*$^{-/-}$ animals. The degree of fibrosis is consistently elevated, but mild, and appears to

contribute little to the greater size of the *Asxl2*$^{-/-}$ heart. Elevated fibrosis was found in both 4 month old and 12-15 month old hearts (Table IX).

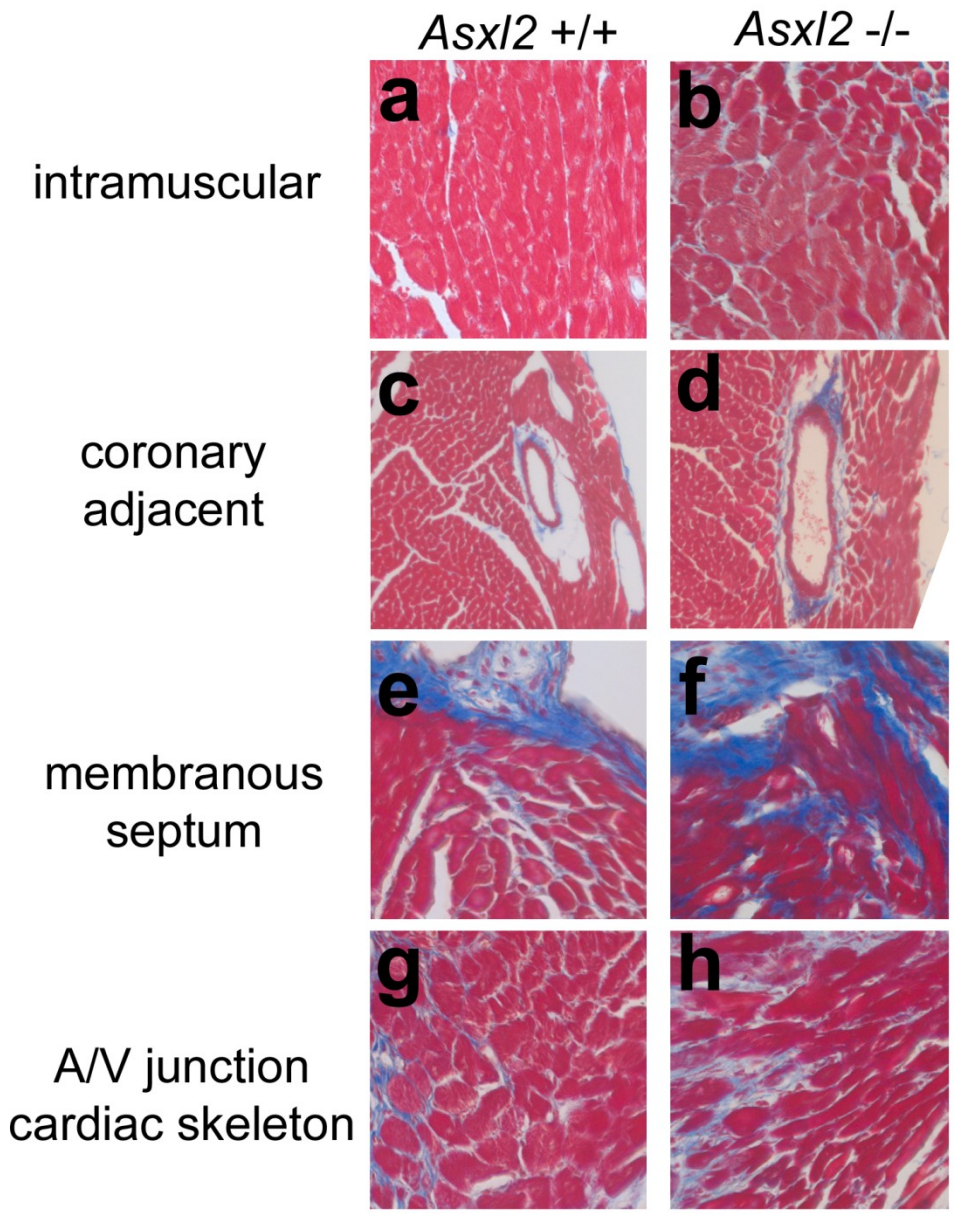

Figure 36: Adult B6;129 *Asxl2*$^{-/-}$ hearts exhibit mild fibrosis.

(a-h) Masson's trichrome staining of wildtype (left) and *Asxl2*$^{-/-}$ (right) hearts. Red: muscle cells. Blue: Extracellular collagen. Normal collagen deposits observed in wildtype hearts appeared expanded in most *Asxl2*$^{-/-}$ hearts in the muscle walls (a-b), next to coronary vessels (c-d), posterior to the attachment of membranous septum (e-f), and extending from the cardiac skeleton at the A/V junctions (g-h).

TABLE IX: ADULT B6;129 HEARTS HAVE MILDLY ELEVATED FIBROSIS

Region	*Asxl2* +/+ 12-15 mo N=3	*Asxl2* -/- 12-15 mo N=4	*Asxl2* +/+ 4 mo N=3	*Asxl2* -/- 4 mo N=4
Intramuscular	2/3	4/4	0/3	1/4
Coronary vessels	1/3	2/4	1/3	3/4
A/V junction	0/3	4/4	0/3	2/4
Membranous septum	1/3	3/4	0/3	1/4
A/V valves	1/3	3/4	0/3	0/4

Number of hearts with elevated fibrosis in a given region is shown.

APPENDIX H. PERMISSION TO REPRINT COPYRIGHTED MATERIALS

JOHN WILEY AND SONS LICENSE TERMS AND CONDITIONS

Jun 09, 2014

This is a License Agreement between Andrea McGinley ("You") and John Wiley and Sons ("John Wiley and Sons") provided by Copyright Clearance Center ("CCC"). The license consists of your order details, the terms and conditions provided by John Wiley and Sons, and the payment terms and conditions.

All payments must be made in full to CCC. For payment instructions, please see information listed at the bottom of this form.

License Number	3404990233953
License date	Jun 09, 2014
Licensed content publisher	John Wiley and Sons
Licensed content publication	genesis
Licensed content title	Additional sex combs-like family genes are required for normal cardiovascular development
Licensed copyright line	Copyright © 2014 Wiley Periodicals, Inc.
Licensed content author	Andrea L. McGinley,Yanyang Li,Zane Deliu,Q. Tian Wang
Licensed content date	Jun 3, 2014
Start page	n/a
End page	n/a
Type of use	Dissertation/Thesis
Requestor type	Author of this Wiley article
Format	Print and electronic
Portion	Full article
Will you be translating?	No
Title of your thesis / dissertation	Additional sex combs-like family genes are required for embryonic development
Expected completion date	Jul 2014
Expected size (number of pages)	150
Total	0.00 USD

CITED LITERATURE

Abdel-Wahab O, Adli M, LaFave LM, Gao J, Hricik T, Shih AH, Pandey S, Patel JP, Chung YR, Koche R, Perna F, Zhao X, Taylor JE, Park CY, Carroll M, Melnick A, Nimer SD, Jaffe JD, Aifantis I, Bernstein BE, Levine RL. 2012. ASXL1 mutations promote myeloid transformation through loss of PRC2-mediated gene repression. Cancer Cell 22: 180–93.

Abdel-Wahab O, Gao J, Adli M, Dey A., Trimarchi T, Chung YR, Kuscu C, Hricik T, Ndiaye-Lobry D, LaFave LM, Koche R, Shih AH, Guryanova OA, Kim E, Li S, Pandey S, Shin JY, Telis L, Liu J, Bhatt PK, Monette S, Zhao X, Mason CE, Park CY, Bernstein BE, Aifantis I, Levine R. 2013. Deletion of Asxl1 results in myelodysplasia and severe developmental defects in vivo. J Exp Med 210: 2641–2659.

Abu-Issa R, Smyth G, Smoak I, Yamamura K, Meyers EN. 2002. Fgf8 is required for pharyngeal arch and cardiovascular development in the mouse. Development 129: 4613–25.

Acharya A, Baek ST, Huang G, Eskiocak B, Goetsch S, Sung CY, Banfi S, Sauer MF, Olsen GS, Duffield JS, Olson EN, Tallquist MD. 2012. The bHLH transcription factor Tcf21 is required for lineage-specific EMT of cardiac fibroblast progenitors. Development 2149: 2139–2149.

Akasaka T, van Lohuizen M, van der Lugt N, Mizutani-Koseki Y, Kanno M, Taniguchi M, Vidal M, Alkema M, Berns A, Koseki H. 2001. Mice doubly deficient for the Polycomb Group genes Mel18 and Bmi1 reveal synergy and requirement for maintenance but not initiation of Hox gene expression. Development 128: 1587–97.

Alonso L, Fuchs E. 2006. The hair cycle. J Cell Sci 119: 391–3.

Anderson RH. 2003. Development of the heart: (2) Septation of the atriums and ventricles. Heart 89: 949–958.

Arrigoni R, Alam SL, Wamstad JA, Bardwell VJ, Sundquist WI, Schreiber-Agus N. 2006. The Polycomb-associated protein Rybp is a ubiquitin binding protein. FEBS Lett 580: 6233–41.

Ashery-Padan R, Gruss P. 2001. Pax6 lights-up the way for eye development. Curr Opin Cell Biol 13: 706–14.

Bainbridge MN, Hu H, Muzny DM, Musante L, Lupski JR, Graham BH, Chen W, Gripp KW, Jenny K, Wienker TF, Yang Y, Sutton VR, Gibbs RA, Ropers HH. 2013. De novo truncating mutations in ASXL3 are associated with a novel clinical phenotype with similarities to Bohring-Opitz syndrome. Genome Med 5: 11.

Baker K, Sanchez-de-Toledo J, Munoz R, Orr R, Kiray S, Shiderly D, Clemens M, Wearden P, Morell VO, Chrysostomou C. 2012. Critical congenital heart disease—utility of routine

screening for chromosomal and other extracardiac malformations. Congenit Heart Dis 7: 145–150.

Bandarchi B, Jabbari CA, Vedadi A, Navab R. 2013. Molecular biology of normal melanocytes and melanoma cells. J Clin Pathol 66: 644–8.

Baragatti B, Brizzi F, Ackerley C, Barogi S, Ballou LR, Coceani, F. 2003. Cyclooxygenase-1 and cyclooxygenase-2 in the mouse ductus arteriosus: individual activity and functional coupling with nitric oxide synthase. Br J Pharmacol 139: 1505–15.

Baskind H, Na L, Ma Q, Patel MP, Geenen DL, Wang QT. 2009. Functional conservation of Asxl2, a murine homolog for the Drosophila enhancer of trithorax and polycomb group gene Asx. PLoS One 4: e4750.

Baumann C, De La Fuente R. 2011. Role of polycomb group protein cbx2/m33 in meiosis onset and maintenance of chromosome stability in the Mammalian germline. Genes (Basel) 2: 59–80.

Bejar R, Stevenson K, Abdel-Wahab O, Galili N, Nilsson B, Garcia-Manero G, Kantarjian H, Raza A, Levine RL, Neuberg D, Ebert BL. 2011. Clinical effect of point mutations in myelodysplastic syndromes. N Engl J Med 364: 2946-506.

Bertrand N, Roux M, Ryckebüsch L, Niederreither K, Dolle P, Moon A, Capecchi M, Zaffran S. 2011. Hox genes define distinct progenitor sub-domains within the second heart field. Dev Biol 353: 266–274.

Beuchle D, Struhl G, Müller J. 2001. Polycomb group proteins and heritable silencing of Drosophila Hox genes. Development 128: 993–1004.

Bhattacharya S, Macdonald ST, Farthing CR. 2006. Molecular mechanisms controlling the coupled development of myocardium and coronary vasculature. Clin Sci (Lond) 111: 35–46.

Botchkareva NV, Botchkarev VA, Gilchrest BA. 2003. Fate of melanocytes during development of the hair follicle pigmentary unit. J Investig Dermatol Symp Proc 8: 76-9.

Boyer LA, Plath K, Zeitlinger J, Brambrink T, Medeiros LA, Lee TI, Levine SS, Wernig M, Tajonar A, Ray MK, Bell GW, Otte AP, Vidal M, Gifford DK, Young RA, Jaenisch R. 2006. Polycomb complexes repress developmental regulators in murine embryonic stem cells. Nature 441: 349–53.

Brade T, Pane LS, Moretti A, Chien KR, Laugwitz KL. 2013. Embryonic heart progenitors and cardiogenesis. Cold Spring Harb Perspect Med 3: a013847.

Brown DD, Martz SN, Binder O, Goetz SC, Price BMJ, Smith JC, Conlon FL. 2005. Tbx5 and Tbx20 act synergistically to control vertebrate heart morphogenesis. Development 132: 553–563.

Bruneau BG, Nemer G, Schmitt JP, Charron F, Robitaille L, Caron S, Conner DA, Gessler M, Nemer M, Seidman CE, Seidman JG. 2001. A murine model of Holt-Oram syndrome defines roles of the T-box transcription factor Tbx5 in cardiogenesis and disease. Cell 106: 709–21.

Burn J, Brennan P, Little J, Holloway S, Coffey R, Somerville J, Dennis NR, Allan L, Arnold R, Deanfield JE, Godman M, Houston A, Keeton B, Oakley C, Scott O, Silove E, Wilkinson J, Pembrey M, Hunter AS. 1998. Recurrence risks in offspring of adults with major heart defects: results from first cohort of British collaborative study. Lancet 351: 311–6.

Bush JO, Jiang R. 2012. Palatogenesis: morphogenetic and molecular mechanisms of secondary palate development. Development 139: 828–828.

Byrd KN, Shearn A. 2003. ASH1, a Drosophila trithorax group protein, is required for methylation of lysine 4 residues on histone H3. Proc Natl Acad Sci 100: 11535-11540.

Cai CL, Liang X, Shi Y, Chu PH, Pfaff SL, Chen J, Evans S. 2003. Isl1 identifies a cardiac progenitor population that proliferates prior to differentiation and contributes a majority of cells to the heart. Dev Cell 5: 877–89.

Cai CL, Martin JC, Sun Y, Cui L, Wang L, Ouyang K, Yang L, Bu L, Liang X, Zhang X, Stallcup WB, Denton CP, McCulluch A, Chen J, Evans SM. 2008. A myocardial lineage derives from Tbx18 epicardial cells. Nature 454: 104–8.

Cao R, Wang L, Wang H, Xia L, Erdjument-Bromage H, Tempst P, Jones RS, Zhang Y. 2002. Role of histone H3 lysine 27 methylation in Polycomb-group silencing. Science 298: 1039-1043.

Chan SS, Shi X, Toyama A, Arpke RW, Dandapat A, Iacovino M, Kang J, Le G, Hagen HR, Garry DJ, Kyba M. 2013. Mesp1 patterns mesoderm into cardiac, hematopoietic, or skeletal myogenic progenitors in a context-dependent manner. Cell Stem Cell 12: 587-601.

Chang C-P, Bruneau BG. 2012. Epigenetics and cardiovascular development. Annu Rev Physiol 74: 41–68.

Chang H-Y, Locker J, Lu R, Schuster VL. 2010. Failure of postnatal ductus arteriosus closure in prostaglandin transporter-deficient mice. Circulation, 121: 529–36.

Chatterjee N, Sinha D, Lemma-Dechassa M, Tan S, Shogren-Knaak MA, Bartholomew B. 2011. Histone H3 tail acetylation modulates ATP-dependent remodeling through multiple mechanisms. Nucleic Acids Res 39: 8378-91.

Chaudhry B, Ramsbottom S, Henderson DJ. 2014. Genetics of cardiovascular development. Prog Mol Biol Transl Sci 124: 19-41.

Chen H, Zhang W, Li D, Cordes T, Payne M, Shou W. 2009. Analysis of ventricular hypertrabeculation and noncompaction using genetically engineered mouse models. Pediatr Cardiol 30: 626–634.

Chen T, Dent SYR. 2013. Chromatin modifiers and remodellers: regulators of cellular differentiation. Nat Rev Genet 1–14.

Chisaka O, Capecchi MR. 1991. Regionally restricted developmental defects resulting from targeted disruption of the mouse homeobox gene hox-1.5. Nature 350: 473–479.

Cho YS, Kim EJ, Park UH, Sin HS, Um SJ. 2006. Additional sex comb-like 1 (ASXL1), in cooperation with SRC-1, acts as a ligand-dependent coactivator for retinoic acid receptor. J Biol Chem 281: 17588–98.

Chow R, Lang R. 2001. Early eye development in vertebrates. Annu Rev Cell Dev 17: 255-296.

Christoffels VM, Moorman AFM. 2009. Development of the cardiac conduction system: why are some regions of the heart more arrhythmogenic than others? Circ Arrhythm Electrophysiol 2: 195–207.

Cichorek M, Wachulska M, Stasiewicz A, Tymińska A. 2013. Skin melanocytes: biology and development. Postepy Dermatol Alergol 30: 30–41.

Clapier CR, Cairns BR. 2009. The biology of chromatin remodeling complexes. Annu Rev Biochem 78: 273-304.

Coléno-Costes A, Jang SM, de Vanssay A, Rougeot J, Bouceba T, Randsholt NB, Gibert JM, Le Crom S, Mouchel-Vielh E, Bloyer S, Peronnet F. 2012. New partners in regulation of gene expression: the enhancer of Trithorax and Polycomb Corto interacts with methylated ribosomal protein l12 via its chromodomain. PLoS Genet 8: e1003006.

Collins H, Moon NS. 2013. The components of Drosophila histone chaperone dCAF-1 are required for the cell death phenotype associated with rbf1 mutation. G3 (Bethesda) 3: 1639–47.

Collop AH, Broomfield JA, Chandraratna RA, Yong Z, Deimling SJ, Kolker SJ, Weeks DL, Drysdale TA. 2006. Retinoic acid signaling is essential for formation of the heart tube in Xenopus. Dev Biol 291: 96-109.

Combs MD, Yutzey KE. 2009. Heart valve development: regulatory networks in development and disease. Circ Res 105: 408–21.

Cordell HJ, Bentham J, Topf A, Zelenika D, Heath S, Mamasoula C, Cosgrove C, Blue G, Granados-Riveron J, Setchfield K, Thornborough C, Breckpot J, Soemedi R, Martin R, Rahman TJ, Hall D, van Engelen K, Moorman AF, Zwinderman AH, Barnett P, Koopmann TT, Adriaens ME, Varro A, George AL Jr., dos Remedios C, Bishopric NH, Bezzina CR, O'Sullivan J, Gewillig M, Bu'Lock FA, Winlaw D, Bhattacharya S, Devriendt K, Brook JD, Mulder BJ, Mital S, Postma AV, Lathrop GM, Farrall M, Goodship JA, Keavney BD. 2013. Genome-wide association study of multiple congenital heart disease phenotypes identifies a susceptibility locus for atrial septal defect at chromosome 4p16. Nat Genet 45: 822–4.

Cossette S, Misra R. 2011. The identification of different endothelial cell populations within the mouse proepicardium. Dev Dyn 240: 2344-53.

Crowley M a, Conlin LK, Zackai EH, Deardorff MA, Thiel BD, Spinner NB. 2010. Further evidence for the possible role of MEIS2 in the development of cleft palate and cardiac septum. Am J Med Genet A 152A: 1326–7.

Dahle Ø, Kumar A, Kuehn MR. 2010. Nodal signaling recruits the histone demethylase Jmjd3 to counteract polycomb-mediated repression at target genes. Sci Signal 22: ra48.

de Napoles M, Mermoud JE., Wakao R, Tang YA, Endoh M, Appanah R, Nesterova TB, Silva J, Otte, AP, Vidal M, Kosecki H, Borckdorff N. 2004. Polycomb group proteins Ring1A/B link ubiquitylation of histone H2A to heritable gene silencing and X inactivation. Dev Cell 7, 663–676.

Déjardin J, Cavalli G. 2005. Epigenetic inheritance of chromatin states mediated by Polycomb and trithorax group proteins in Drosophila. Prog Mol Subcell Biol 38: 31–63.

Delgado-Olguín P, Huang Y, Li X, Christodoulou D, Seidman CE, Seidman JG, Tarakhovsky A, Bruneau BG. 2012. Epigenetic repression of cardiac progenitor gene expression by Ezh2 is required for postnatal cardiac homeostasis. Nat Genet 44: 343–7.

Deschamps J, van Nes J. 2005. Developmental regulation of the Hox genes during axial morphogenesis in the mouse. Development 132: 2931–42.

Dey A, Seshasayee D, Noubade R, French DM, Liu J, Chaurushiya MS, Kirkpatrick DS, Pham VC, Lill JR, Bakalarski CE, Wu J, Phu L, Katavolos P, LaFave LM, Abdel-Wahab O, Modrusan Z, Seshagiri S, Dong K, Lin Z, Balazs M, Suriben R, Newton K, Hymowitz S, Garcia-Manero G, Martin F, Levine RL, Dixit VM. 2012. Loss of the tumor suppressor BAP1 causes myeloid transformation. Science 337: 1541–6.

Dinwiddie DL, Soden SE, Saunders CJ, Miller NA, Farrow EG, Smith LD, Kingsmore SF. 2013. De novo frameshift mutation in ASXL3 in a patient with global developmental delay, microcephaly, and craniofacial anomalies. BMC Med Genomics 6: 32.

Dixon MJ, Marazita ML, Beaty TH, Murray JC. 2011. Cleft lip and palate: understanding genetic and environmental influences. Nat Rev Genet 12: 167–78.

Drayton MR, Skidmore R. 1987. Ductus arteriosus blood flow during first 48 hours of life. Arch Dis Child 62: 1030–4.

Echtler K, Stark K, Lorenz M, Kerstan S, Walch A, Jennen L, Rudelius M, Seidl S, Kremmer E, Emambokus NR, von Bruehl ML, Frampton J, Isermann B, Genzel-Boroviczény O, Schreiber C, Mehilli J, Kastrati A, Schwaiger M, Shivdasani RA, Massberg S. 2010. Platelets contribute to postnatal occlusion of the ductus arteriosus. Nat Med 16: 75–82.

Eckardt N. 2006. Functional divergence of AP3 genes in the MAD world of flower development. Plant Cell 18: 1779–1781.

Endoh M, Endo TA, Endoh T, Isono K, Sharif J, Ohara O, Toyoda T, Ito T, Eskeland R, Bickmore WA, Vidal M, Bernstein BE, Koseki H. 2012. Histone H2A mono-ubiquitination is a crucial step to mediate PRC1-dependent repression of developmental genes to maintain ES cell identity. PLoS Genet 8: e1002774.

Ernfors P. 2010. Cellular origin and developmental mechanisms during the formation of skin melanocytes. Exp Cell Res 316: 1397–407.

Evans SM, Yelon D, Conlon FL, Kirby ML. 2010. Myocardial lineage development. Circ Res 107: 1428–44.

Ezhkova E, Lien WH, Stokes N, Pasolli Ha, Silva Jm, Fuchs E. 2011. EZH1 and EZH2 cogovern histone H3K27 trimethylation and are essential for hair follicle homeostasis and wound repair. Genes Dev 25: 485–498.

Ezhkova E, Pasolli HA, Parker JS, Stokes N, Su IH, Hannon G, Tarakhovsky A, Fuchs E. 2009. Ezh2 orchestrates gene expression for the stepwise differentiation of tissue-specific stem cells. Cell 136: 1122–1135.

Fisher C, Berger J, Randazzo F, Brock HW. 2003. A human homolog of Additional sex combs, ADDITIONAL SEX COMBS-LIKE 1, maps to chromosome 20q11. Gene 306: 115–126.

Fisher C, Lee I, Bloyer S, Bozza S, Chevalier J, Dahl A, Bodner C, Helgason CD, Hess JL, Humphries RK, Brock HW. 2010a. Additional sex combs-like 1 belongs to the enhancer of trithorax and polycomb group and genetically interacts with Cbx2 in mice. Dev Biol 337: 9–15.

Fisher CL, Fisher AG. 2011. Chromatin states in pluripotent, differentiated, and reprogrammed cells. Curr Opin Genet Dev 21:140-6.

Fisher CL, Pineault N, Brookes C, Helgason CD, Ohta H, Bodner C, Hess JL, Humphries RK, Brock HW. 2010b. Loss-of-function Additional sex combs like 1 mutations disrupt hematopoiesis but do not cause severe myelodysplasia or leukemia. Blood 115: 38–46.

Fisher CL, Randazzo F, Humphries RK, Brock HW. 2006. Characterization of Asxl1, a murine homolog of Additional sex combs, and analysis of the Asx-like gene family. Gene 369: 109–18.

Fisher CL. 2004. Characterization of mammalian ASX-Like genes and role of ASX-Like-1 in development and hematopoiesis. Dissertation, University of British Columbia.

Force A, Lynch M, Pickett FB, Amores A, Yan YL, Postlethwait J. 1999. Preservation of duplicate genes by complementary, degenerative mutations. Genetics 151: 1531-45.

Franco D, Meilhac SM, Christoffels VM, Kispert A, Buckingham M, Kelly RG. 2006. Left and right ventricular contributions to the formation of the interventricular septum in the mouse heart. Dev Biol 294: 366–75.

Frey N, Olson EN. 2003. Cardiac hypertrophy: the good, the bad, and the ugly. Annu Rev Physiol 65: 45–79.

Fuchs A, Inthal A, Herrmann D, Cheng S, Nakatomi M, Peters H, Neubüser A. 2010. Regulation of Tbx22 during facial and palatal development. Dev Dyn 239: 2860-74.

Fuhrmann S. 2008. Wnt signaling in eye organogenesis. Organogenesis 4: 60–7.

García E, Marcos-Gutiérrez C, del Mar Lorente M, Moreno JC, Vidal M. 1999. RYBP, a new repressor protein that interacts with components of the mammalian Polycomb complex, and with the transcription factor YY1. EMBO J 18: 3404–18.

Gelsi-Boyer V, Brecqueville M, Devillier R, Murati A, Mozziconacci M-J, Birnbaum D. 2012. Mutations in ASXL1 are associated with poor prognosis across the spectrum of malignant myeloid diseases. J Hematol Oncol 5: 12.

Gelsi-Boyer V, Trouplin V, Adélaïde J, Bonansea J, Cervera N, Carbuccia N, Lagarde A, Prebet T, Nezri M, Sainty D, Olschwang S, Xerri L, Chaffanet M, Mozziconacci MJ, Vey N, Birnbaum D. 2009. Mutations of polycomb-associated gene ASXL1 in myelodysplastic syndromes and chronic myelomonocytic leukaemia. Br J Haematol 145: 788–800.

Gill HK, Splitt M, Sharland GK, Simpson JM. 2003. Patterns of recurrence of congenital heart disease. J Am Coll Cardiol 42: 923–929.

Gitler AD, Lu MM, Jiang YQ, Epstein JA, Gruber PJ. 2003. Molecular markers of cardiac endocardial cushion development. Dev Dyn 228: 643–50.

Goddeeris MM, Rho S, Petiet A, Davenport CL, Johnson GA, Meyers EN, Klingensmith J. 2008. Intracardiac septation requires hedgehog-dependent cellular contributions from outside the heart. Development 135: 1887–95.

Goding CR. 2007. Melanocytes: the new Black. Int J Biochem Cell Biol 39: 275–9.

Goldberg AD, Allis CD, Bernstein E. 2007. Epigenetics: a landscape takes shape. Cell 128: 635–8.

Granados-Riveron J, Pope M, Bu'lock FA, Thornborough C, Eason J, Setchfield K, Ketley A, Kirk EP, Fatkin D, Feneley MP, Harvey RP, Brook JD. 2012. Combined Mutation Screening of NKX2.5, GATA4, and TBX5 in Congenital Heart Disease: Multiple Heterozygosity and Novel Mutations. Congenit Heart Dis 7: 151–159.

Graw J. 2010. Eye development. Curr Top Dev Biol 90: 343–86.

Grego-Bessa J, Luna-Zurita L, del Monte G, Bolós V, Melgar P, Arandilla A, Garratt AN, Zang H, Mukouyama YS, Chen H, Shou W, Ballestar E, Esteller M, Rojas A, Perez-Pomares JM, de la Pompa JL. 2007. Notch signaling is essential for ventricular chamber development. Dev Cell 12: 415–29.

Gritli-Linde A. 2007. Molecular control of secondary palate development. Dev Biol 301: 309–26.

Hamilton BA, Yu BD. 2012. Modifier genes and the plasticity of genetic networks in mice. PLoS Genet 8: e1002644.

Hang CT, Yang J, Han P, Cheng HL, Shang C, Ashley E, Zhou B, Chang CP. 2010. Chromatin regulation by Brg1underlies heart muscle development and disease. Nature 466: 62–7.

Hastings R, Cobben J-M, Gillessen-Kaesbach G, Goodship J, Hove H, Kjaergaard S, Kemp H, Kingston H, Lunt P, Mansour S, McGowan R, Metcalfe K, Murdoch-Davis C, Ray M, Rio M, Smithson S, Tolmie J, Turnpenny P, van Bon B, Wieczorek D, Newbury-Ecob R. 2011. Bohring-Opitz (Oberklaid-Danks) syndrome: clinical study, review of the literature, and discussion of possible pathogenesis. Eur J Hum Genet 19: 513–9.

Hatcher CJ, Diman NY, McDermott DA, Basson CT. 2003. Transcription factor cascades in congenital heart malformation. Trends Mol Med 9: 512–5.

He A, Ma Q, Cao J, von Gise A, Zhou P, Xie H, Zhang B, Hsing M, Christodoulou DC, Cahan P, Daley GQ, Kong SW, Orkin SH, Seidman CE, Seidman JG, Pu WT. 2012. Polycomb repressive complex 2 regulates normal development of the mouse heart. Circ Res 110: 406–15.

He F, Xiong W, Yu X, Espinoza-Lewis R, Liu C, Gu S, Nishita M, Suzuki K, Yamada G, Minami Y, Chen Y. 2008. Wnt5a regulates directional cell migration and cell

proliferation via Ror2-mediated noncanonical pathway in mammalian palate development. Development 135: 3871-9.

Hill CR, Sanchez NS, Love JD, Arrieta JA, Hong CC, Brown CB, Austin AF, Barnett JV. 2012. BMP2 signals loss of epithelial character in epicardial cells but requires the Type III TGFβ receptor to promote invasion. Cell Signal 24: 1012–22.

Hizume K, Araki S, Hata K, Prieto E, Kundu TK, Yoshikawa K, Takeyasu K. 2010. Nano-scale analyses of the chromatin decompaction induced by histone acetylation. Arch Histol Cytol 73: 149–63.

Hochgreb T, Linhares VL, Menezes DC, Sampaio AC, Yan CY, Cardoso WV, Rosenthal N, Xavier-Neto J. 2003. A caudorostral wave of RALDH2 conveys anteroposterior information to the cardiac field. Development 130: 5363–74.

Hoffmann AD, Peterson MA, Friedland-Little JM, Anderson SA, Moskowitz IP. 2009. sonic hedgehog is required in pulmonary endoderm for atrial septation. Development 136: 1761–70.

Hoischen A, van Bon BWM, Rodríguez-Santiago B, Gilissen C, Vissers LELM, de Vries P, Janssen I, van Lier B, Hastings R, Smithson SF, Newbury-Ecob R, Kjaergaard S, Goodship J, McGowan R, Bartholdi D, Rauch A, Peippo M, Cobben JM, Wieczorek D, Gillessen-Kaesbach G, Veltman JA, Brunner HG, de Vries BB. 2011. De novo nonsense mutations in ASXL1 cause Bohring-Opitz syndrome. Nat Genet 43: 729–31.

Hsu Y, Osinski J, Campbell C. 2011. Mesenchymal nuclear factor IB regulates cell proliferation and epithelial differentiation during lung maturation. Dev Biol 354: 242–252.

Huang J, Cheng L, Li J, Chen M, Zhou D, Lu MM, Proweller A, Epstein JA, Parmacek MS. 2008. Myocardin regulates expression of contractile genes in smooth muscle cells and is required for closure of the ductus arteriosus in mice. J Clin Invest 118: 515–25.

Huang X, Gao X, Diaz-Trelles R, Ruiz-Lozano P, Wang Z. 2008. Coronary development is regulated by ATP-dependent SWI/SNF chromatin remodeling component BAF180. Dev Biol 319: 258–66.

Huntington K, Hunter AG, Chan KL. 1997. A prospective study to assess the frequency of familial clustering of congenital bicuspid aortic valve. J Am Coll Cardiol 30: 1809–12.

Ieda M, Tsuchihashi T, Ivey KN, Ross RS, Hong T-T, Shaw RM, Srivastava D. 2009. Cardiac fibroblasts regulate myocardial proliferation through beta1 integrin signaling. Dev Cell 16: 233–44.

Ingham PW. 1985. A clonal analysis of the requirement for the trithorax gene in the diversification of segments in Drosophila. J Embryol Exp Morphol 89: 349-65.

Iourov IY, Vorsanova SG, Kurinnaia OS, Yurov YB. 2013. An interstitial 20q11.21 microdeletion causing mild intellectual disability and facial dysmorphisms. Case Rep Genet 2013: 9–13.

Isono K, Fujimura Y, Shinga J, Yamaki M, O-wang J, Takihara Y, Murahashi Y, Takada Y, Mizutani-koseki Y, Koseki H. 2005. Mammalian Polyhomeotic Homologues Phc2 and Phc1 Act in Synergy To Mediate Polycomb Repression of Hox Genes. 25: 6694–6706.

Jankowska AM, Makishima H, Tiu RV, Szpurka H, Huang Y, Traina F, Visconte V, Sugimoto Y, Prince C, O'Keefe C, Hsi ED, List A, Sekeres MA, Rao A, McDevitt MA, Maciejewski JP. 2011. Mutational spectrum analysis of chronic myelomonocytic leukemia includes genes associated with epigenetic regulation: UTX, EZH2, and DNMT3A. Blood 118: 3932–41.

Janody F, Lee JD, Jahren N, Hazelett DJ, Benlali A, Miura GI, Draskovic I, Treisman JE. 2004. A mosaic genetic screen reveals distinct roles for trithorax and polycomb group genes in Drosophila eye development. Genetics 166: 187–200.

Katoh M, Katoh M. 2003. Identification and characterization of ASXL2 gene in silico. Int J Oncol 23: 845–50.

Katoh M, Katoh M. 2004. Identification and characterization of ASXL3 gene in silico. Int J Oncol 24: 1617–22.

Katoh M. 2013. Functional and cancer genomics of ASXL family members. Br J Cancer 109: 299–306.

Kattman SJ, Huber TL, Keller GM. 2006. Multipotent flk-1+ cardiovascular progenitor cells give rise to the cardiomyocyte, endothelial, and vascular smooth muscle lineages. Dev Cell 11: 723–32.

Katz TC, Singh MK, Degenhardt K, Rivera-Feliciano J, Johnson RL, Epstein JL , Tabin CJ. 2012. Distinct compartments of the proepicardial organ give rise to coronary vascular endothelial cells. Dev Cell 22: 639-650

Kauffman SL. 1975. Kinetics of pulmonary epithelial proliferation during prenatal growth of the mouse lung. Anat Rec 183: 393-403.

Kelly TK, De Carvalho DD, Jones PA. 2010. Epigenetic modifications as therapeutic targets. Nat Biotechnol 28: 1069-1078.

Kelsh R, Harris ML, Colanesi S, Erickson CA. 2009. Stripes and belly-spots—a review of pigment cell morphogenesis in vertebrates. Semin Cell Dev Biol 20: 90–104.

Kennison JA, Tamkun JW. 1988. Dosage-dependent modifiers of polycomb and antennapedia mutations in Drosophila. Proc Natl Acad Sci 85:8136-40.

Kennison JA. 1995. The Polycomb and trithorax group proteins of Drosophila: trans-regulators of homeotic gene function. Annu Rev Genet 29: 289–303.

Keyte A, Hutson MR. 2012. The neural crest in cardiac congenital anomalies. Differentiation 84: 25–40.

Kim H, Kang K, Ekram MB, Roh TY, Kim J. 2011. Aebp2 as an epigenetic regulator for neural crest cells. PLoS One 6: e25174.

Kim TG, Chen J, Sadoshima J, Lee Y. 2004. Jumonji Represses Atrial Natriuretic Factor Gene Expression by Inhibiting Transcriptional Activities of Cardiac Transcription Factors. Mol Cell Biol 24: 10151–10160.

Kirby ML, Waldo KL. 1995. Neural crest and cardiovascular patterning. Circ Res 77:211-5.

Kitajima S1, Takagi A, Inoue T, Saga Y. 2000. MesP1 and MesP2 are essential for the development of cardiac mesoderm. Development 127: 3215-26.

Klymenko T, Müller J. 2004. The histone methyltransferases Trithorax and Ash1 prevent transcriptional silencing by Polycomb group proteins. EMBO Rep 5: 373–7.

Koga H, Kaji Y, Nishii K, Shirai M, Tomotsune D, Osugi T, Sawada A, Kim JY, Hara J, Miwa T, Yamauchi-Takihara K, Shibata Y, Takihara Y. 2002. Overexpression of Polycomb-group gene rae28 in cardiomyocytes does not complement abnormal cardiac morphogenesis in mice lacking rae28 but causes dilated cardiomyopathy. Lab Invest 82: 375–85.

Köhler C, Villar CB. 2008. Programming of gene expression by Polycomb group proteins. Trends Cell Biol 18: 236–43.

Kondo T, Isono K, Kondo K, Endo T a, Itohara S, Vidal M, Koseki H. 2014. Polycomb potentiates meis2 activation in midbrain by mediating interaction of the promoter with a tissue-specific enhancer. Dev Cell 28: 94–101.

Kumar JP, Moses K. 1997. Transcription factors in eye development: a gorgeous mosaic? Genes Dev 11: 2023–2028.

Kuo CT, Morrisey EE, Anandappa R, Sigrist K, Lu MM, Parmacek MS, Soudais C, Leiden JM. GATA4 transcription factor is required for ventral morphogenesis and heart tube formation. Genes Dev. 1997;11: 1048–1060.

Lai H, Grachoff M, McGinley AL, Khan FF, Warren CM, Chowdhury SA, Wolska BM, Solaro RJ, Geenen DL, Wang QT. 2012. Maintenance of adult cardiac function requires the chromatin factor Asxl2. J Mol Cell Cardiol 53: 734–741.

Lai HL, Wang QT. 2013. Additional sex combs-like 2 is required for polycomb repressive complex 2 binding at select targets. PLoS One 8: e73983.

Lane J, Kaartinen V. 2014. Signaling networks in palate development. Wiley Interdiscip Rev Syst Biol Med 6: 271–8.

Lau C, Rogers JM, Desai M, Ross MG. 2011. Fetal programming of adult disease: implications for prenatal care. Obstet Gynecol 117: 978–85.

Laumonnier F, Holbert S, Ronce N, Faravelli F, Lenzner S, Schwartz CE, Lespinasse J, Van Esch H, Lacombe D, Goizet C, Phan-Dinh Tuh F, van Bokhoven H, Fryns JP, Chelly J, Ropers HH, Moraine C, Hamel BC, Briault S. 2005. Mutations in PHF8 are associated with X linked mental retardation and cleft lip/cleft palate. J Med Genet 42: 780–6.

Lavine KJ, Long F, Choi K, Smith C, Ornitz DM. 2008. Hedgehog signaling to distinct cell types differentially regulates coronary artery and vein development. Development 135: 3161–71.

Lee SW, Cho YS, Na JM, Park UH, Kang M, Kim EJ, Um SJ. 2010. ASXL1 represses retinoic acid receptor-mediated transcription through associating with HP1 and LSD1. J Biol Chem 285: 18–29.

Lee Y, Song AJ, Baker R, Micales B, Conway SJ, Lyons GE. 2000. Jumonji, a Nuclear Protein That Is Necessary for Normal Heart Development. Circ Res 86: 932–938.

Levin MD, Lu MM, Petrenko NB, Hawkins BJ, Gupta TH, Lang D, Buckley PT, Jochems J, Liu F, Spurney CF, Yuan LJ, Jacobson JT, Brown CB, Huang L, Beermann F, Margulies KB, Madesh M, Eberwine JH, Epstein JA, Patel VV. 2009. Melanocyte-like cells in the heart and pulmonary veins contribute to atrial arrhythmia triggers. J Clin Invest 119: 3420-36.

Levy C, Khaled M, Fisher DE. 2006. MITF: master regulator of melanocyte development and melanoma oncogene. Trends Mol Med 12: 406–14.

Liakath-Ali K, Vancollie VE, Heath E, Smedley DP, Estabel J, Sunter D, Ditommaso T, White JK, Ramirez-Solis R, Smyth I ,Steel KP, Watt FM. 2014. Novel skin phenotypes revealed by a genome-wide mouse reverse genetic screen. Nat Commun 5: 3540.

Lien CL, Wu C, Mercer B, Webb R, Richardson JA, Olson EN. 1999. Control of early cardiac-specific transcription of Nkx2-5 by a GATA-dependent enhancer. Development 126: 75-84.

Lints TJ, Parsons LM, Hartley L, Lyons I, and Harvey RP. 1993. Nkx-2.5: a novel murine homeobox gene expressed in early heart progenitor cells and their myogenic descendants. Development 119: 419–431.

Lorente M, Pérez C, Sánchez C, Donohoe M, Shi Y, Vidal M. 2006. Homeotic transformations of the axial skeleton of YY1 mutant mice and genetic interaction with the Polycomb group gene Ring1/Ring1A. Mech Dev 123: 312–20.

MacLellan WR, Schneider MD. 2000. Genetic dissection of cardiac growth control pathways. Ann Rev Physiol 62: 289–319.

Magini P, Monica MD, Uzielli MLG, Mongelli P, Scarselli G, Gambineri E, Scarano G, Seri M. 2012. Two novel patients with Bohring-Opitz syndrome caused by de novo ASXL1 mutations. Am J Med Genet A 158A: 917–21.

Margueron R, Reinberg D. 2010.Chromatin structure and the inheritance of epigenetic information. Nature 11: 285-96.

Margueron R, Reinberg D. 2011. The Polycomb complex PRC2 and its mark in life. Nature 469: 343–349.

Marino B, Digilio MC. 2000. Congenital heart disease and genetic syndromes: specific correlation between cardiac phenotype and genotype. Cardiovasc Pathol 9: 303–15.

Maron BJ, Towbin JA, Thiene G, Antzelevitch C, Corrado D, Arnett D, Moss AJ, Seidman CE, Young JB. 2006. Contemporary definitions and classification of the cardiomyopathies: an American Heart Association Scientific Statement from the Council on Clinical Cardiology, Heart Failure and Transplantation Committee; Quality of Care and Outcomes Research and Functional Genomics and Translational Biology Interdisciplinary Working Groups; and Council on Epidemiology and Prevention. Circulation 113:1807–16.

Martínez-Morales JR, Rodrigo I, Bovolenta P. 2004. Eye development: a view from the retina pigmented epithelium. Bioessays 26: 766–77.

Marvin MJ, Di Rocco G, Gardiner A, Bush SM, Lassar AB. 2001. Inhibition of Wnt activity induces heart formation from posterior mesoderm. Genes Dev 15: 316-27.

Matarazzo MR, Bonis MLDE, Strazzullo M, Cerase A, Ferraro M, Vastarelli P, Ballestar E, Esteller M, Kudo S, Esposito MD. 2007. Multiple Binding of Methyl-CpG and Polycomb Proteins in Long-Term Gene Silencing Events. J Cell Physiol 719: 711–719.

McCulley DJ, Black BL. 2012. Transcription factor pathways and congenital heart disease. Curr Top Dev Biol 100: 253–77.

McGinley AL, Li Y, Deliu Z, Wang QT. 2014. Additional sex combs-like family genes are required for normal cardiovascular development. Genesis 16: 1–16.

Mikawa T, Brand T. 2010. Epicardial Lineage : Origins and Fates. In Heart Development and Regeneration, Elsevier Inc. pp. 325–344.

Milgrom-Hoffman M, Harrelson Z, Ferrara N, Zelzer E, Evans SM, Tzahor E. 2011. The heart endocardium is derived from vascular endothelial progenitors. Development 138: 4777–87.

Milne TA, Sinclair DA, Brock HW. 1999. The Additional sex combs gene of Drosophila is required for activation and repression of homeotic loci, and interacts specifically with Polycomb and super sex combs. Mol Gen Genet 261: 753–761.

Minette MS, Sahn DJ. 2006. Ventricular septal defects. Circulation 114: 2190–2197.

Mitchell ME, Sander TL, Klinkner DB, Tomita-Mitchell A. 2007. The molecular basis of congenital heart disease. Semin Thorac Cardiovasc Surg 19: 228–37.

Mommersteeg MT, Soufan AT, de Lange FJ, van den Hoff MJ, Anderson RH, Christoffels VM, Moorman AF. 2006. Two distinct pools of mesenchyme contribute to the development of the atrial septum. Circ Res 99: 351–3.

Moss JB, Xavier-Neto J, Shapiro MD, Nayeem SM, McCaffery P, Drager UC, Rosenthal N. 1998. Dynamic Patterns of retinoic acid synthesis and response in the developing mammalian heart. Dev Biol 199: 55-71.

Moxham BJ. 2003. The development of the palate – a brief review. Eur J Anat 7: 53–74.

Mullen AC, Orlando DA, Newman JJ, Lovén J, Kumar RM, Bilodeau S, Reddy J, Guenther MG, DeKoter RP, Young RA. 2011. Master transcription factors determine cell-type-specific responses to TGF-β signaling. Cell 147: 565–76.

Nebbioso A, Carafa V, Benedetti R, Altucci L. 2012. Trials with “epigenetic” drugs: an update. Mol Oncol 6: 657–82.

Nemer M. 2008. Genetic insights into normal and abnormal heart development. Cardiovasc Pathol 17: 48–54.

Nishimoto S, Minguillon C, Wood S, Logan MP. 2014. A combination of activation and repression by a colinear Hox code controls forelimb-restricted expression of Tbx5 and reveals Hox protein specificity. PLoS Genet 10: e1004245.

Nishimura EK. 2011. Melanocyte stem cells: a melanocyte reservoir in hair follicles for hair and skin pigmentation. Pigment Cell Melanoma Res 24: 401–10.

Oka T, Maillet M, Watt AJ, Schwartz RJ, Aronow BJ, Duncan SA, Molkentin JD. 2006. Cardiac-specific deletion of Gata4 reveals its requirement for hypertrophy, compensation, and myocyte viability. Circ Res 98: 837-45.

Olivey HE, Mundell NA, Austin AF, Barnett JV. 2006. Transforming growth factor-beta stimulates epithelial-mesenchymal transformation in the proepicardium. Developmental dynamics. 235: 50–9.

Olivey HE, Svensson EC. 2010. Epicardial-myocardial signaling directing coronary vasculogenesis. Circ Res 106: 818–32.

Ordovás JM, Smith CE. 2010. Epigenetics and cardiovascular disease. Nat Rev Cardiol 7: 510–9.

Oudesluijs G, Grange DK, Bohring A, Zampino G, Thierry P. 2006. New Cases of Bohring – Opitz Syndrome, update, and critical review of the literature. Am J Med Genet A 1263: 1257–1263.

Øyen N, Poulsen G, Boyd HA, Wohlfahrt J, Jensen PK, Melbye M. 2009. Recurrence of congenital heart defects in families. Circulation 120: 295–301.

Park DS, Tompkins RO, Liu F, Zhang J, Phoon CK, Zavadil J, Fishman GI. 2013. Pocket proteins critically regulate cell cycle exit of the trabecular myocardium and the ventricular conduction system. Biol Open 2: 968–78.

Park UH, Yoon SK, Park T, Kim EJ, Um SJ. 2011. Additional sex comb-like (ASXL) proteins 1 and 2 play opposite roles in adipogenesis via reciprocal regulation of peroxisome proliferator-activated receptor {gamma}. J Biol Chem 286: 1354–63.

Pasumarthi KBS, Field LJ. 2002. Cardiomyocyte Cell Cycle Regulation. Circ Res 90: 1044–1054.

Philips GT, Stair CN, Young Lee H, Wroblewski E, Berberoglu MA, Brown NL, Mastick GC. 2005. Precocious retinal neurons: Pax6 controls timing of differentiation and determination of cell type. Dev Biol 279: 308-21.

Philips GT, Stair CN, Young Lee H, Wroblewski E, Berberoglu MA, Brown NL, Mastick GS. 2005. Precocious retinal neurons: Pax6 controls timing of differentiation and determination of cell type. Dev Biol 279: 308-321.

Pietersen AM, van Lohuizen M. 2008. Stem cell regulation by polycomb repressors: postponing commitment. Curr Opin Cell Biol 20: 201–7.

Piette D, Hendrickx M, Willems E, Kemp CR, Leyns L. 2008. An optimized procedure for whole-mount in situ hybridization on mouse embryos and embryoid bodies. Nat Protoc 3:1194-1201.

Pirity MK, Wang WL, Wolf L , Tamm ER, Schreiber-Agus N, Cvekl A. 2007. Rybp, a polycomb complex-associated protein, is required for mouse eye development. BMC Dev Biol 7: 39.

Pu WT. 2009. Identification of a cardiac disease modifier gene using forward genetics in the mouse. PLoS Genet 5: e1000643.

Raes J, Peer Y Van de. 2003. Gene duplication, the evolution of novel gene functions, and detecting functional divergence of duplicates in silico. Appl Bioinformatics 2: 91-101.

Rajagopal SK, Ma Q, Obler D, Shen J, Manichaikul A, Tomita-Mitchell A, Boardman K, Briggs C, Garg V, Srivastava D, Goldmuntz E, Broman KW, Benson DW, Smoot LB, Pu WT. 2007. Spectrum of heart disease associated with murine and human GATA4 mutation. J Mol Cell Cardiol 43: 677–85.

Ramirez MI, Millien G, Hinds A, Cao Y, Seldin DC, Williams MC. 2003. T1α, a lung type I cell differentiation gene, is required for normal lung cell proliferation and alveolus formation at birth. Dev Biol 256: 62–73.

Red-Horse K, Ueno H, Weissman IL, Krasnow, MA. (2010). Coronary arteries form by developmental reprogramming of venous cells. Nature, 464: 549–53.

Richards AA, Garg V. 2010. Genetics of congenital heart disease. Curr Cardiol Rev 6: 91-97.

Riley PR, Smart N. 2011. Vascularizing the heart. Cardiovasc Res 91: 260–8.

Rochais F, Mesbah K, Kelly RG. 2009. Signaling pathways controlling second heart field development. Circ Res 104: 933–42.

Runge MS, Patterson C. 2005. Principles of Molecular Cardiology. Humana Press Inc. 617 pp.

Russell B, Graham JM. 2013. Expanding our knowledge of conditions associated with the ASXL gene family. Genome Med 5: 16.

Ryckebusch L, Wang Z, Bertrand N, Lin SC, Chi X, Schwartz R, Zaffran S, Niederreither K. 2008. Retinoic acid deficiency alters second heart field formation. Proc Natl Acad Sci U S A 105: 2913–8.

Sakata Y, Koibuchi N, Xiang F, Youngblood JM, Kamei CN, Chin MT. 2006. The spectrum of cardiovascular anomalies in CHF1/Hey2 deficient mice reveals roles in endocardial cushion, myocardial and vascular maturation. J Mol Cell Cardiol 40: 267–73.

Saladi SV, Wong PG, Trivedi AR, Marathe HG, Keenen B, Aras S, Liew ZQ, Setaluri V, de la Serna IL. 2013. BRG1 promotes survival of UV-irradiated melanoma cells by cooperating with MITF to activate the melanoma inhibitor of apoptosis gene. Pigment Cell Melanoma Res 26: 377–91.

Salic A, Mitchison TJ. 2008. A chemical method for fast and sensitive detection of DNA synthesis in vivo. Proc Natl Acad Sci U S A 105: 2415–20.

Samsa LA, Yang B, Liu J. 2013. Embryonic cardiac chamber maturation: Trabeculation, conduction, and cardiomyocyte proliferation. Am J Med Genet C Semin Med Genet 163C: 157–68.

Scapoli L, Martinelli M, Pezzetti F, Palmieri A, Girardi A, Savoia A, Bianco AM, Carinci F. 2010. Expression and association data strongly support JARID2 involvement in nonsyndromic cleft lip with or without cleft palate. Hum Mutat 31: 794–800.

Scheuermann JC, de Ayala Alonso AG, Oktaba K, Ly-Hartig N, McGinty RK, Fraterman S, Wilm M, Muir TW, Müller J. 2010. Histone H2A deubiquitinase activity of the Polycomb repressive complex PR-DUB. Nature 465: 243–7.

Scheuermann, Johanna C; Gutierrez, Luis; Muller J. 2012. Histone H2A monoubiquitination and Polycomb repression. Fly (Austin) 6: 162–168.

Schuettengruber B, Chourrout D, Vervoort M, Leblanc B, Cavalli G. 2007. Genome regulation by polycomb and trithorax proteins. Cell 128: 735–45.

Schuettengruber B, Ganapathi M, Leblanc B, Portoso M, Jaschek R, Tolhuis B, van Lohuizen M, Tanay A, Cavalli G. 2009. Functional anatomy of polycomb and trithorax chromatin landscapes in Drosophila embryos. PLoS Biol 7: e13.

Schultheiss, TM, Burch JB, Lassar AB. 1997. A role for bone morphogenetic proteins in the induction of cardiac myogenesis. Genes Dev. 11: 451–462.

Schwartz YB, Pirrotta V. 2007. Polycomb silencing mechanisms and the management of genomic programmes. Nat Rev Genet 8: 9–22.

Schwartz YB, Pirrotta V. 2008. Polycomb complexes and epigenetic states. Curr Opin Cell Biol 20: 266–73.

Sedmera D, McQuinn T. 2008. Embryogenesis of heart muscle. Heart Fail Clin 4: 235–245.

Shaham O, Menuchin Y, Farhy C, Ashery-Padan R. 2012. Pax6: a multi-level regulator of ocular development. Prog Retin Eye Res 31: 351–76.

Shaham O, Menuchin Y, Farhy C, Ashery-Padan R. 2012. Pax6: a multi-level regulator of ocular development. Prog Retin Eye Res 31: 351–76.

Shieh JTC, Srivastava D. 2009. Heart malformation: what are the chances it could happen again? Circulation 120: 269–71.

Shirai M, Osugi T, Koga H, Kaji Y, Takimoto E, Komuro I, Hara J, Miwa T, Yamauchi-Takihara K, Takihara Y. 2002. The Polycomb-group gene Rae28 sustains Nkx2.5/Csx expression and is essential for cardiac morphogenesis. J Clin Invest 110: 177–184.

Sinclair DA, Campbell RB, Nicholls F, Slade E, Brock HW. 1992. Genetic analysis of the a*dditional sex combs* locus of *Drosophila melanogaster*. Genetics 130:817–825.

Sinclair DA, Milne TA, Hodgson JW, Shellard J, Salinas CA, Kyba M, Randazzo F, Brock HW. 1998. The Additional sex combs gene of Drosophila encodes a chromatin protein that binds to shared and unique Polycomb group sites on polytene chromosomes. Development 125: 1207-1216.

Sirbu IO, Zhao X, Duester G. 2008. Retinoic acid controls heart anteroposterior patterning by down-regulating Isl1 through the Fgf8 pathway. Dev Dyn 237: 1627–35.

Slominski A, Wortsman J, Plonka PM, Schallreuter KU, Paus R, Tobin DJ. 2005. Hair follicle pigmentation. J Invest Dermatol 124: 13–21.

Smith TM, Lozanoff S, Iyyanar PP, Nazarali AJ. 2012. Molecular signaling along the anterior-posterior axis of early palate development. Front Physiol 3: 488.

Snider P, Standley KN, Wang J, Azhar M, Doetschman T, Conway SJ. 2009. Origin of cardiac fibroblasts and the role of periostin. Circ Res 105: 934–47.

Song LB, Li J, Liao WT, Feng Y, Yu CP, Hu JL, Kong QL, Xu LH, Zhang X, Liu W, Li MZ, Zhang L, Kang TB, Fu LW, Huang WL, Xia YF, Tsao SW, Li M, Band V, Dand H, Shi QH, Zeng YX, Zeng MS. 2009. The polycomb group protein Bmi-1 represses the tumor suppressor PTEN and induces epithelial-mesenchymal transition in human nasopharyngeal epithelial cells. J Clin Invest 119: 3626-36.

Sparmann A, van Lohuizen M. 2006. Polycomb silencers control cell fate, development and cancer. Nat Rev Cancer 6: 846-856.

Später D, Abramczuk MK, Buac K, Zangi L, Stachel MW, Clarke J, Sahara M, Ludwig A, Chien KR. 2013. A HCN4+ cardiomyogenic progenitor derived from the first heart field and human pluripotent stem cells. Nat Cell Biol 15: 1098–106.

Stankunas K, Hang CT, Tsun ZY, Chen H, Lee NV, Wu JI, Shang C, Bayle JH, Shou W, Iruela-Arispe ML, Chang CP. 2008. Endocardial Brg1 represses ADAMTS1 to maintain the microenvironment for myocardial morphogenesis. Dev Cell 14: 298–311.

Steffen PA, Ringrose L. 2014. What are memories made of? How Polycomb and Trithorax proteins mediate epigenetic memory. Nat Rev Mol Cell Biol 15: 340–56.

Stock JK, Giadrossi S, Casanova M, Brookes E, Vidal M, Koseki H, Brockdorff N, Fisher AG, Pombo A. 2007. Ring1-mediated ubiquitination of H2A restrains poised RNA polymerase II at bivalent genes in mouse ES cells. Nat Cell Biol 9: 1428–35.

Stoller JZ, Demauro SB, Dagle JM, Reese J. 2011. Current Perspectives on Pathobiology of the Ductus Arteriosus. J Clin Exp Cardiolog 8: 1–29.

Takihara Y, Tomotsune D, Shirai M, Katoh-Fukui Y, Nishii K, Motaleb MA, Nomura M, Tsuchiya R, Fujita Y, Shibata Y, Higashinakagawa T, Shimada K. 1997. Targeted disruption of the mouse homologue of the Drosophila polyhomeotic gene leads to altered anteroposterior patterning and neural crest defects. Development 124: 3673–82.

Tamura Y, Matsumura K, Sano M, Tabata H, Kimura K, Ieda M, Arai T, Ohno Y, Kanazawa H, Yuasa S, Kaneda R, Makino S, Nakajima K, Okano H, Fukuda K. 2011. Neural crest-derived stem cells migrate and differentiate into cardiomyocytes after myocardial infarction. Arterioscler Thromb Vasc Biol 31: 582–9.

Tanimura S1, Tadokoro Y, Inomata K, Binh NT, Nishie W, Yamazaki S, Nakauchi H, Tanaka Y, McMillan JR, Sawamura D, Yancey K, Shimizu H, Nishimura EK. Cell Stem Cell. 2011 Hair follicle stem cells provide a functional niche for melanocyte stem cells. Cell Stem Cell 8:177-87.

Tomanek, RJ, Ishii Y, Holifield JS, Sjogren CL, Hansen HK, Mikawa T. 2006. VEGF family members regulate myocardial tubulogenesis and coronary artery formation in the embryo. Circ Res 98: 947-53.

Tomita Y, Matsumura K, Wakamatsu Y, Matsuzaki Y, Shibuya I, Kawaguchi H, Ieda M, Kanakubo S, Shimazaki T, Ogawa S, Osumi N, Okano H, Fukuda K. 2005. Cardiac neural crest cells contribute to the dormant multipotent stem cell in the mammalian heart. J Cell Biol 170: 1135–46.

Toyoda M, Shirato H, Nakajima K, Kojima M, Takahashi M, Kubota M, Suzuki-Migishima R, Motegi Y, Yokoyama M, Takeuchi T. 2003. jumonji downregulates cardiac cell proliferation by repressing cyclin D1 expression. Dev Cell 5: 85–97.

Trompouki E, Bowman TV, Lawton LN, Fan ZP, Wu DC, DiBiase A, Martin CS, Cech JN, Sessa AK, Leblanc JL, Li P, Durand EM, Mosimann C, Heffner GC, Daley GQ, Paulson RF, Young RA, Zon LI. 2011. Lineage regulators direct BMP and Wnt pathways to cell-specific programs during differentiation and regeneration. Cell 147: 577–89.

Tse C, Sera T, Wolffe AP, Hansen JC. 1998. Disruption of higher-order folding by core histone acetylation dramatically enhances transcription of nucleosomal arrays by RNA polymerase III. Mol Cell Biol 18: 4629–38.

Turgeon B, Meloche S. 2009. Interpreting neonatal lethal phenotypes in mouse mutants : insights into gene function and human diseases. Physiol Rev 89: 1–26.

Vallaster M, Vallaster CD, Wu SM. 2012. Epigenetic mechanisms in cardiac development and disease. Acta Biochim Biophys Sin (Shanghai) 44: 92–102.

van der Bom T, Bouma BJ, Meijboom FJ, Zwinderman AH, Mulder BJM. 2012. The prevalence of adult congenital heart disease, results from a systematic review and evidence based calculation. Am Heart J 164: 568–75.

Van Speybroeck L. 2002. From epigenesis to epigenetics: the case of C. H. Waddington. Ann N Y Acad Sci 981: 61–81.

Van Weerd JH, Koshiba-Takeuchi K, Kwon C, Takeuchi JK. 2011. Epigenetic factors and cardiac development. Cardiovasc Res 91: 203–11.

VanderSluis B, Bellay J, Musso G, Costanzo M, Papp B, Vizeacoumar FJ, Baryshnikova A, Andrews B, Boone C, Myers CL. 2010. Genetic interactions reveal the evolutionary trajectories of duplicate genes. Mol Syst Biol 6: 429.

Verzi MP, McCulley DJ, De Val S, Dodou E, Black BL. 2005. The right ventricle, outflow tract, and ventricular septum comprise a restricted expression domain within the secondary/anterior heart field. Dev Biol 287: 134–45.

Voigt P, Tee W-W, Reinberg D. 2013. A double take on bivalent promoters. Genes Dev 27: 1318–38.

Wang D, Chang PS, Wang Z, Sutherland L, Richardson JA, Small E, Krieg PA, Olson EN. 2001. Activation of cardiac gene expression by myocardin, a transcriptional cofactor for serum response factor. Cell 105: 851–862.

Wang J, Kumar RM, Biggs VJ, Lee H, Chen Y, Kagey MH, Young RA, Abate-Shen C. 2011. The Msx1 Homeoprotein Recruits Polycomb to the Nuclear Periphery during Development. Dev Cell 21: 575–88.

Wang J, Li Z, He Y, Pan F, Chen S, Rhodes S, Nguyen L, Yuan J, Jiang L, Yang X, Weeks O, Liu Z, Zhou J, Ni H, Cai CL, Xu M, Yang FC. 2013. Loss of Asxl1 leads to myelodysplastic syndrome-like disease in mice. Blood 123:541-53.

Wang J, Li Z, He Y, Pan F, Chen S, Rhodes S, Nguyen L, Yuan J, Jiang L, Yang X, Weeks O, Liu Z, Zhou J, Ni H, Cai CL, Xu M, Yang FC. 2014. Loss of Asxl1 leads to myelodysplastic syndrome-like disease in mice. Blood 123: 541-553.

Wang QT. 2012. Epigenetic regulation of cardiac development and function by polycomb group and trithorax group proteins. Dev Dyn 241: 1021–33.

Wang W, Li Q, Xu J, Cvekl A. 2010. Lens Fiber Cell Differentiation and Denucleation Are Disrupted through Expression of the N-Terminal Nuclear Receptor Box of Ncoa6 and Result in p53-dependent and p53-independent apoptosis. Mol Biol Cell 21: 2453–2468.

Warburton D, Schwarz M, Tefft D, Flores-Delgado G, Anderson KD, Cardoso WV. 2000. The molecular basis of lung morphogenesis. Mech Dev 92: 55–81.

Warnes CA, Williams RG, Bashore TM, Child JS, Connolly HM, Dearani JA, del Nido P, Fasules JW, Graham TP Jr., Hijazi ZM, Hunt SA, King ME, Landzberg MJ, Miner PD, Radford MJ, Walsh EP, Webb GD. 2008. ACC/AHA 2008 guidelines for the

management of adults with congenital heart disease: a report of the American College of Cardiology/American Heart Association Task Force on Practice Guidelines (Writing Committee to Develop Guidelines on the Management of Adults with Congenital Heart Disease). J Am Coll Cardiol 52: e143–263.

Webb S, Brown NA, Anderson RH. 1998. Formation of the atrioventricular septal structures in the normal mouse. Circ Res 82: 645–656.

Wheeler FC, Tang H, Marks OA, Hadnott TN, Chu PL, Mao L, Rockman HA, Marchuk DA. 2009. Tnni3k modifies disease progression in murine models of cardiomyopathy. PLoS Genet 5: e1000647.

Wilkie AL, Jordan SA, Jackson IJ. 2002. Neural crest progenitors of the melanocyte lineage: coat colour patterns revisited. Development 129: 3349–57.

Wilting J, Buttler K, Schulte I, Papoutsi M, Schweigerer L, Männer J. 2007. The proepicardium delivers hemangioblasts but not lymphangioblasts to the developing heart. Dev Biol 305: 451–9.

Winston JB, Erlich JM, Green CA, Aluko A, Kaiser KA, Takematsu M, Barlow RS, Sureka AO, LaPage MJ, Janss LL, Jay PY. 2010. Heterogeneity of genetic modifiers ensures normal cardiac development. Circulation 121: 1313–21.

Xie L, Hoffmann AD, Burnicka-Turek O, Friedland-Little JM, Zhang K, Moskowitz IP. 2012. Tbx5-hedgehog molecular networks are essential in the second heart field for atrial septation. Dev Cell 23: 280–91.

Xu K, Nieuwenhuis E, Cohen BL, Wang W, Canty AJ, Danska JS, Coultas L, Rossant J, Wu MYJ, Piscione TD, Nagy A, Gossler A, Hicks GG, Hui CC, Henkelman RM, Yu LX, Sled JG, Gridley T, Egan SE. 2010. Lunatic Fringe-mediated Notch signaling is required for lung alveogenesis. Am J Physiol Lung Cell Mol Physiol 298: 45–56.

Yokoyama U, Minamisawa S, Quan H, Ghatak S, Akaike T, Segi-Nishida E, Iwasaki S, Iwamoto M, Misra S, Tamura K, Hori H, Yokota S, Toole BP, Sugimoto Y, Ishikawa Y. 2006. Chronic activation of the prostaglandin receptor EP4 promotes hyaluronan-mediated neointimal formation in the ductus arteriosus. J Clin Invest 116: 3026–34.

Zhang M, Bolfing MF, Knowles HJ, Karnes H, Hackett BP. 2004. Foxj1 regulates asymmetric gene expression during left-right axis patterning in mice. Biochem Biophys Res Commun 26: 1413-20.

Zhang M, Chen M, Kim JR, Zhou J, Jones RE, Tune JD, Kassab GS, Metzger D, Ahlfeld S, Conway SJ, Herring BP. 2011. SWI/SNF complexes containing Brahma or Brahma-related gene 1 play distinct roles in smooth muscle development. Mol Cell Biol 31(13): 2618–31.

Zhou B, MA Q, Rajagopal S, Wu SM, Domian I, Rivera-Feliciano J, Jiang D, von Gise A, Ikeda S, Chien KR, Pu WT. 2008. Epicardial progenitors contribute to the cardiomyocyte lineage in the developing heart. Nature 454: 109-13.

Zhou L, Lim L, Costa RH, Whitsett JA. 1996. Thyroid transcription factor-1, hepatocyte nuclear factor-3beta, surfactant protein B, C, and Clara cell secretory protein in developing mouse lung. J Histochem Cytochem 44: 1183-1193.

Zhou W, Zhu P, Wang J, Pascual G, Ohgi KA, Lozach J, Glass CK, Rosenfeld MG. 2008. Histone H2A monoubiquitination represses transcription by inhibiting RNA polymerase II transcriptional elongation. Mol Cell 29: 69–80.

Zhou Y, Kim J, Yuan X, Braun T. 2011. Epigenetic modifications of stem cells: a paradigm for the control of cardiac progenitor cells. Circ Res 109: 1067–81.

Zuber ME, Gestri G, Viczian AS, Barsacchi G, Harris WA. 2003. Specification of the vertebrate eye by a network of eye field transcription factors. Development 130: 5155–67.

VITA

EDUCATION

University of Illinois at Chicago, Chicago, Illinois. Ph.D. Candidate, Biological Sciences, 2008-2014.

Marietta College, Marietta, Ohio. B.S. in Biology, 2004-2007.

RESEARCH EXPERIENCE

Asxl2 and *Asxl1* regulate mouse heart development. Doctoral research. Department of Biological Sciences, University of Illinois at Chicago, 2008-2014. Adviser: Qun-Tian Wang, Ph.D.

Beta-actin and metastasis in B16 melanoma.Undergraduate Capstone Project. Department of Biology, Marietta College, 2006-2007. Adviser: Steven R. Spilatro, Ph.D.

PUBLICATIONS

McGinley, AL, Li, YY, Deliu, ZD, and Wang, QT. (2014). Additional sex combs-like family genes are required for normal cardiac development. Genesis. In press.

Lai, HL, Grachoff, M, McGinley, AL, Khan, FF, Warren, CM, Chowdhury, SAK, Wolska, BM, Solaro, RJ, Geenen, DL, and Wang, QT. (2012). Maintenance of adult cardiac function requires the chromatin factor Asxl2. Journal of Molecular and Cellular Cardiology, 53:5 p.734-741.

TEACHING EXPERIENCE

Instructor, Vertebrate Embryology, University of Illinois at Chicago, 2014.

Teaching Assistant, Microbiology, Vertebrate Embryology, Developmental Biology, Cell Biology, Mendelian and Molecular Genetics, Biology of Populations and Communities, Biology of Cells and Organisms. University of Illinois at Chicago, 2008-2013.

Curriculum Development, Explaining Science, BIOS 594, University of Illinois at Chicago, 2013.

Guest Lecturer, Developmental Biology, BIOS 320, University of Illinois at Chicago, 2012.

Teaching Assistant, Human Physiology, BIOL 203, Marietta College, 2008.

Teaching Assistant, Environmental Biology Lab, BIOL 106, Marietta College, 2007.

HONORS AND AWARDS

Excellence in Teaching – Microbiology, 2014; Mendelian & Molecular Genetics, 2013; Vertebrate Embryology, 2013, 2011; Developmental Biology, 2012. University of Illinois at Chicago.

Chancellor's Student Service Award, University of Illinois at Chicago, 2012, 2013.

Peer Mentor of the Year, University of Illinois at Chicago, 2012.

Excellence in Research Mentorship, University of Illinois at Chicago, 2010.

UNIVERSITY SERVICES

Advisory Board Member, Women in Science and Engineering, University of Illinois at Chicago, 2013.

Mentor, Summer Research Opportunities Program, University of Illinois at Chicago, 2013.

President, Biology Graduate Student Association, University of Illinois at Chicago, 2012-2013.

Peer Mentor, Women in Science and Engineering, University of Illinois at Chicago, 2011-2013.

Co-Chair, Career Seminar Series Committee, University of Illinois at Chicago, 2011-2013.

Judge, Chicago Area Undergraduate Research Symposium, 2011.

Representative, Graduate Student Council, University of Illinois at Chicago, 2010-2011.

PRESENTATIONS

Marion, AL, Lin, A, Lee, MC, Baskind, HA, Svensson, EC, and Wang, QT. (2011). The Enhancer of trithorax and Polycomb Group gene Additional sex combs-like 2 regulates mouse embryonic heart development. Society for Developmental Biology 70th Annual Meeting, Chicago, IL.

Marion, AL, Lee, MC, Lai, HL, Dao, NK, Svensson, EC, and Wang, QT. (2010). Additional Sex Combs Like 2 regulates mouse embryonic heart development. Birth, Life and Death of the Cardiac Myocyte Conference. Napa Valley, CA.

Marion, AL, Lee, MC, Patel, MP, Baskind, HA, Svensson, EC, and Wang, QT. (2010). The Enhancer of Trithorax and Polycomb group gene Additional Sex Combs Like 2 regulates mouse embryonic heart development. 49th Annual Midwest Developmental Biology Meeting. Cincinnati, OH.